MODELING AND SYSTEM IMPROVEMENTS FOR WAVELENGTH CONVERSION IN OPTICAL SWITCHING NODES

LI HAILONG

(M.Eng, Beijing University of Posts and Telecommunications)

A THESIS SUBMITTED

FOR THE DEGREE OF DOCTOR OF PHILOSOPHY

DEPARTMENT OF ELECTRICAL AND COMPUTER ENGINEERING

NATIONAL UNIVERSITY OF SINGAPORE

2005

ACKNOWLEDGEMENTS

First of all, I would like to express my most sincere gratitude to my supervisor Dr Ian Li-Jin Thng, for his patient guidance and supervision during my Ph.D. program. This work would not have been possible without his concerted efforts and involvement. I appreciate his insightful guidance, substantial assistance, and enthusiastic encouragement at every step of my research.

I also deeply appreciate the many fruitful discussions with many of my colleagues-Liu Yong, Qin Zheng, Zhao Qun, Tan Wei Liak, Lim Kim Hui, Neo Hanmeng, Lim Boon Tiong and Choo Zhiwei.

Last, but not least, I am deeply indebted to my parents and my wife. Their love and commitment have been a great source of encouragement and incentive for me to continue to succeed in this endeavor.

TABLE OF CONTENTS

SUMMARY

This thesis presents a plethora of new and novel techniques for reducing the cost of wavelength conversion in Optical Switching (OS) nodes. The techniques are useful for reducing cost in OS nodes like Optical Burst Switching (OBS), Optical Packet Switching (OPS) and Optical Circuit Switching (OCS) where it is often assumed that full wavelength conversion (FWC) is available. In this thesis, an extensive range of non-FWC (NFWC) architectures, which can achieve similar performance with FWC but at low Wavelength Converter (WC) costs in an OS node, are presented. In this thesis, we focus on asynchronous traffic scenario for the performance analysis.

First of all, for OS node employing PWC-only (partial wavelength converters-only) architecture, we develop a new one-dimensional Markov chain analysis method, which can provide both upper and lower bound for the performance of the node.. The results show that the PWC-only OS node hardly achieves similar performance with that of FWC. In addition, there is not much WC savings gained compared to a FWC node.

Secondly, for OS node employing CWC-SPF (a limited number of Complete Wavelength Converters in a share-per-fiber system), we develop a novel two-dimensional Markov chain analysis, which provides exact performance of CWC-SPF. The results show that CWC-SPF can achieve similar drop performance as a FWC node. The achievable WC saving of CWC-SPF is only around 10-20% WC compared to a FWC OS node, due to poor sharing efficiency of the SPF architecture.

Thirdly, for CWC-SPN (a limited number of CWC in a share-per-node (SPN) system) OS node, we contribute a novel multi-dimensional Markov chain analysis, which provides an exact drop performance of CWC-SPN. However, due to intractability of solving the multi-dimensional problem set, we develop a set of new mathematical tools: Randomized States (RS), Self-constrained Iteration (SCI) and Sliding Window Update (SWU), which elegantly reduce the intractable multi-dimensional Markov chain problem to a simple two-dimensional Markov chain problem for which an approximated performance is easily obtained. The results show that 50% WC costs saving (depending on the configurations) can be achieved compared to FWC, due to high sharing efficiency of SPN architecture.

Fourthly, a new NFWC architecture, combining CWCs and PWCs termed Two-Layer Wavelength Converter (TLWC), is contributed. In the TLWC architecture, the PWC is assigned to convert an input wavelength to a near output wavelength while the CWC is to convert from an input wavelength to a far output wavelength. The CWCs are shared using SPF or SPN. For TLWC-SPF, by combining the analytical models of PWC-only and CWC-SPF, we develop a novel two-dimensional Markov chain analysis method, which can provide a tight lower bound for the performance of TLWC-SPF. The results show that TLWC-SPF can save 40-60% wavelength converter compared to FWC at high load. This saving of WC costs in TLWC-SPF is much higher than in CWC-SPF. In addition, due to fewer number of CWCs used in TLWC-SPF, more switch fabric costs can be saved in TLWC-SPF compared to CWC-SPF.

Fifthly, for TLWC-SPN, by combining the analytical model of PWC-only and CWC-SPN, we develop an exact multi-dimensional Markov chain analytical model. Therefore, to reduce the complexity of the multi-dimensional method, we

contribute an approximated two-dimensional analysis method by introducing a set of mathematical tools: RS, SCI and SWU. The results show that TLWC-SPN can save 80% WC (depending on configuration) compared to FWC at high load. This saving of WC in TLWC-SPN is much higher than in CWC-SPN. In addition, due to the fewer number of CWCs used in TLWC-SPN, more switch fabric cost can be saved in TLWC-SPN compared to CWC-SPN.

Lastly, we prove that our Markov chain analysis methods presented in this thesis for all five NFWC architectures are also applicable to general optical data size distribution. This means that the analyses are applicable for OCS, OPS and OBS technologies, where the data distribution size is not necessarily exponential.

In summary, the contributions of the thesis are useful on two considerations. Firstly, we demonstrate that NFWC architectures can achieve similar performance as FWC architecture, while making significant savings on WC. The new TLWC-SPF/SPN architectures are the most cost-conscious NFWC architecture. Secondly, the analytical models presented in the thesis are also practically useful for the designer of the optically switched node to evaluate the performance and costs without performing tedious simulations.

LIST OF TABLES

LIST OF FIGURES

LIST OF ABBREVIATIONS

Abbr.	Description
WDM	Wavelength-Division-Multiplexing
NGI	Next Generation Internet
OCS	Optical Circuit Switching
OPS	Optical Packet Switching
OBS	Optical Burst Switching
OS	Optical Switching
OXC	Optical Cross-Connects
CP	Control Packet
OT	Offset Time
FDL	Fiber Delay Line
WC	Wavelength Converter
CWC	Complete Wavelength Converter
PWC	Partial Wavelength Converter
RWA	Routing and Wavelength Assignment
FWC	Full Wavelength Conversion
NFWC	Non-Full Wavelength Conversion
LLC	Link Load Correlation
TLWC	Two-Layer Wavelength Conversion
PWC-only	An NFWC architecture, which uses only PWCs.
CWC-SPF	An NFWC architecture, which uses only CWCs. All CWCs are shared by SPF mode
CWC-SPN	An NFWC architecture, which uses only CWCs. All CWCs are shared by SPN mode
TLWC-SPF	An NFWC architecture, which uses TLWC. All CWCs are shared by SPF mode
TLWC-SPN	An NFWC architecture, which uses TLWC. All CWCs are shared by SPN mode
RS	Randomized States method
SCI	Self-Constrained Iteration
SWU	Sliding Window Update
Near-WC	Near wavelength conversion
Far-WC	Far wavelength conversion

1 Introduction

With recent research progress in Wavelength-Division-Multiplexing (WDM) technology, more data can be transmitted using one fiber. Therefore, all Optical Switching (OS) network technology has emerged based on WDM. In OS technology, the processing of data is purely on the optical domain. Thus, OS technology allows high-speed traffic to be transmitted transparently in the network; and it needs fewer network layers, leading to a vast reduction of cost and complexity of the networks [1][2]. It is well-acknowledged that the next generation internet (NGI) should be based on an all OS technology.

In this chapter, a brief review of three available OS technologies is presented first. Then, the four existing contention resolution methods used in OS node are introduced. Wavelength conversion, being one of the more efficient contention resolution methods, is further discussed in terms of wavelength conversion architectures and its application to different OS technologies. We show that little research has been done on the performance analysis of wavelength conversion in a single OS node, and we will contribute some new wavelength conversion architectures in this thesis. Lastly, we present the purpose, method and contribution of this thesis in the area of architecture and performance modeling of wavelength conversion.

1.1 Optical switching technologies for next generation networks

Generally, there are three possible all-optical switching (OS) technologies for NGI: optical circuit switching (OCS, in some literatures, is referred as wavelength switching or wavelength routed) [3], optical packet switching (OPS) [4] and optical burst switching (OBS) [5]. In the following sections, a brief review of these three technologies is provided.

1.1.1 Optical Circuit Switching (OCS)

OCS is based on the wavelength routed technique, where a lightpath is set up on some dedicated wavelength(s) along the route between source destination pair via nodes equipped with Optical cross-Connects (OXC) (or wavelength routers) [1].

At each OXC along the route from source to destination, the switching configuration is controlled by the signaling sent from the source (distributed signaling) or the central server (centralized signaling) [3][6][7]. The switching configuration will reserve switching resources from the input wavelength (at an input fiber) to the output wavelength (at an output fiber). Accordingly, the lightpath is setup. The teardown procedure is initiated by the source via the use of the release signaling to each OXC node along the route, causing the intermediate OXCs to release the lightpath.

In OCS technology, no optical buffer is required at the intermediate OXC nodes of the network. This enables data to be transported transparently in the optical domain. OCS technology is a simple extension of traditional WDM network, and can be relatively easily implemented.

However, in OCS there are several drawbacks that make it an unsuitable technology for NGI deployment. Firstly, the traffic granularity of OCS is one

wavelength whose transmission speed can be 10-40 Gbps or higher. This may lead to bandwidth wastage if the required traffic intensity is less than the capacity of one wavelength. If the traffic is bursty (i.e., IP traffic), then bandwidth will be wasted due to reservation according to peak traffic intensity. Secondly, OCS requires that the duration of a lightpath be long enough, i.e., several minutes. This is because that the lightpath processing for setup and teardown is often a high overhead and may require at least several hundred milliseconds. Lastly, when the number of wavelengths is not enough to support the full mesh connectivity, load distribution in the network may be uneven given that the traffic intensity varies over time, and some source-destination pairs have to use two or more lightpaths to relay the data leading to longer route and higher volume of traffic.

1.1.2   Optical Packet Switching (OPS)

In OPS, the optical data is transmitted based on packet technology. The header and payload of one optical packet is transmitted continuously on one of the wavelengths in the fiber with no need for a lightpath setup or teardown [4], [8]-[11]. In the intermediate OPS node, the header is processed in the electrical domain by O/E conversion, and then converted to the optical domain again before being forwarded to the next node [3]-[6]. The traffic granularity of OPS technology is per-packet based, thus rendering a finer degree of service flexibility for the IP over WDM integration (e.g., statistical multiplexing performance by bandwidth sharing, traffic balance, and contract duration).

However, if OPS is implemented it needs a large number of expensive O/E/O devices (at least one per wavelength) as well as header extraction/insertion mechanism. In addition, Fiber Delay Lines (FDL) is required to delay the payload of

the optical packet, in order to compensate the processing delay of the header in the electronic domain. Owing to variations in the processing time of the packet header at the intermediate nodes, OPS also requires stringent synchronization and a complicated control mechanism. All these requirements in OPS are expensive and cannot be easily implemented based on current industry technologies. Another problem inherent to OPS is that the sizes of the data packets are usually too small (normally one optical IP packet size is around 1 KB). Given the high capacity of each wavelength, relatively high control overheads are clearly expected. Therefore, the OPS technology is still evolving and may need some more time to mature for its commercial value to be visible.

1.1.3   Optical Burst Switching (OBS)
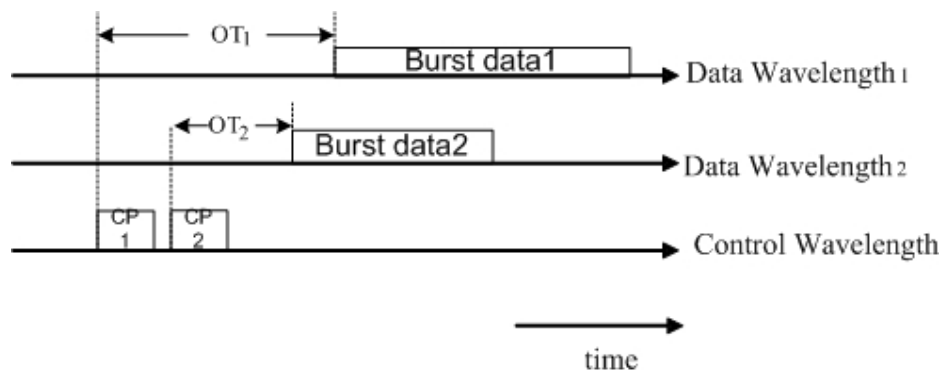
Figure 1-1:   OBS timing diagram.

A new all-optical network technology, OBS, was proposed in [12][13][14], in order to provide an all-optical switching ability with practical simplicity in implementation. In OBS paradigm [12][13], the burst data is transmitted on data wavelengths. Control packet (CP), which contains all control information of an associated burst data, is transmitted on one or more control wavelength(s). In OBS, a

CP, which is followed by the corresponding burst after some Offset Time (OT), is sent out from the ingress edge node. Each core node in the route processes the control information of the CP in the electronic domain. Using these control information, the core node can route, schedule, and reserve bandwidth for the future incoming burst data. Then the core OBS node will release this control packet to the next hop. When the burst data arrives at the core node after OT, the burst will be processed in the optical domain entirely. By arranging for an OT that is of suitable duration, this scheme ensures that the burst data cannot overtake the corresponding CP, whose information is processed in the electronic domain. The timing diagram of OBS is shown in the Figure 1-1.

The OT enables the bufferless all-optical data delivery, because the OT compensates for the processing delay of the CP in the electronic domain. In contrast, OPS needs FDL to compensate for the processing delay as well as a levy of O/E/O devices for each wavelength. OBS does not need complicated header extract/insertion mechanism, and requires only one (or small number of) O/E device for extraction of information from the CP transmitted on the control wavelength(s).
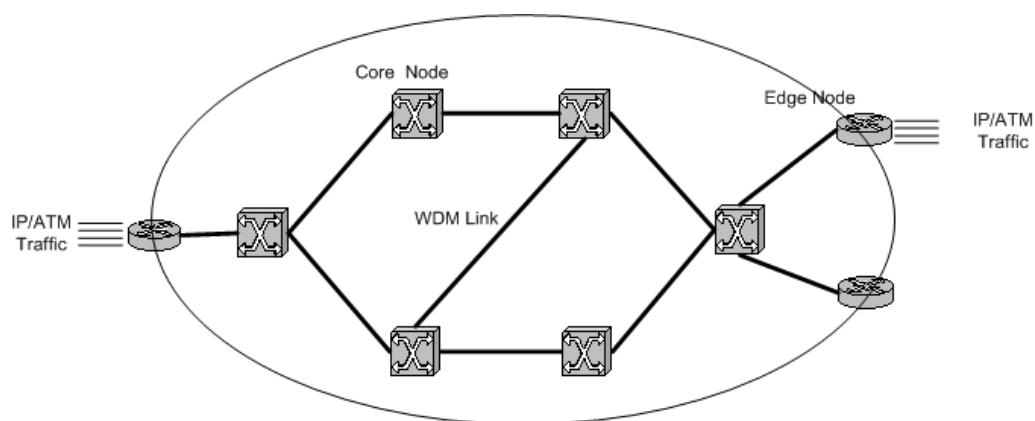
Figure 1-2:   OBS Network architecture

In OBS, to reduce control information processing overhead, many IP/ATM packets/cells are electronically assembled into one burst data at the edge nodes located at the network ingress. The burst data are then routed over a purely optical transport core network using dynamic wavelength assignment, and disassembled into IP/ATM packets/cells at the egress edge node in the electronic domain again. Therefore, in the OBS network, the edge node plays an important role in assembling the burst data, deciding burst starting time and assigning a suitable OT. The network architecture of OBS is shown in Figure 1-2

In summary, OBS combines the benefits of both OPS and OCS. The OBS burst data size is midway between OPS packet size and the OCS connection duration. Compared to OCS, OBS achieves better statistical multiplexing and accommodates delivery of short information. Compared to OPS, the OBS node is significantly simpler with less O/E/O and does not require expensive header insertion/extraction mechanisms as well as FDLs.

Thus, OBS combines the benefit of the OCS and OPS, while leveraging on the optical switching granularity and the electrical processing of control information. All these advantages enable OBS to be perhaps the most promising technology for the optical NGI.

The three OS technologies aim to exploit the bandwidth of multi-wavelengths within one fiber or to utilize bandwidth more efficiently. However, due to the dynamic property of data traffic, contention for resources in an OS node will still arise. The next section describes a number of contention resolution methods.

1.2 Resolving contention in optical switching technologies
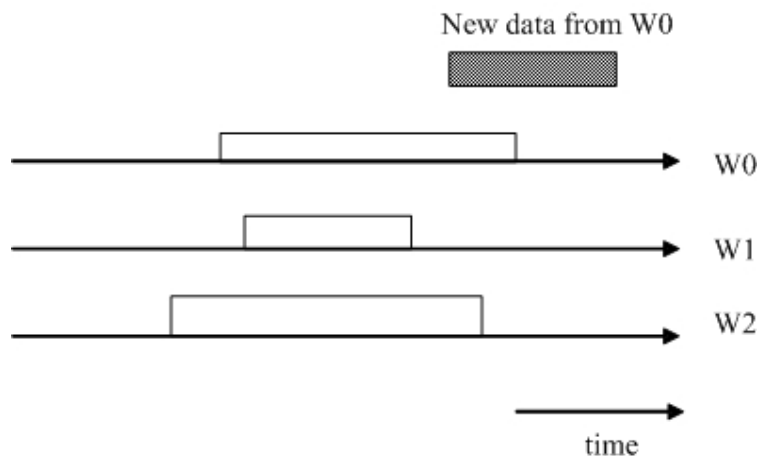
Figure 1-3:   Example of contention on one output fiber in one OS node

In OS, it is crucial to exploit bandwidth efficiently; therefore, resolving contention is a very important feature to achieve low drop probability of optical data. Contention in OS is defined as two or more optical data competing for the same resources (usually the same bandwidth on a particular wavelength). If contention happens, one of the optical data has to be dropped due to the lack of resources. A simple example is demonstrated in Figure 1-3, where there are three available wavelengths (W0, W1 and W2) within one output fiber on one OS node. All three wavelengths are serving optical data currently. When a new optical data with wavelength W0 arrives at an input fiber and is routed to this output fiber, the new data will be dropped as there is no available time slot on the W0 output wavelength. This contention can be resolved by: (1) searching for an available W0 on another output fiber which can reach the destination via an alternative route; (2) delaying the new data for some time until W0 is available, (3) using the new data to pre-empt the data being served on W0 if the priority of the new data is higher than the data being

served on W0 and; (4) converting the new data from W0 to W1, where the bandwidth is available. It can be seen that these four different solutions represent different ways to solve contention: the first solution represents the space domain solution, the second represents the time domain solution, the third represents the data domain resolution, and the last represents the wavelength domain. More details on these four solutions are discussed in the following sections.

1.2.1 Contention resolution in the space domain by using deflection routing

In the space domain, when a new optical data cannot find a suitable output wavelength on the output fiber, the optical data can be routed to another output fiber so that the optical data transmits on an alternative route to its destination from the current OS node. This is know as deflection routing [18][19][20]. In deflection routing, the entire network resources are pooled together to solve the contention.

There are some restrictions to the use of deflection routing. In OBS, because the offset time of the burst data is fixed, there is a limit on the number of hops in the alternative route that the burst can transverse within the network. In addition, Deflection routing technology relies heavily on the topology of the network. This means that the network with high connectivity, i.e., more fibers from one node to other nodes, can gain better performance than the network with the low connectivity. Previous research works in [18][19] showed that deflection routing can reduce drop probability significantly under low traffic load condition, but may destabilize the network under high traffic load condition [20].

1.2.2 Contention resolution in the time domain by using Fiber Delay Line

In the time domain, when a new optical data cannot find a suitable output wavelength on the output fiber, the data will be fed into a Fiber Delay Line (FDL) to delay some time until at least one wavelength is available. It is noticed that the FDL only provides fixed time delay, unlike an electronic buffer where the delay time can vary. The fixed delay of the FDL cannot be very long because it is restricted by the length of the FDL. Otherwise the signal degradation due to length of FDL becomes a non-negligible value and may need to be compensated by an optical signal amplifier. Therefore, this method is used mainly in OBS [15][21] and OPS [22][23], whose data size is relatively small. In OCS, the connection time of a lightpath may be too long (several minutes or even longer) for a conventional FDL to provide sufficient delay.

1.2.3 Contention resolution in the data domain by using pre-emption

In the data domain, when a new high priority optical data cannot find a suitable output wavelength on the output fiber, it will pre-empt some data being served on the output wavelength. This technique only protects the high priority data and does not improve the drop probability. The technique can be implemented in OCS, OPS, and OBS. However, there is a variant in OBS called burst segmentation in [24][25] or OCBS in [26], in which the burst data is segmented into several parts. Only the contentious parts of the burst data (either an existing burst or a new incoming burst) will be dropped/ deflected. The remaining parts of the burst data can be transmitted smoothly. Therefore, the drop performance based on the amount of segmented parts can be improved.

1.2.4 Contention resolution in the wavelength domain by using wavelength conversion

In the wavelength domain, the new optical data contending with an existing data will be sent to another available wavelength via wavelength conversion. The device which conducts the conversion, is called wavelength converter (WC) or sometimes known as tunable WC. This technique can be implemented in OCS, OBS, and OPS. Researches in [22][23][27][28][29] showed that by using WC, the drop performance can be improved significantly because the optical data can achieve high multiplexing performance with multi-wavelengths in one fiber.

1.2.5 Focus on wavelength conversion

Table 1-1:   Comparison of contention resolution techniques.

Contention Resolution	OCS	OPS	OPS	Performance Improvement
Deflection routing	✓	✓	✓	Restricted to topology and redundant routes
FDL	✗	✓	✓	Medium
Pre-emption	✓	✓	✓	Depends on whether segmented or not.
Wavelength Conversion	✓	✓	✓	High

The comparison of all these contention resolutions is listed in Table 1-1. In Table 1-1, it shows wavelength conversion is applicable to all three OS technologies and can achieve higher performance enhancement. In this thesis, we will study the wavelength conversion technology in OS. As one of contention resolution methods, wavelength conversion can also be used with the combination of other methods,

such as WC+FDL, WC + deflection routing, WC + pre-empt, and WC+ FDL + deflection routing + pre-emption. However, in order to simplify the problem studied in this thesis, only wavelength conversion method is considered. This means no FDL, deflection routing, or pre-emption method is considered in this thesis.

In this thesis, the main focus is to reduce the cost of WC while achieving a pre-defined drop performance by wavelength conversion to solve contention. We now present more details of wavelength conversion in optical switching technologies.

1.3 Wavelength conversion in optical switching technologies

The following sections present the various classes of WCs firstly. Thereafter, various possible architectures of OS node equipped with WC are reviewed. Lastly, the cost analyses and the performance models of the WC in different OS technologies are reviewed.

1.3.1 Classifications of wavelength conversion node architecture

Normally, there are two kinds of wavelength conversion node architectures: Full Wavelength Conversion (FWC) and NFWC. In FWC, whenever an input wavelength needs to be converted, there is a converter available. This means the drop probability will not impacted by wavelength conversion. However, such architecture needs many WC so that it is expensive. In order to lower the cost, there are some NFWC architectures available. In NFWC, the drop due to lack of WC is possible. Before introduce the architecture of FWC and NFWC, in the following, we will present the classification of WC first.

1.3.2 Classifications of wavelength converters

There are two classes of WCs: Partial Wavelength Converter (PWC) and Complete Wavelength Converter (CWC). PWC (referred to as limited-range tunable WC in certain literature), can only convert an input wavelength to a subset range of output wavelengths in the vicinity of the input wavelength. CWC (referred to as full-range tunable WC in certain literature), can convert any input wavelength to any output wavelength within the complete range of the fiber. The PWC is more compatible (compared to CWCs) with the hardware constraints of wavelength converters whereby after a certain range of direct conversion, the noise margin is too low for reliable conversion [30][31][32]. CWC, on the other hand, is relatively hard to manufacture directly under current technology [33]. Therefore, CWC is normally manufactured by concatenated PWCs with the help of an optical switch (detailed explanations are presented in Section 3.2.2). Of course, the drop performance of CWC is significantly better than PWC and, accordingly, there are more research interests in CWC than PWC.

1.3.3 Wavelength conversion switch architecture

In this section, we discuss three different WC switch architectures: dedicated, share-per-fiber (SPF) and share-per-node (SPN).

The dedicated WC OS node architecture is shown in Figure 1-4. The node has N input/output fiber, each with K wavelengths. There is one dedicated WC for each wavelength on each output fiber. The dedicated WC can also be located at the input side between the demux and switch. For simplicity, only the output style

dedicated architecture is shown. For the dedicated architecture, WC can be either CWC or PWC.

For an OS node, there are N number of $1 \times K$ wavelength demultiplexers, N number of $K \times 1$ multiplexer, a $NK \times NK$ non-blocking optical switch, and NK number of WC. If CWC is used in this architecture, obviously full wavelength conversion (FWC) is achieved, in which every new coming optical data can find an available WC to convert itself to an available output wavelength.
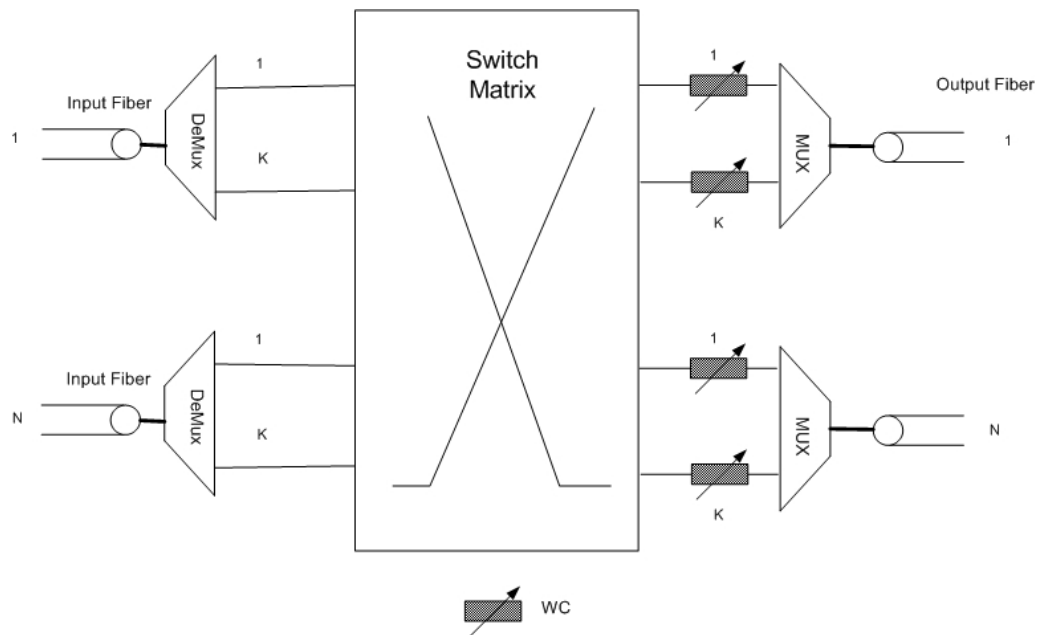
Figure 1-4:   OS node architecture with dedicated WC

However, FWC requires too many WCs, thus increasing the cost of implementation. In the operation of the actual network, the probability of using all WCs at the same time is expected to be low. Therefore, it is possible that only a few WCs are required to satisfy the of drop probability performance in OS network. Some cost effective solutions of OS switching architectures were proposed based on

the sharing of a limited number of WCs. The sharing methodology can be share-per-fiber (SPF) and share-per-node (SPN), by which we can construct NFWC architectures
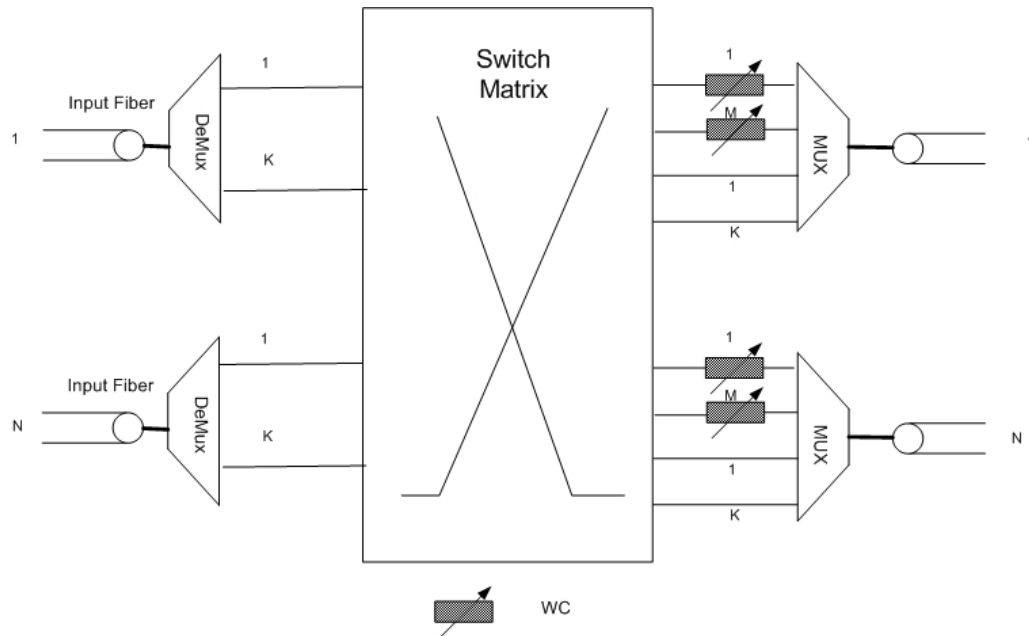
Figure 1-5:   OS switch and conversion architecture with share-per-fiber WC.

In a SPF switch and conversion architecture shown in Figure 1-5, a limited number of WCs are shared within one output fiber.

Assuming there are M ($M<K$) WCs for each output fiber, the cost of WCs using SPF is less than the dedicated architecture. However, it needs more switch fabric, i.e., $NK \times (NK + NM)$, compared to the dedicated WC architecture. This is a trade-off, which means when we want to save WC, we may need some other resources, i.e., switch, to compensate. In addition, the sharing efficiency of SPF is not high because the sharing of WCs is only localized within one fiber.
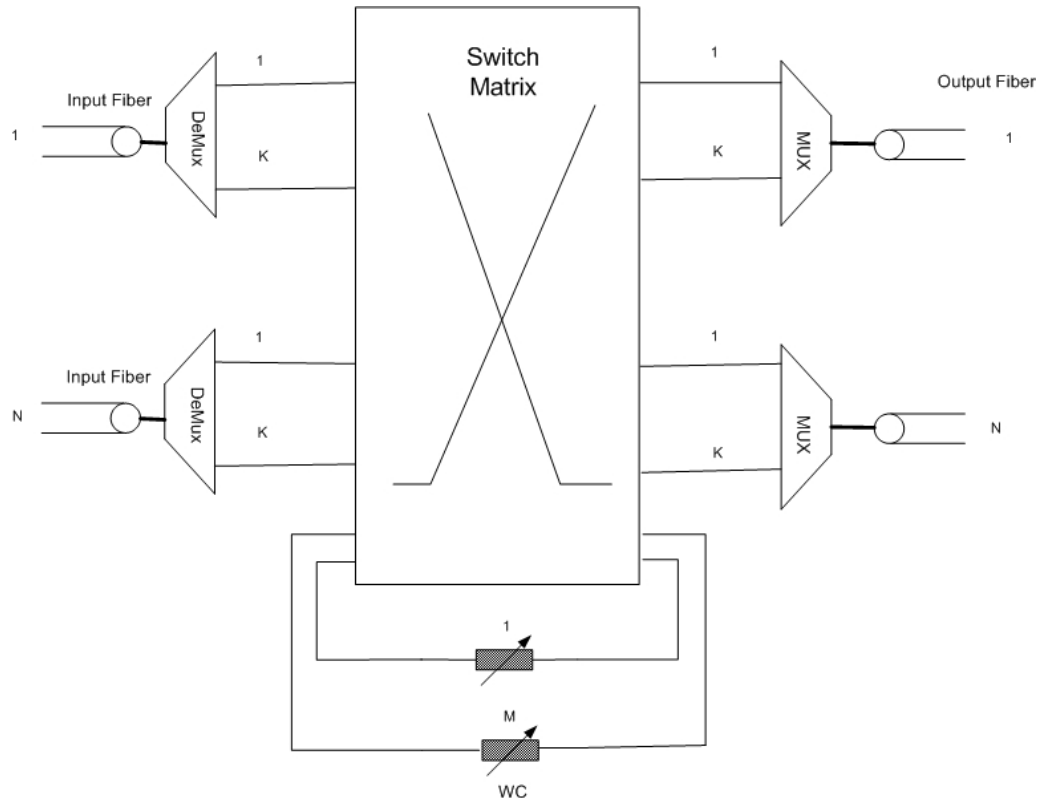
Figure 1-6:   OS switch and conversion architecture with share-per-node WC

The OS architecture with SPN WC is shown in Figure 1-6. In SPN architecture, WC is normally CWC as in SPF architecture. A total of M number of WCs are shared for the whole OS node, using a $(NK+M) \times (NK+M)$ non-blocking switching fabric. If an incoming optical data needs conversion, it will be placed on one of the shared WCs. After conversion, the data can be switched back to its output fiber. Because all WCs are shared for the whole OS node, the sharing potential is maximized, and the drop probability performance is expected to be better than that of SPF for the same number of WCs in the OS node.

1.3.4 Literature on wavelength conversion in OCS and its peculiarity compared to wavelength conversion in OBS and OPS.

The issue of wavelength conversion was first studied in OCS networks. In the majority of OCS literature, it is assumed full wavelength conversion (FWC) is available. FWC architecture can be constructed by using CWC and dedicated switch architecture shown in Figure 1-4 [27]. Therefore, the drop probability performance of OCS with FWC is only restricted by the following factors: network topology and size, the number of wavelengths per fiber, the routing and wavelength assignment algorithm (RWA), and the traffic pattern.

However, FWC architecture is expensive [34][35] to be implemented in the network, since each fiber needs one dedicated CWC to convert an input wavelength to any output wavelength. A cheaper alternative, Non-Full wavelength conversion (NFWC), which may not convert any input wavelength to any output wavelength, motivates further investigation.

In the literature on NFWC, in order to lower the cost of WC, it is normally assumed that only a limited number of WCs are available on the whole network. Therefore, the issue in OCS is to try to maximize the drop performance by selecting a *good* scheme to distribute these WCs on the networks. In this area, two possible options were considered. Firstly, WC-placement [36]-[45], is defined as follows: Given there are A nodes in network, in which B ($<A$) nodes can have FWC, a solution is sought for choosing B nodes out of all A nodes, such that best drop performance can be achieved [35]. The WC-placement problem for an arbitrary network is NP-complete [36]. By using some simple assumption about the independence of the network traffics between neighboring nodes, the authors in [36]

showed that the optimal solution of WC-placement can by found with time complexity $O(H^2 A)$, where H is the length of the lightpath. However, such assumption may not be true, and the optimal solution is expected to depend heavily on the Routing and Wavelength Assignment algorithm (RWA) [37] [38].

Secondly, WC-allocation, is defined as follows: Given C number of CWCs are available in whole network and each node can use sharing architecture like SPF/SPN, the WC-allocation problem is to distribute the CWCs over networks such that the drop performance can be optimized [35] [47] [48] [49]. In [35] [47] [49], the authors use SPN architecture and a simulation-based optimization approach, in which utilization statistics of CWCs from computer simulations are collected and then optimized to allocate the CWCs. The results show that the drop probability performance can be dramatically reduced by carefully allocating the CWCs among the network. It is also demonstrated that the drop probability performance is on par with FWC network after the number of CWCs available in the network exceeds a certain threshold. In [48], the authors evaluate the minimum number of CWCs, which are necessary to be implemented in the ring network to achieve the same performance as a FWC network.

In both WC-placement and WC-allocation, the behavior of the whole network using WC is studied, rather than behavior of one single OS node. This is because of the following two reasons. Firstly, OCS is a kind of circuit switching technique. A lightpath should be setup in the network from source to destination before data is transmitted. Therefore, the setup of a lightpath has influence on the whole network rather than a single node. Secondly, the feature of Link Load Correlation (LLC) [35], which is the correlation between load or wavelength in use

on successive links, make the link/node states of the whole network correlate together. Therefore, in OCS, the network topology, size, and traffic pattern must be considered for both WC-placement and WC-allocation.

However, in OPS and OBS networks, the basic data transmission unit is packet or burst, whose behavior in the network is more like traditional IP packet. The optical data can be momentarily delayed (by FDL) and forwarded in a connectionless or connection-oriented manner. The data can also be dropped at any intermediate node along the route from source to destination. In OCS, such drops do not occur. In addition, the traffic intensity of each connection/session is not as heavy as OCS (a wavelength). Therefore, the correlation between successive node and link is not as severe as in OCS. Thus, in OPS and OBS, the performance issues (i.e., scheduling, QoS and wavelength conversion issue) are normally studied for a single OS node instead of the whole network.

1.3.5 Wavelength conversion in OPS and OBS and implementation cost

In OPS and OBS, because of the distinctive feature of packet switching, every OS node in the network needs to provide low drop probability for the optical data. It is well known that in queuing theory [76], having more servers (wavelengths in OS) to serve many data at the same time can reduce drop probability dramatically. Obviously, by assuming full wavelength conversion (FWC) in the OS node, all wavelengths within one fiber can be considered identical, thus, multi-server queuing theory can be used to evaluate drop performance such as *M/G/K/K* [76]. By assuming FWC, a lot of important issues in OPS and OBS networks have been

studied recently, such as QoS [51]-[59], scheduling algorithm [60]-[67], theoretical performance analysis [68]-[72].

However, as stated before, the implementation cost of FWC is expensive. Therefore, an important question in OPS and OBS has surfaced in recent years: Is it possible to use NFWC to achieve the similar performance as FWC? If so, how is the performance of NFWC architecture evaluated, what kind of NFWC architecture can be achieved with the least cost?

Most research works on NFWC architectures consider only a limited number of CWCs to provide wavelength conversion capability [73]-[78]. In this case, a CWC is not dedicated to a particular wavelength; instead, all CWCs are placed in a common pool and shared amongst the wavelengths by SPF mode or SPN mode. In this thesis, the former will be referred to as CWC-SPF and the latter as CWC-SPN.

So far mathematical methods to evaluate the minimum number of CWCs required for a *synchronous slotted* optical packet network operating with CWC-SPF [77] and CWC-SPN [78] architecture have been contributed. The "**minimum number of CWCs**" is defined to be that number of CWCs required so that the drop performance of a CWC-SPF or a CWC-SPN node is similar to the drop performance of a FWC node. The saving of the CWC can reach about 95%, when extreme light load is considered.

In addition to the use of limited number of CWCs, PWC [79] can also be employed in *synchronous slotted* optical packet network. A PWC can convert an input wavelength to only a limited range of output wavelengths in the vicinity of the input wavelength. Thus, normally each PWC is dedicated to one particular wavelength at input side. In this thesis, this kind of structure is referred to as PWC-

only model. There are certain advantages in the use of PWC. Firstly, the cost of implementation can be reduced as PWC is substantially cheaper compared to CWC. Another advantage with limiting the range of outgoing wavelengths is that the level of noise introduced into the signal by the conversion process can be reduced [81]. Eramo also showed in [79] that the performance of PWC can only achieve similar performance as FWC when the range of PWC nearly reaches CWC.

1.3.6 Open problems for Non-full wavelength conversion for OPS and OBS

From the above literature review, there are still a number of unanswered questions in the NFWC research area for OPS and OBS networks.

- The traffic type in OPS/OBS may be synchronous or asynchronous depending on the politics of the various standardization boards. If the traffic type is designed/chosen/voted to be asynchronous with variable data size distribution, what is the performance model for NFWC architectures in such scenarios and how many WCs can be saved using these NFWC architectures?

- Other than CWC-SPF, CWC-SPN and PWC-only model, are there any other alternative architecture to save WC?

1.4 Purpose and method of the analysis of non-full wavelength conversion

The purpose of this thesis is to address the stated questions in section 1.3.6. The thesis will provide mathematical analysis for the performance and the cost of existing NFWC architectures under asynchronous traffic.

The traffic model considered in this thesis will be Poisson traffic with optical data length of some general distribution. We consider Poisson arrivals mainly for its amenability to bring forth further theoretical analysis/conclusions so that certain trends in the saving of wavelength cost can be highly illustrated and elucidated. While there are suggestions that in certain optical networks, traffic is Poisson or short term Poisson [83][84][85], we are also aware that there are other studies which suggest that traffic in optical networks is sub-exponential. Of course, further simulation studies on more difficult traffic types can be conducted on OS node with NFWC; and should there be any unexplainable numerical results, the Poisson-traffic-based theoretical studies presented here may be able to shed some light.

In this thesis, we will use traditional Markov chain state transition to analyze the bufferless NFWC architectures. This type of state transition analysis normally is only applicable to the queuing system, where the arrival process is Poisson and data size distribution is exponential. However, the results in the **Appendix** show that Markov chain state transition analytical model is also applicable to general data size distribution. Recent research works have shown that the optical data size distribution in OBS networks is either Gaussian or Fixed [86][87], and possibly, the data size is Fixed in OPS [77]-[80]. Our analytical results in this thesis are applicable to all three optical switching techniques, i.e., OCS, OBS, OPS, only if the arrival process of optical data is Poisson.

In this thesis, besides the use of basic theoretical Markov chain analysis, some other mathematical tools are contributed to analyze the performance, such as Randomized States, Self-Constrained Iteration and Sliding Window Update. Several

cost functions are defined to evaluate the costs of different NFWC architectures as well.

In order to compare the implementation costs on the different wavelength conversion architecture, a simple linear cost structure is adopted such that the cost of a PWC or CWC is linearly proportional to its conversion range. This linear cost model is a conservative cost increase model since practical CWCs are constructed via the concatenation of many PWCs with the help of optical switches. The direct manufacture of CWCs without the use of concatenated PWCs is also impractical. It is thus expected that the cost increase per additional wavelength range is higher than a linear model [79]. For the detailed explanation of the linear cost function, please refer to section 3.2.2.

1.5   Contributions of the thesis

The objective of this thesis is to present novel analytical methods techniques for saving the cost of WCs in NFWC architectures, while achieving similar performance as the FWC. Specifically, the thesis makes significant contributions in the following areas:

(1) For the existing PWC-only architecture,

- A novel one-dimensional Markov chain analytical model providing both lower and upper bounds for the PWC-only performance is contributed.

- New numerical results show that the PWC-only architecture can achieve similar performance as FWC only when the conversion range of the PWC is almost the same as CWC.

(2) For the existing CWC-SPF architecture,

- A novel two-dimensional Markov chain analytical model providing exact theoretical performance of the CWC-SPF node is contributed.

- New numerical results show that the CWC-SPF node has an effective cost saving percentage of only 10-20% under high load conditions compared to FWC. The low cost saving percentage is due to the sharing inefficiency of the SPF scheme.

(3) For the existing CWC-SPN architecture,

- A novel multi-dimensional Markov chain analytical model providing exact theoretical performance of the CWC-SPN node is contributed.

- A set of novel mathematical tools: RS, SCI and SWU, to simplify the intractable multi-dimensional Markov chain to a more tractable two-dimensional Markov chain model, is contributed.

- New numerical results are contributed to accurately show that the approximated two-dimensional Markov chain is able to predict the right NFWC configuration that gives maximum WC saving.

- New numerical results are contributed to show that CWC-SPN can save more WC costs than CWC-SPF because of the high sharing efficiency of the SPN system. Under high load condition, around 50% WCs (depending the configuration of CWC-SPN) can be saved compared to FWC.

(4) A novel NFWC architecture, called Two-Layer Wavelength Conversion (TLWC), to achieve similar performance as FWC is contributed. Two sub-

architectures of TLWC are contributed: TLWC-SPF and TLWC-SPN, which use different sharing modes to utilize a limited number of CWCs.

(5) For the new TLWC-SPF architecture,

- A novel two-dimensional Markov chain analytical model providing a very tight lower bound theoretical performance is contributed.

- New numerical results show that the TLWC-SPF node has a WC saving performance of 40-60% compared to FWC under high load conditions. This WC saving percentage value is much higher compared to CWC-SPF.

- New numerical results show that, due to fewer numbers of CWCs used in TLWC-SPF, more switch fabric costs can be saved in TLWC-SPF compared to CWC-SPF.

(6) For the new TLWC-SPN architecture,

- A novel and exact multi-dimensional Markov chain analytical model is contributed.

- A set of new method to reduce the multi-dimensional Markov chain to an approximated two-dimensional analytical model is contributed. Thereafter, the solution set of mathematical tools: RS, SCI and SWU are used to solve for the solution.

- New numerical results show that the TLWC-SPN can save 80% WC (depending on configurations) compared to FWC under high load conditions. The saving percentage of WC in TLWC-SPN is much higher compared to CWC-SPN.

- New numerical results show that, due to fewer numbers of CWCs used in TLWC-SPN, more switch fabric costs can be saved in TLWC-SPF than in CWC-SPN.

(7) Extension of performance study for general data size distribution

- A theoretical proof is contributed to demonstrate that all the analytical models contributed in this thesis are also applicable for general data size distribution. This means the work in this thesis can be used for all three OS technologies, which are based on different data size distributions.

1.6 Outline of the thesis

This thesis consists of five chapters and they are organized as follows.

In chapter 2, a simple one dimensional Markov chain analysis for PWC-only architecture is contributed. In this analysis, both lower and upper bounds of performance are obtained theoretically. Relevant numerical results for the PWC-only architecture are also demonstrated.

In chapter 3, the architectures and the mathematical analysis for CWC-SPF and CWC-SPN model are presented. For CWC-SPF, an exact two-dimensional Markov chain analytical model is presented first, followed by the relevant numerical results. For CWC-SPN, an exact multi-dimensional Markov chain analytical model is presented first. Thereafter, in order to lower the complexity of the exact multi-dimensional analytical model, we present a set of mathematical tools, called Randomized States, Self-Constrained Iteration and Sliding-Window Update. The numerical results show that these tools are able to provide a good approximation to

the performance of the CWC-SPN model. The results also show that CWC-SPN save more WC than CWC-SPF, but at the expense of higher switch costs

In Chapter 4, the architectures and the mathematical analysis for the TLWC-SPF and the TLWC-SPN model are presented. An important link between PWC and CWC sections in TLWC is presented. The link simplifies the analysis of TLWC to be similar to that of CWC-SPF/SPN model. The numerical results show that the TLWC-SPF/SPN architecture can save more WC and switch fabric cost than CWC-SPF/SPN architecture.

Chapter 5 concludes the thesis and proposes several possible future research works.

Finally, in the Appendix, we demonstrate that all the theoretical analyses presented in the thesis are also applicable to general data size distribution.

2 Architecture and its Modeling of Partial Wavelength Converter

Partial wavelength converters (PWCs) can convert one input wavelength to a subset range of output wavelengths in the vicinity of the input wavelength. The PWC is more suited for the hardware implementation. This is because it is widely known that after a certain range of direct conversion, the noise margin is too low for reliable conversion, thereby increasing manufacturing cost [30]. Therefore, if only the PWC is used to solve contention in OS node, it can reduce the cost of the implementation. We refer to this architecture as PWC-only.

In this chapter, the architecture of PWC-only is presented first. Thereafter, a novel analytical model based on Markov chain analysis is contributed. Lastly, numerical results show that this novel model can provide better performance prediction than existing analytical models.

The theoretical analysis in this Chapter and in the following Chapters are also applicable to general data size distribution. For more details, please refer to the **Appendix**.

2.1 Architecture of PWC-only model and related work

Assume there are K wavelengths within one fiber. We number the wavelengths within one fiber from 0 to K-1. For the architecture of PWC, without

loss of generality, we assume that an optical data arriving on input wavelength k can only be converted to a wavelength m by the PWC.

$$m \in \Omega(k) \triangleq \{k \bmod K \mid k - d_1 \leq m \leq k + d_2\}, \ d_1, d_2 \geq 0 \qquad (2.1)$$

This means that an input optical data may be converted to an output wavelength range $S = d_1 + d_2 + 1$, where $S \leq K$. When $S = K$, PWC will become CWC. The modulation used in (2.1) means the conversion range of the PWC will wrap around when the conversion range reaches the edge of wavelength index (i.e., 0 or *K-1*).
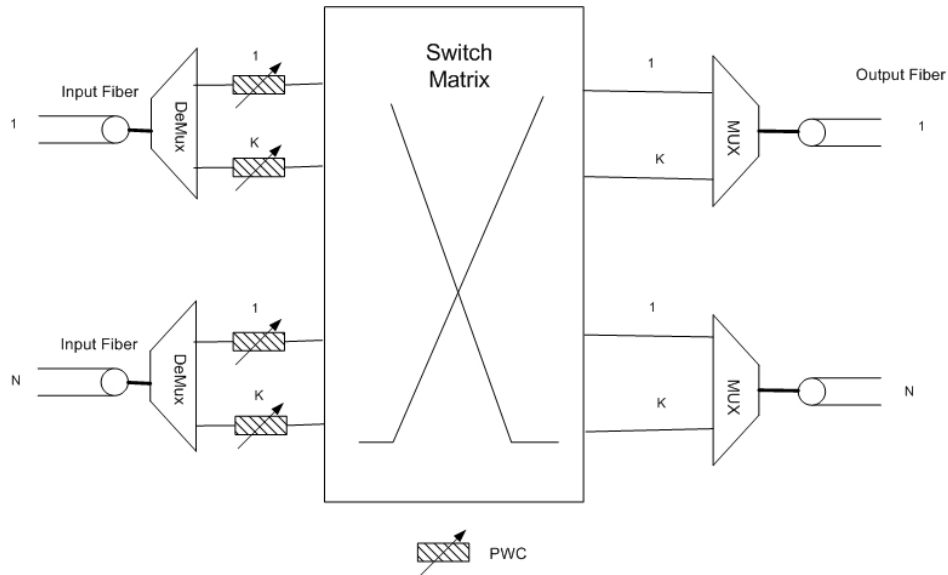
Figure 2-1:   OS switch and conversion architecture of PWC-only.

Figure 2-1 illustrates an OS node architecture with PWCs, termed as PWC-only. In PWC-only architecture, every input wavelength has one associated PWC. This is because PWC is a single-input multi-output wavelength converter device (hence inexpensive), so that PWC cannot be shared by several different input wavelengths and PWC cannot be put at the outside of the switch.

A conventional cross-bar switching fabric is assumed. Other more efficient switching fabrics are also possible but are beyond the scope of work presented here. In the context of this thesis, it is assumed that the cross-bar switch is used for the OS node.

The PWC contribution in [79] predicts the drop performance in synchronous slotted OPS, and the contribution in [81] was to present theoretical drop performance of an OS network with asynchronous traffic, using PWCs with different conversion range. The contribution in [81] proposed a multi-dimensional Markov chain analysis, where the number of Markov states is 2^S. The method may result in intractable problem set and loose lower bound, when S is larger.

In this chapter, we concentrate on obtaining the drop performance of a single OS node using a new and different solution method. The new solution method does not require any restrictions on S since the solution method utilizes a simple one-dimensional Markov chain analysis with $K+1$ number of Markov states. Theoretical solution methods for both upper and lower bound drop performance of an OS node with PWC are presented. Numerical studies will also demonstrate that the new solution method provides a much tighter upper and lower bound on drop probability compared to the method presented in [81]. In fact, for the new solution method, the larger the S, the tighter the lower bound is to the actual drop performance.

2.2   Performance analysis of PWC-only architecture

In this thesis, the case of asynchronous Poisson traffic with variable optical data length is studied. We denote λ to be the arrival rate of optical data on the fiber, and μ be the service rate of each wavelength respectively. Therefore, the traffic

load on each wavelength is $\rho = \lambda/(K\mu)$. We assume that optical data arrives on each wavelength with equal probability, i.e., uniformly distributed amongst the wavelengths.

Theorem 2-1: The ErlangB formula based on *M/G/S/S* model gives an upper bound on the drop probability of the OS node with PWC-only architecture.

Proof:

For both the *M/G/S/S* and PWC-only OS node model, all arriving optical data can be converted to one of *S* output wavelengths. Specifically, in the *M/G/S/S* model, all input arrivals (irrespective of its input wavelength) must share a common range of *S* output wavelengths.

For the case of the PWC-only node, an arriving optical data also has *S* output wavelength choices, but this range of *S* wavelength choices is different with another arriving optical data that is of another input wavelength. Let us define $\Omega(k,t)$ as the set of output wavelengths, associated with PWC_k, in use at time *t*, and $0 \leq |\Omega(k,t)| \leq S$ as the number of these output wavelengths currently in use. If $|\Omega(k,t)| = S$ when an optical data arrives with input wavelength *n*, then this optical data is dropped. Now, it is clear that in PWC-only, $\Omega(k,t)$ is different from $\Omega(k',t)$, where *k'* represents another input wavelength. Hence when $|\Omega(k,t)| = S$, it does not necessarily mean that $|\Omega(k',t)| = S$. However, for the case of the *M/G/S/S* model, $\Omega(k,t)$ is exactly equal to $\Omega(k',t)$. Clearly, the drop probability of the PWC-only node cannot be higher than the *M/G/S/S* model. Hence the *M/G/S/S* model gives an upper bound on drop probability of the PWC-only.

End proof

In the following, we will present a simple one-dimensional Markov chain analysis, comparing with a multi-dimensional Markov chain analysis in [81], to obtain the drop performance of PWC. Let us define the one-dimensional state i to mean there are i wavelengths in use by optical data, and P_i as the state probability.

Theorem 2-2: The state probability can be obtained from the following simultaneous equations

$$\begin{cases} P_{i+1} = \dfrac{\lambda(1-\alpha_i)}{(i+1)\mu} P_i \quad , \quad 0 \le i \le K \\ \displaystyle\sum_{i=0}^{K} P_i = 1 \end{cases} \tag{2.2}$$

where α_i is an important parameter to be explained in the following.

Proof:
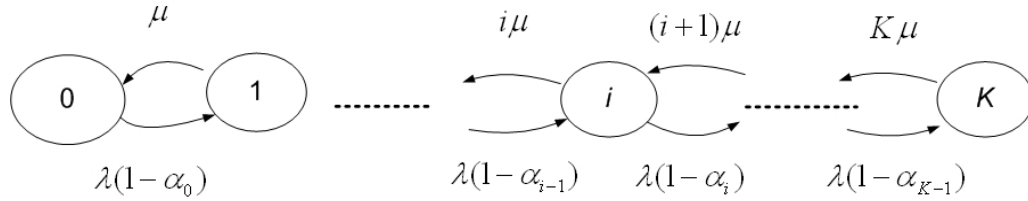
Figure 2-2:   Markov chain state transition diagram

Firstly, the one-dimensional Markov state transition diagram for solving P_i is illustrated in Figure 2-2. In Figure 2-2, α_i is an important probability measure representing the probability that for an input optical data arrival, say at a certain PWC, all the associated S consecutive output wavelengths of that PWC are already in use. The probability α_i is also evaluated at state i. Hence the probability $1-\alpha_i$ is the probability that for an optical data's arrival, say at a certain PWC, there is at

least an available wavelength amongst the associated S consecutive output wavelengths associated with that PWC. Accordingly, the new arrival can be converted to any available wavelength and accepted. Hence, based on Figure 2-2, the state probabilities P_i can be easily obtained by solving the stable state equations in (2.2).

End proof

The result in above **Theorem 2-2** is also applicable to general data size distribution. Please refer to the **Appendix**.

Corollary 2-1: By solving (2.2), the drop probability of the OS node with PWCs can be evaluated by (2.3).

$$P_{drop} = \sum_{i=0}^{K} \alpha_i P_i \qquad (2.3)$$

Approximation for α_i: In state i, there are i wavelengths in use, out of a total of K wavelengths. It is assumed that when a new optical data arrives, the optical data is uniformly filled amongst all of its K - i available wavelengths. This is not true for the real system as will be demonstrated later. The use of this assumption allows us to evaluate α_i easily as follows:

$$\alpha_i = \frac{i}{K} \times \frac{i-1}{K-1} \times ... \times \frac{i-(S-1)}{K-(S-1)} = \prod_{q=0}^{S-1} \frac{i-q}{K-q} \ , \ 0 \leq i \leq K \qquad (2.4)$$

The first term in (2.4), i.e., i/K, represents the probability that the first output wavelength of the PWC is occupied. The second term, i.e., $(i-1)/(K-1)$, represents the probability that the next consecutive output wavelength of the PWC is also occupied.

The α_i probability is complete once all the probabilities for wavelength occupation in all the consecutive output wavelengths in the associated S range of the PWC are included. It is also noted in (2.4) that $\alpha_i = 0$ for all $i < S$. Now the following theorem is important:

Theorem 2-3 : The use of α_i in (2.4) to obtain the drop probability P_{drop} via (2.2) and (2.3) will result in a lower bound to the actual drop probability of the OS node. In other words, the actual α_i is larger than the α_i given in (2.4).

Proof:

This is due to the inherent property of PWC where the conversion range is limited. Consequently, available wavelengths next to filled wavelengths will have a higher probability to be filled by new arrivals compared to available wavelengths situated in an area where there are also many available wavelengths. This means that when a wavelength is filled, the available wavelengths next to the filled wavelength have a higher probability of being filled, compared to other unfilled wavelengths far from these filled wavelengths.

A simple example as illustrated in Figure 2-3 is now presented, where $S = 2$ ($d_1 = 0, d_2 = 1$), and $K = 4$. It is noted in the figure that currently, wavelength 0 (W0) is in use. Because of uniform distribution of new arrival optical data amongst K wavelengths, it is noted that the probability that the next arrival will be filled in W1 will be higher than the probability that the arrival will be filled in W2 or in W3. The reason being that arrivals with input W0 and W1 will be filled in W1 so that W1 is twice more likely to be filled compared to W2 and W3. We refer to this phenomenon as the "***grouping tendency***".

The same grouping tendency can also be seen for any other combination of S and K. The grouping tendency makes the wavelengths in use group together rather than uniformly distributed. For the case α_i in (2.4), uniform filling distribution is assumed. Hence there is no grouping tendency phenomenon in the assumption, which will clearly result in a lower α_i, and lower drop probability. This is because the following reason. α_i makes the data be dropped even though there is resource (i.e., empty wavelength), so that the whole system becomes a non-conservative system. A lower α_i will lead the whole system become a less conservative system. For example when α_i=0, the whole system will become a M/G/K/K, which is a conservative system. It is well-known that the performance of a more conservative system is always better than the less conservative one. Thus the smaller α leads to lower drop probability.

End proof.
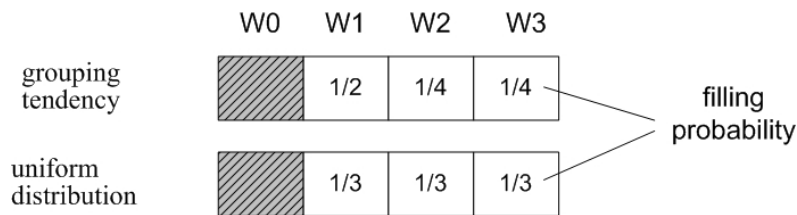
Figure 2-3:   Grouping tendency example

Theorem 2-4 : As S approaches K (or K approaches S), the approximation of α_i in (2.4) becomes more accurate.

Proof:

As *S* approaches *K*, the grouping tendency will become weaker and weaker since the range of output wavelengths for the PWC increases. If we consider the limit $S = K$, grouping tendency is totally eliminated in the real system since it is clear that any available wavelength will now have exactly the same probability of being used by a new arrival. When $S = K$, α_i ($i<K$) in (2.4) will always be zero, which means the Markov chain transition diagram in Figure 2-2 is the same as *M/M/K/K* model.

End proof.

2.3   Numerical results of PWC-only

In this section, we compare the numerical results obtained through theoretical means for comparison with actual simulation. The theoretical results include: (a) the *M/G/S/S* upper bound, henceforth denoted as UpperB; (b) the new lower bound obtained by equations (2.2), (2.3), (2.4) and henceforth referred to as LowerB; (c) the lower bound obtained by the multi-dimensional method proposed in [81] and henceforth referred to as MLowerB [1]. In addition, we use Gaussian, Fixed and Exponential data size distribution to simulate, and they all generate same drop performance as stated in the **Appendix**. In order to simplify the results shown in the following figures, only "Sim" legend is used to represent the simulation results for all these three size distributions.

---

[1] The contribution in [81] presented numerical results for an OS network, but not for a single OS node. The single node MLowerB results illustrated here are obtained with the best effort of the authors and after several email consultations with MLowerB authors, who also agree with our comments and results.
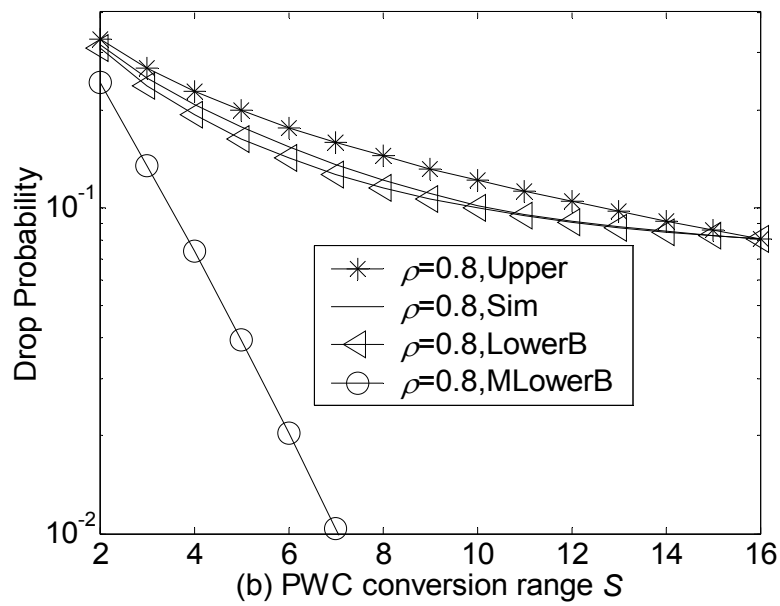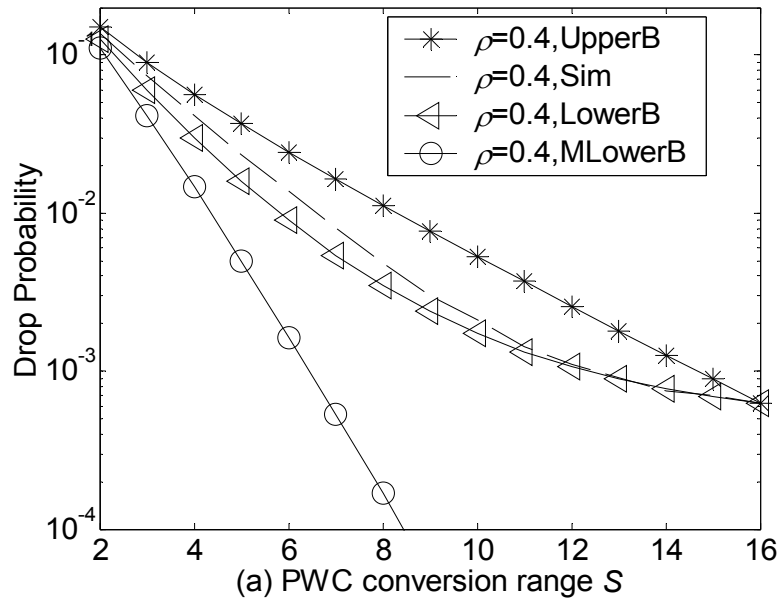
Figure 2-4:   Drop probability vs. range of PWC S, for simulation and different theoretical values, with $K = 16$,(a) $\rho = 0.4$, (b) $\rho = 0.8$.

Figure 2-4 illustrates the drop probabilities vs. range of PWC when $K=16$, $\rho = 0.8, 0.4$. It can be seen that both the UpperB and LowerB results are very close to the simulation results. The MLowerB results, although a lower bound, deviate

significantly from simulation. This is because in the analysis of MLowerB results, the formulation had to assume independence in the analysis for each PWC. Due to the fact that each PWC's conversion range will overlap with the conversion range of its neighboring PWCs, the independence assumption is inaccurate. Thus when S increases, the degree of correlation between neighboring PWCs becomes higher. It is therefore expected that in Figure 2-4, the MLowerB results deviates more from the simulated results as S increases. In contrast, the new LowerB results get closer to the simulated results as S increases, as illustrated in Figure 2-4. This is expected from **Theorem 2-4**. In addition, it is observed that when S is large enough, i.e., S=15, the drop performance of the PWC-only node become similar to FWC (when S=16, PWC is CWC). This means that when the range of a PWC is close to the range of a CWC, the performance of the PWC-only node will approach that of a FWC node. Therefore, although PWC is cheap to be implemented in OS node, the higher conversion range requirements for desirable performance makes it impractical.

(a) Number of Wavelengths K
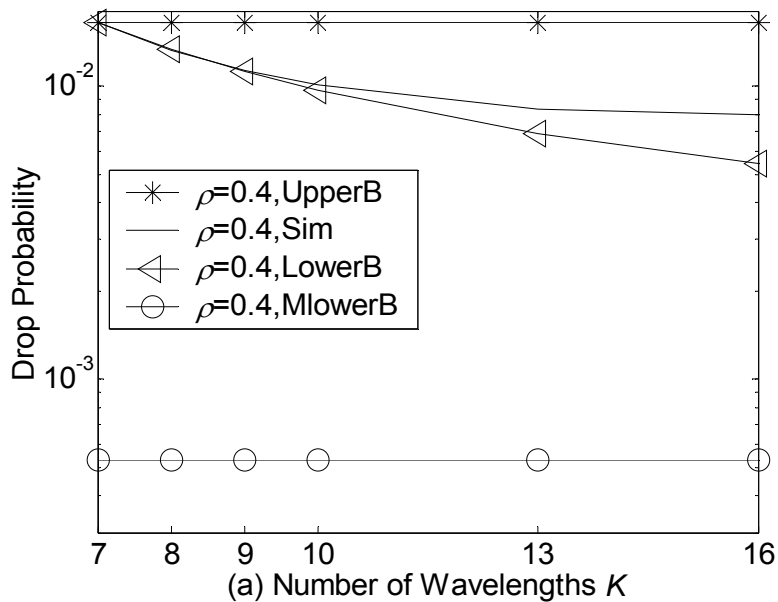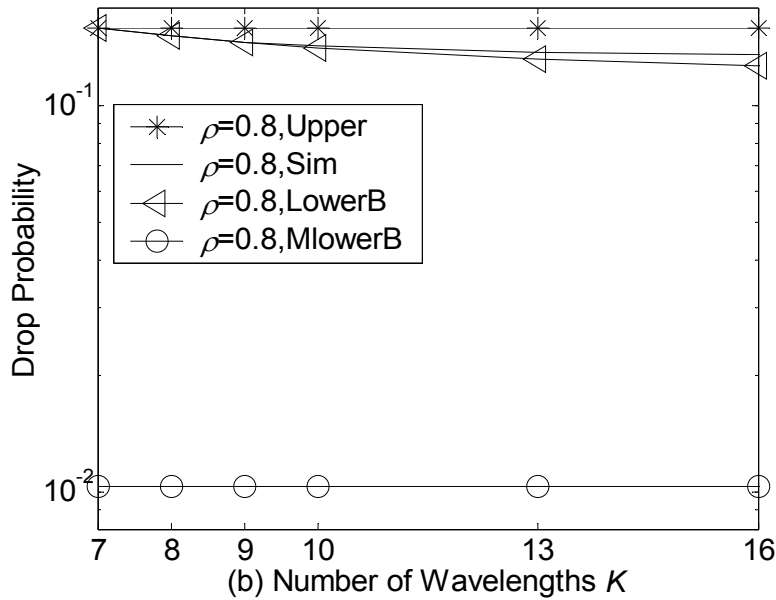
Figure 2-5:   Drop probability vs. number of wavelength for *S*=7 (a) $\rho = 0.4$, (b) ρ =0.8.

Figure 2-5 illustrates the drop probability results of the OS node with fixed load and *S* (=7), but varying *K* (from 7 to 16). When *K* is larger, i.e., *S* is far away from *K*, it is noted that the LowerB results deviate from the simulation results. But when *K* approaches *S*, i.e., $K \rightarrow S$, it is noted that the simulation results and LowerB results converge. This is expected in view of *Theorem 2-4*. Figure 2-5 also demonstrates that both UpperB and MlowerB do not vary according to *K*, since their formulations do not consider *K*. It is clear from Figure 2-5 that the MLowerB result is a significantly looser bound compared to the LowerB result.

2.4   Summary

In this chapter, a novel one-dimensional Markov chain analytical model was contributed for the PWC-only architecture. From this model, both lower and upper

bounds of performance of the system can be obtained. Simulation results show that the contributed bounds provide very close approximation.

However, it is found that the PWC-only architecture, as one of NFWC, is not a suitable architecture for achieving similar performance as a FWC node. This is because the PWC-only architecture can achieve desirable performance only when the range of the PWC is close to CWC ($S \approx K$). This makes the costs of the PWC-only architecture roughly similar to FWC architecture with dedicated CWC as shown in Figure 1-4.

Therefore, we will now consider using a limited number of complete wavelength converter (CWC) to achieve similar performance as FWC. As stated before, when using CWC, a sharing mode for pooling a limited number of CWCs has to be defined. In the next chapter, the architectures of using a limited number of CWCs by share-per-fiber and share-per-node are analyzed.

3   Architecture and Modeling of Complete Wavelength Converter

3.1   Introduction

From chapter 2, it is demonstrated that the PWC-only architecture is not suitable for achieving similar drop performance as the FWC. Therefore, in this chapter, we will consider the use of a limited number of complete wavelength converter (CWC), which can convert an input wavelength to a full range of output wavelength used in one fiber, for achieving similar drop performance as the FWC.

When a limited number of CWCs is used, some form of sharing policy must be implemented as well. The sharing mode can be share-per-fiber (SPF), where every output fiber has its own pool of CWCs only for use by wavelengths belonging to that output fiber. Alternatively, the sharing mode can be share-per-node (SPN), where all CWCs in the optical node are pooled together for use by any output wavelength belonging to any output fiber in the node. In this thesis, the former architecture will be referred to as CWC-SPF and the latter as CWC-SPN

So far, mathematical methods to evaluate the minimum number of CWCs required for a **synchronous slotted** optical packet network operating with CWC-SPF and CWC-SPN [77][78] architecture have been contributed. Through theoretical analysis and simulations, Eramo [77][78] showed that both CWC-SPN and CWC-SPF can achieve similar drop performance with FWC. The "*minimum number of CWCs*" is defined to be that number of CWCs required so that the drop performance of a CWC-SPF or a CWC-SPN node is similar to the drop performance

of a FWC node. Eramo showed that both CWC-SPF and CWC-SPN architecture can save cost of WC, while CWC-SPN saves more than CWC-SPF because of better sharing efficiency. Eramo's analysis and results can also be extended to synchronous slotted OBS, because the issue of wavelength conversion in OBS is the same as synchronous slotted OPS.

However, there is currently little or no theoretical analysis for the performance evaluation of CWC-SPF/SPN in the case of **asynchronous** traffic in OS network. In this thesis, the case of asynchronous Poisson traffic with variable optical data length is studied. New mathematical analyses, modeled upon a Markov chain, are presented to evaluate the performance of an OS node employing a limited number of CWCs. The wavelength converter savings of CWC-SPF/SPN are studied as well.

This chapter is organized as follows. In section 3.2, we analyze the performance of CWC-SPF by two-dimensional Markov chain, and numerical results by both simulation and theoretical calculations are demonstrated for CWC-SPF as well. In section 3.3, we present the analysis of CWC-SPN by multi-dimensional Markov chain, and then we contribute a set of methods to simplify the multi-dimensional Markov chain to multi-plane Markov chain by Randomized States, Self-Constrain Iteration and Sliding-window update. Section 3.3 demonstrates numerical results by both simulation and theoretical calculations for CWC-SPN as well. Finally in section 3.4, we summarize the results.

3.2 Architecture and analysis of CWC-SPF

3.2.1 Architecture of CWC-SPF

The architecture of CWC-SPF is shown in Figure 3-1. There are M CWCs shared by each output fiber with K wavelengths. If a new optical input needs to use a CWC to convert itself to another wavelength on this output fiber, one available CWC will be assigned to this new optical input. If the data input doesn't need to convert wavelength, it can be switched to one of K output ports to the output fiber. A conventional cross-bar switching fabric is assumed here.
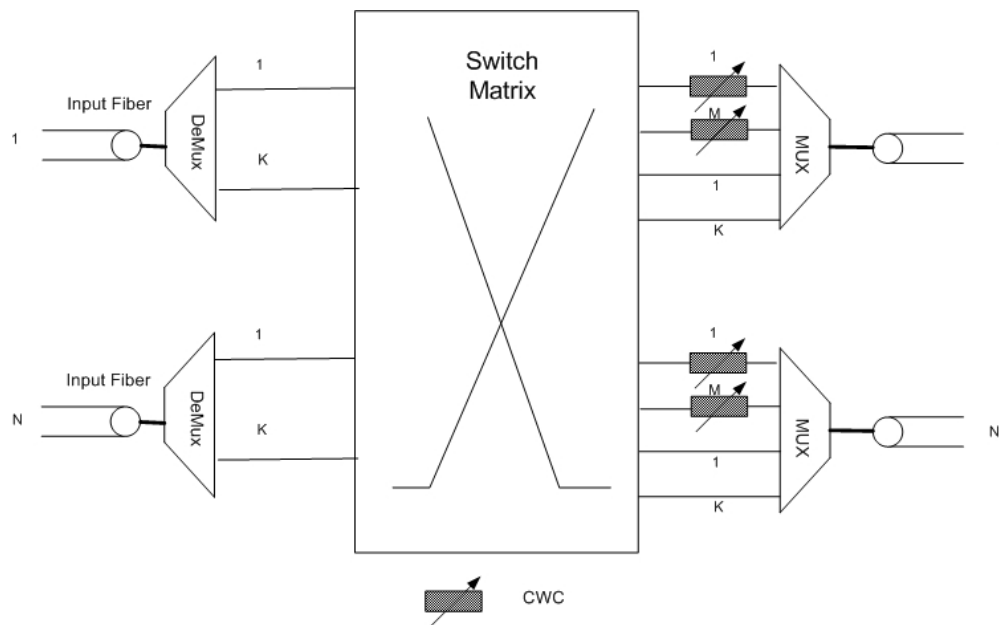
Figure 3-1:   Switch and conversion architecture of CWC-SPF.

3.2.2 Cost function of CWC-SPF

As stated in section 1.4, in this thesis we use linear cost model to gauge the cost of the WC, which means the cost of WC is linearly proportional to its conversion range. For CWC its conversion range is the number of wavelengths

within one fiber, i.e., *K*. Accordingly, the WC cost of FWC and CWC-SPF can be expressed in (3.1) and (3.2) respectively. The switch cost of the CWC-SPF architecture can be expressed in (3.3)

$$WcCost_{FWC} = K \times K \qquad\qquad (3.1)$$

$$WcCost_{CWC-SPF} = K \times M \qquad\qquad (3.2)$$

$$SwCost_{CWC-SPF} = NK \times (NK + NM) \qquad\qquad (3.3)$$
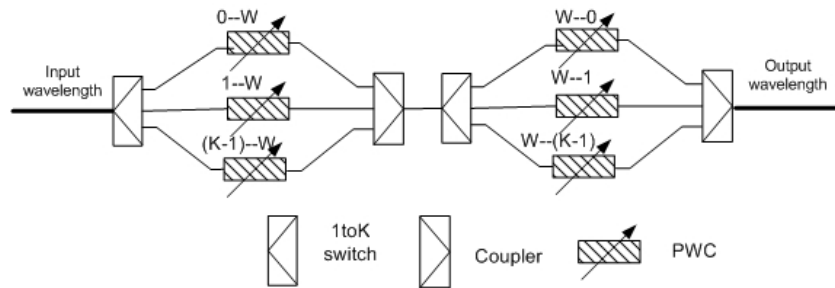
Figure 3-2   A possible two-stage CWC structure using concatenated PWCs.

This linear cost model is a conservative cost increase model since practical CWCs are constructed via the concatenation of many PWCs with the help of optical switches. The direct manufacture of CWCs without the use of concatenated PWCs is also impractical. It is thus expected that the cost increase per additional wavelength range is more severe than a linear model [79]. For example, Figure 3-2 illustrates a CWC structure that is constructed using two PWC stages. Noting that there are *2K* PWCs and a system of optical cross-connects, the cost of this CWC example is expected to be more than *2K*. The first stage converts any input optical signal to a common wavelength *W* and the second stage converts *W* to any output wavelength, and it is assumed in this example that each PWC can only convert one input to one output. The linear cost model, for simplicity, will conservatively assume that the

cost of a CWC is K, which is less than half the cost of the CWC example in Figure 3-2.

3.2.3 Analysis of CWC-SPF

In this section, we will analyze the performance of one particular output fiber, because all output fibers are independent in terms of switch structure and traffic input. Thus, the overall performance of the OS node can be obtained via simple combination of each output fiber.

We denote λ and μ to be the arrival rate of optical data on the output fiber and the service rate of each wavelength. Therefore, the traffic load on each wavelength is $\rho = \lambda/(K\mu)$. The two-dimensional state (i,j) indicates that there are i wavelengths in use by optical data in the output fiber, and j CWCs in use by some of these i wavelengths at the same time. It is clear that $0 \le j \le i \le K$ and $j \le M < K$. We now determine the state probability $P_{i,j}$ of the state (i,j). The state probabilities $P_{i,j}$ provide the elementary building blocks to obtain all other probability measures related to the overall performance of the CWC-SPF architecture, for example the overall drop probability (see *Corollary 3-3*). We now present the analysis for determining $P_{i,j}$

Theorem 3-1: the state probability $P_{i,j}$ (for all valid states $0 \le j \le i \le K$ and $j \le M$) can be obtained from the following simultaneous equations

$$\begin{cases} (A_{i,j} + B_{i,j} + C_{i,j} + D_{i,j})P_{i,j} = \\ A_{i-1,j}P_{i-1,j} + B_{i-1,j-1}P_{i-1,j-1} + C_{i+1,j}P_{i+1,j} + D_{i+1,j+1}P_{i+1,j+1} \\ \sum_{i,j} P_{i,j} = 1 \quad \text{(for all } 0 \le j \le i \le K \text{ and } j \le M < K) \end{cases} \qquad (3.4)$$

where $A_{i,j}$, $B_{i,j}$, $C_{i,j}$ and $D_{i,j}$ are transition speeds for various scenarios to be described later.

Proof:

In Markov chain analysis, the state transition probability in/out of each valid state is required. To simplify our analysis, we will only present the transition which is outgoing from state (i, j), since any incoming transition is also an outgoing transition from some other state (i', j').

Case 1: (i, j) to $(i+1, j)$, for $i+1 \leq K$. This scenario indicates that the wavelength of the incoming optical data can be scheduled on an available wavelength of the output fiber. The incoming optical data does not require any CWC to find a suitable output wavelength. Thus the input wavelength of the new optical data must correspond to one of the currently unused $(K-i)$ wavelengths in the output fiber. Thus, the transition speed is $A_{i,j} = (K-i)\lambda / K$.

Case 2: (i, j) to $(i+1, j+1)$, for $i+1 \leq K$ and $j+1 \leq M$. This case indicates that the wavelength of the incoming optical data corresponds to one of the i wavelengths currently in use. Thus, the optical data has to use one CWC to find a suitable output wavelength. Thus, the transition speed is $B_{i,j} = i\lambda / K$.

Case 3: (i, j) to $(i-1, j)$, for $i-1 \geq 0$ and $i > j$. This case indicates that an optical data not using any CWC has just been sent out completely. As there are $i-j$ optical data not using CWCs, the transition speed is therefore $C_{i,j} = (i-j)\mu$.

Case 4: (i, j) to $(i-1, j-1)$, for $i-1 \geq 0$ and $j-1 \geq 0$. This case indicates that a optical data using one CWC has just been sent out completely. As there are j optical data using CWCs, the transition speed is therefore $D_{i,j} = j\mu$.

From the description of the four transition cases, the state transition for state (i, j) is shown in the Figure 3-3(a). It can be seen that there are at most eight transitions in/out of the state (i, j). Including the fact that the sum of all state probabilities is equal to unity, the simultaneous equations in (3.4) are valid. The entire state transition is shown on Figure 3-3(b), which is a trapezium.

End Proof.

The result in above analysis is also applicable to general data size distribution. Please refer to the **Appendix**.

(a)

(b)
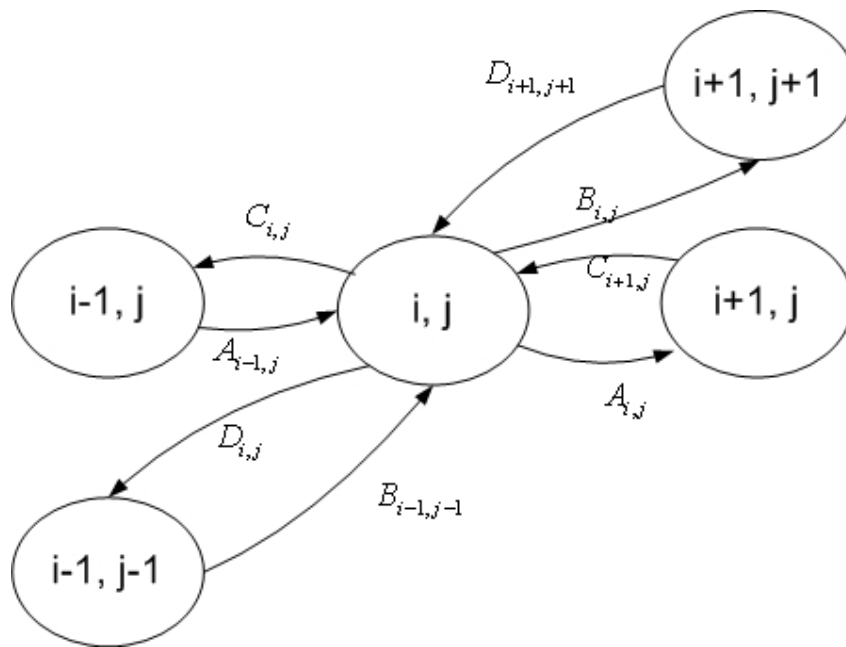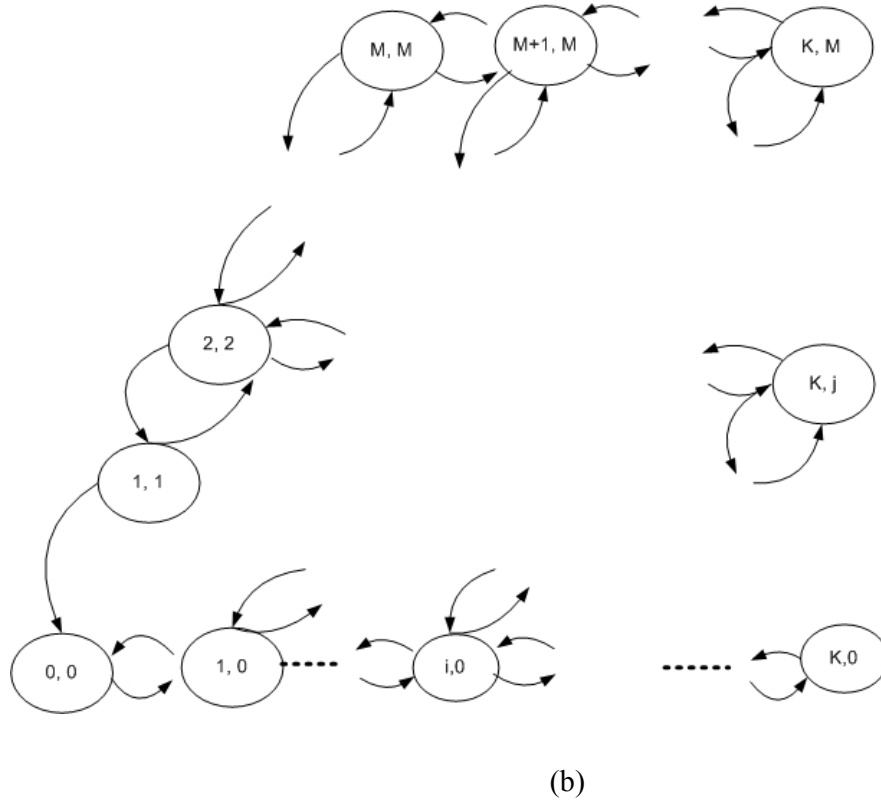
Figure 3-3:   Markov chain state transition diagram of CWC-SPF. (a) State transition for state (i, j). (b) Entire state transition diagram

Corollary 3-1 The number of states in the simultaneous equations of (3.4) is

$$V = (2K - M + 2)(M + 1)/2.$$

This is because the state transition diagram in Figure 3-3(b) is a trapezium. The number of states in the bottom row is $K+1$, and the number of rows in Figure 3-3(b) is $M+1$. The difference in the number of states between neighboring rows is one. Therefore, it can be verified that the number of overall states is

$$V = (2K - M + 2)(M + 1)/2.$$

Corollary 3-2 The simultaneous equations in (3.4) are solvable.

Proof:

There are V state equations (one equation per state) and an additional sum-to-unity equation in (3.4). Noting that for Markov transition diagram, there is always one redundant state equation in (3.4), which (any one) can be deleted. Therefore, combining with the unity equation, there are enough equations to solve for the state probabilities $P_{i,j}$.

End proof

Corollary 3-3: From state probabilities $P_{i,j}$, many useful parameters can be obtained as follows.

We denote random variable W as the number of CWCs being used. Thus the tail distribution function of used CWCs, $f(w)$, can be written as (3.5) and drop probability as (3.6)

$$f(w) = \Pr\{W \geq w\} = \sum_{i,j \geq w} P_{i,j} \tag{3.5}$$

$$P_{Drop} = \sum_{i=M}^{K-1} \frac{i}{K} P_{i,M} + \sum_{j=0}^{M} P_{K,j} \tag{3.6}$$

In (3.6), the first term on the right side is the drop probability due to lack of CWC. For this probability, we have to consider those new optical data arrivals whose wavelength corresponds to one of the i wavelengths currently in use. This explains the i/K factor. The second term is the drop probability due to lack of available output wavelength

3.2.4 Numerical results of CWC-SPF

In this section, we compare the theoretical results obtained by simultaneously solving (3.4) (using Matlab software) with numerical results obtained through simulation. The numerical simulations include optical data with distributions that are Exponential, Gaussian and Fixed. Figure 3-4 illustrates the theoretical value of the tail distribution function $f(w)$ [see (3.5)] for different number of CWCs M, and for $K=16$ and $\rho = 0.8$. The simulation results obtained for Exponential, Gaussian and Fixed optical data size distribution are the same. The results clearly show that the CWC-SPF analytical model is in agreement with the simulation results. The function $f(w)$ decreases faster than exponentially with increasing w. Thereby, after a certain point, the usage probability of these CWC are negligible. This means it is not necessary to provide the ideal number of wavelength converters for the CWC-SPF model. After some point as illustrated in Figure 3-5 (see later), a limited number of CWCs is able to achieve almost identical performance compared to having an ideal number of wavelength converters.
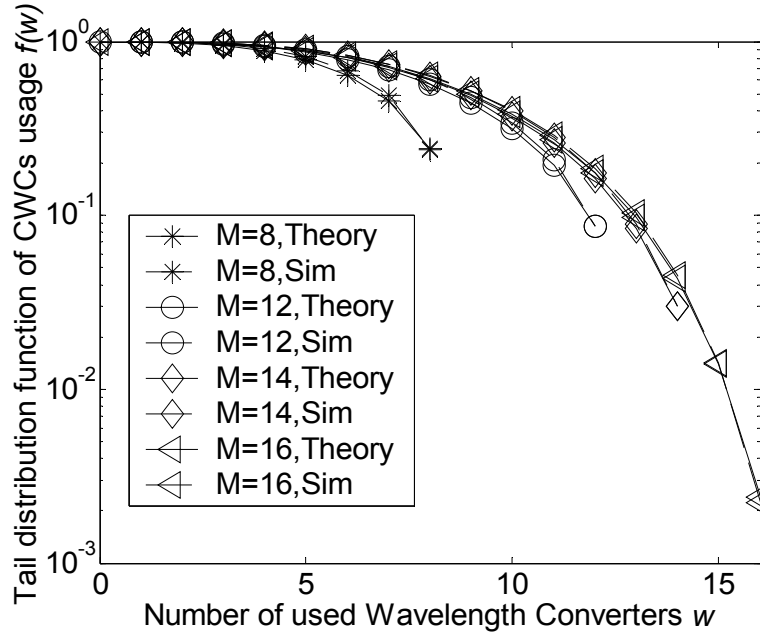
Figure 3-4:   Tail distribution function of CWC-SPF with different number of CWCs. Both theoretical and simulation values are plotted with Gaussian, Exp, Fix optical data size distributions with $K = 16$, $\rho = 0.8$, $M = 8, 12, 16$.

Figure 3-5 illustrates the drop probability vs. M, for $K=16$ and for $\rho = 0.4, 0.8$. Similar to Figure 3-4, the simulation results apply also for Exponential, Gaussian, and Fixed optical data size distribution. Similar to Figure 3-4, the simulation results verify the theoretical results obtained from **Theorem 3-1**. It is also noted when M increases, the drop probability decreases dramatically. After certain point, the drop probability decreases very slowly and then levels out. The leveling of the drop probability indicates that after some point, operating with a limited number of CWCs gives similar drop probability performance with operating with an ideal number of CWCs. This is due to the effect of statistical multiplexing for both wavelength and CWCs in the CWC-SPF architecture.
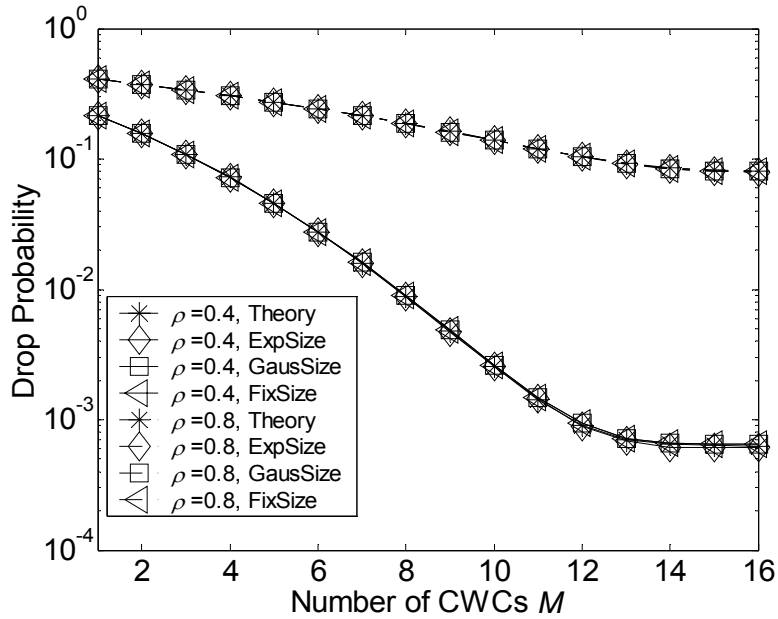
Figure 3-5:   CWC-SPF drop probability vs. number of WCs. Both simulation and theory results are plotted with different data size distributions for $K = 16$, $\rho = 0.4$, 0.8.

From Figure 3-4 and Figure 3-5, we can conclude that the theoretical analysis presented in section 3.2.3 is accurate and can predict the drop probability of CWC-SPF without deviation. Therefore, in the following figures, only theoretical analysis results will be presented. In addition, it is noted that all simulations with different data size distributions give same results, which are stated in **Appendix**. Therefore, in order to simplify the presentation of the results, in the rest of the thesis, we won't compare the simulation results of different size distributions, although the remaining simulation results in the thesis are run under different size distributions and they all gave same results as well.

As mentioned earlier, the CWC-SPF system, while being able to save wavelength converter cost, should ensure that its drop performance is also not compromised. In Figure 3-5, when the number of available CWCs, i.e., M increases,

the drop probability of the system decreases and slowly approaches to that of a FWC system. This demonstrates that the blocking performance of the CWC-SPF system will approach that of a FWC system monotonically. However, the performance of CWC-SPF only approaches the performance of FWC asymptotically. It will not exactly achieve same performance as FWC. Therefore, a target performance threshold of the drop probability is set to be achieved by the CWC-SPF. Therefore, if $P_{CWC-SPFdrop} / P_{FWCdrop} \leq \xi$, where $\xi > 1$ is a user-defined performance threshold, we consider the performance of CWC-SPF similar to that of FWC. The performance threshold adopted throughout in this thesis is $\xi = 1.2$. It should be noted that $P_{FWCdrop}$ can be obtained from the *M/G/K/K* or ErlangB formula.

We can see that $P_{CWC-SPFdrop,M}$ will monotonically decrease with increasing of *M*. Therefore, there must be a $\overline{M}_{CWC-SPF}$ to be the minimum number of CWCs required for the CWC-SPF architecture such that the performance threshold requirement is satisfied, i.e

$$\overline{M}_{CWC-SPF} = \min\{M \mid P_{CWC-SPFdrop,M} / P_{FWCdrop} \leq \xi\} \tag{3.7}$$

Accordingly, the minimum WC cost and minimum switch cost of CWC-SPF can be expressed as

$$\min WcCost_{CWC-SPF} = K \times \overline{M}_{CWC-SPF} \tag{3.8}$$

$$\min SwCost_{CWC-SPF} = NK \times (NK + N\overline{M}_{CWC-SPF}) \tag{3.9}$$

The saving of WC of CWC-SPF against FWC $\theta_1^{CWC-SPF}$ can be expressed as

$$\theta_1^{CWC-SPF} = (1 - \frac{\min WcCost_{CWC-SPF}}{WcCost_{FWC}}) \times 100\% \tag{3.10}$$

Figure 3-6 shows the saving of WC against FWC $\theta_1^{CWC-SPF}$ for both low load and high load, under different number of wavelengths. Figure 3-6 demonstrates that when load is low, the saving of WC is high and vice versa. The saving is around 12% to 20%, which is not a very high saving. This may be due to the low sharing efficiency of CWC-SPF architecture. The fluctuation of the saving curves is due to the integer value effect, since both the number of wavelengths and number of CWCs are integer values while the threshold drop probability is a real number. Thus when the threshold drop probability is achieved, the saving may fluctuate. Table 3-1 shows the number of saved WC corresponding to the Figure 3-6. From the table, we can find that the number of saved WC is non-increasing. In addition, because the integer value of both number of wavelengths and number of CWCs are relative small, the saving of WCs fluctuate.
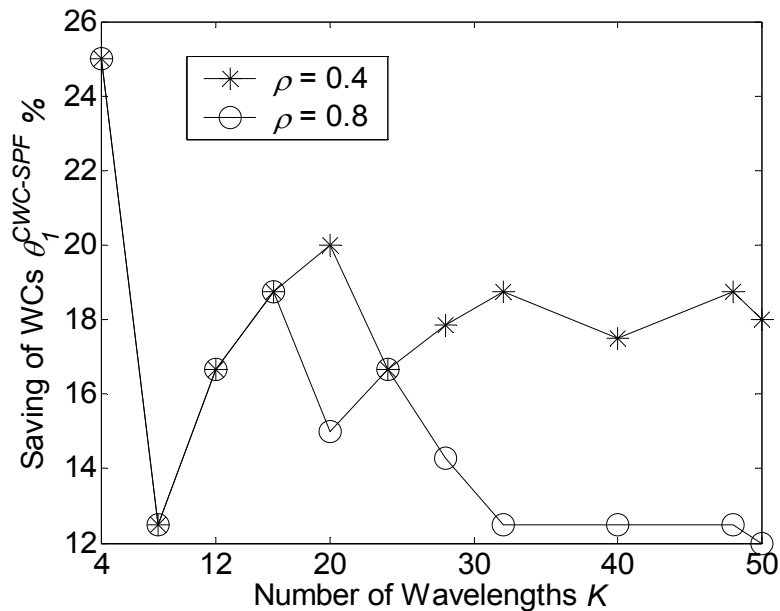
Figure 3-6: Saving of WC of CWC-SPF against FWC for different number of wavelengths under both low load and high load.

Table 3-1:   The number of saved WC in CWC-SPF.

No. of Wavelength	4	8	12	16	20	24	28	32	40	48	50
Saved WC at load=0.4	1	1	2	3	4	4	5	6	7	9	9
Saved WC at load=0.8	1	1	2	3	3	4	4	4	5	6	6

3.3   Architecture and analysis of CWC-SPN

3.3.1   Architecture of CWC-SPN
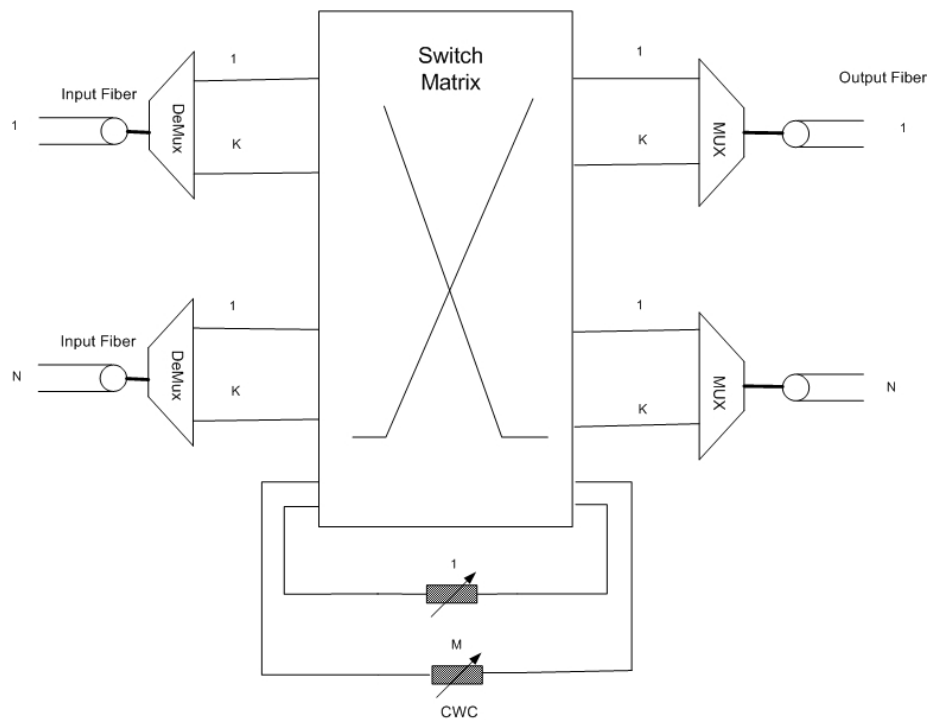
Figure 3-7:   Switch and conversion architecture of CWC-SPN

Consider the optical switch of CWC-SPN architecture in Figure 3-7. There are N input/output fibers, and each fiber supports K wavelength. All M WCs are

shared among all N output fibers in this OS node. SPN needs the support of a central switch matrix, whose switching capacity is $(NK+M)\times(NK+M)$. As stated before, in this thesis it is assumed that the crossbar structure is used. If a new optical input needs to use a CWC to convert itself to another wavelength on one output fiber, the data will be switched to CWC pool and one available CWC will be assigned to this new optical input. After conversion, the data will be switched back to the output fiber directly. If the data input does not need to convert wavelength, it can be switched to one of K output ports to the output fiber.

It is well known that for the case of ideal number of CWCs, M, is equal to the number of output wavelengths: $M=NK$; the CWC-SPN will become FWC, because there is enough number of CWC to convert any input wavelength to available output wavelength. In this architecture, for the case of limited CWCs, the scenarios $M<NK$ is now considered.

3.3.2 Cost function of CWC-SPN

As stated in section 3.2.2, we use linear cost function for CWC, i.e., cost proportional to its conversion range. Accordingly, the WC cost of CWC-SPN per fiber can be expressed in (3.11) (WC cost of FWC has been presented in (3.1)). Here, the reason why we use WC cost per fiber is that comparison between CWC-SPF and CWC-SPN can be made. The switch cost of the CWC-SPN architecture can be expressed in (3.12)

$$WcCost_{CWC-SPN} = K \times M / N \tag{3.11}$$

$$SwCost_{CWC-SPN} = (NK+M)\times(NK+M) \tag{3.12}$$

3.3.3 Theoretical analysis of CWC-SPN using multi-dimensional Markov chain

In this section, we will analyze the performance of each output fiber and the node for CWC-SPN. We denote λ_n as the optical data arrival rate of output fiber n ($1 \leq n \leq N$), so that the overall arrival rate at the node is $\lambda = \sum_n \lambda_n$, μ is the service rate of each wavelength. Therefore, the load on the output fiber n is $\rho_n = \lambda_n /(K\mu)$, and the overall load on the node is $\rho = \lambda /(KN\mu)$. For generality, we consider traffic as asymmetric, which means that the traffic intensity λ_n on every output fiber may be different. We also assume that optical data arrive on each wavelength with equal probability, i.e., uniformly distributed amongst the wavelengths. In this thesis, we do not consider deflection routing. That means once the data has been routed to an output fiber, it cannot be rerouted to any other output fiber even though it may be dropped due to contention.

We use (i_n, j_n) to indicate the state of the fiber n, where there are i_n wavelengths in use by optical data and j_n CWCs in use by some of these i_n wavelengths at the same time. It is clear that $0 \leq j_n \leq i_n \leq K$ and $j_n \leq \min(M,K)$. Thus, the state of a CWC-SPN architecture is defined by $(i_1 j_1 ... i_n j_n ... i_N j_N)$. We now proceed to determine the state probability $P_{i_1 j_1 ... i_n j_n ... i_N j_N}$ of the state $(i_1 j_1 ... i_n j_n ... i_N j_N)$. The state probabilities $P_{i_1 j_1 ... i_n j_n ... i_N j_N}$ provide the elementary building blocks to obtain all other probability measures related to the overall performance of the CWC-SPN

node, for example the overall drop probability. We now present the analysis for determining $P_{i_1 j_1 \ldots i_n j_n \ldots i_N j_N}$.

Theorem 3-2: the state probability $P_{i_1 j_1 \ldots i_n j_n \ldots i_N j_N}$ (for all valid states) can be obtained from the following simultaneous equations

$$
\begin{cases}
P_{i_1 j_1 \ldots i_n j_n \ldots i_N j_N} \times \sum_{n=1}^{N} (A_{i_n, j_n} + B_{i_n, j_n} + C_{i_n, j_n} + D_{i_n, j_n}) = \\
\sum_{n=1}^{N} \left\{ \begin{array}{l} A_{i_n-1, j_n} P_{i_1 j_1 \ldots (i_n-1) j_n \ldots i_N j_N} + B_{i_n-1, j_n-1} P_{i_1 j_1 \ldots (i_n-1),(j_n-1) \ldots i_N j_N} \\ + C_{i_n+1, j_n} P_{i_1 j_1 \ldots (i_n+1),(j_n-1) \ldots i_N j_N} + D_{i_n+1, j_n+1} P_{i_1 j_1 \ldots (i_n+1),(j_n+1) \ldots i_N j_N} \end{array} \right\} \\
\sum P_{i_1 j_1 \ldots i_n j_n \ldots i_N j_N} = 1 \quad (\text{for all } 0 \le j_n \le i_n \le K \text{ and } \sum_{n=1}^{N} j_n \le M)
\end{cases}
\tag{3.13}
$$

where A_{i_n, j_n}, B_{i_n, j_n}, C_{i_n, j_n} and D_{i_n, j_n} are transition speeds for various scenarios to be described later

Proof:

　　In Markov chain analysis, the state transition probability in/out of each valid state is required. To simplify our analysis, we will only present the transition which is outgoing from state $(i_1 j_1 \ldots i_n j_n \ldots i_N j_N)$, since any incoming transition is also an outgoing transition from some other state. It should be noticed that the transitions of this Markov chain only happen within a particular fiber state (no deflection routing), since the output fiber of any optical data is determined and cannot be changed.

　　Case 1: From $(i_1 j_1 \ldots i_n j_n \ldots i_N j_N)$ to $(i_1 j_1 \ldots (i_n+1) j_n \ldots i_N j_N)$, when $i_n + 1 \le K$ for all $n \in [1, N]$. This scenario indicates that the input data will be switched to the output fiber *n*, and that the wavelength of the incoming optical data can be scheduled on the corresponding available wavelength of the output fiber. The incoming data does not require any CWC to find a suitable output wavelength. Thus the

wavelength of the new optical data must correspond to one of the currently unused $(K - i_n)$ wavelengths. Therefore, the transition speed is $A_{i_n,j_n} = (K - i_n)\lambda_n / K$.

Case 2: From $(i_1 j_1 ... i_n j_n ... i_N j_N)$ to $(i_1 j_1 ...(i_n + 1)(j_n + 1)...i_N j_N)$, when $i_n + 1 \le K$ and $1 + \sum_{k=1}^{N} j_k \le M$ for all $n \in [1, N]$. This case indicates that the input data will be switched to the output fiber n, and that the wavelength of the incoming optical data corresponds to one of the i_n wavelengths currently in use. Thus, the optical data has to use one CWC to find a suitable output wavelength. Thus, the transition speed is $B_{i_n,j_n} = i_n \lambda_n / K$.

Case 3: From $(i_1 j_1 ... i_n j_n ... i_N j_N)$ to $(i_1 j_1 ...(i_n - 1) j_n ... i_N j_N)$, when $i_n - 1 \ge 0$ and $i_n > j_n$ for all $n \in [1, N]$. This case indicates that an optical data not using any CWC has just been sent out completely from the fiber n. As there are $i_n - j_n$ data not using CWCs, the transition speed is therefore $C_{i_n,j_n} = (i_n - j_n)\mu$.

Case 4: From $(i_1 j_1 ... i_n j_n ... i_N j_N)$ to $(i_1 j_1 ...(i_n - 1)(j_n - 1)...i_N j_N)$, when $i_n - 1 \ge 0$ and $j_n - 1 \ge 0$ for all $n \in [1, N]$. This case indicates that an optical data using one CWC has just been sent out completely from the fiber n. As there are j_n optical data using CWCs, the transition speed is therefore $D_{i_n,j_n} = j_n \mu$.

Based on these four scenarios and the fact that the sum of all state probabilities is equal to unity, simultaneous equations in (3.13) are obtained. It should be noticed if the transition conditions specified in any of the above scenarios are not satisfied, then the corresponding transition speeds A_{i_n,j_n} , B_{i_n,j_n} , C_{i_n,j_n} and D_{i_n,j_n} are zero.

End proof

From above analysis, it can be seen that the equation (3.13) is quite similar to (3.4), which is used to analyze the performance of CWC-SPF . Therefore, equation (3.13) also has some features that equation (3.4) owns.

Firstly, we will analyze the solvability of (3.13) by the number of variables and equations. For convenience, we define $V^{(N)}$ to be the total number of variables in the simultaneous equation (3.13), where the superscript (N) indicating the total number of fibers in the CWC-SPN node.

Corollary 3-4 : The number of variables $V^{(N)}$ in the simultaneous equations of (3.13) is

$$V^{(N)} \sim O(V^N) \sim O((K^2/2)^N) \tag{3.14}$$

where $V = (2K - \min(M,K) + 2)(\min(M,K)+1)/2$

Proof:

It is only valid to have a state $(i_1 j_1 ... i_n j_n ... i_N j_N)$ if $0 \le j_n \le i_n \le K$ and $\sum_{n=1}^{N} j_n \le M$ for all $n \in [1, N]$. For one particular fiber $n \in [1, N]$, the number of possible states is $V = (2K - \min(M,K) + 2)(\min(M,K)+1)/2$ (Please refer to ***Corollary 3-1***), therefore, for N fibers, the number of possible states is $O(V^N)$. This is just a rough estimation of the number of states, because the states among each fiber are not independent, so that the number of states will be less than $O(V^N)$. In addition, because of $V \sim O(K^2/2)$, the (3.14) can be obtained.

End proof

Corollary 3-5: The simultaneous equations in (3.13) are theoretically solvable, but in practice, they are numerically intractable

Proof

There are $V^{(N)}$ state equations (one equation representing one state) and an additional sum-to-unity equation in (3.13). Because of Markov chain properties, there is one redundant state equation in (3.13), which (any one) can be deleted. Therefore, combining with the sum-to-unity equation, the simultaneous equations are solvable, and therefore, the state probability $P_{i_1 j_1 \ldots i_n j_n \ldots i_N j_N}$ can be obtained theoretically.

However, the number of variables $V^{(N)}$ is too large for tractable calculations. When solving a set of linear simultaneous equations, a $V^{(N)} \times V^{(N)}$ matrix is typically required. If Gaussian elimination is used to solve the equations, then the computation complexity is $O((V^{(N)})^3)$. It is noted that such high space and running time requirement are not easy to be satisfied under current computer technology.

End proof

As the simultaneous equations (3.13) are numerically intractable, a method, called Randomized States (RS), for reducing the number of variables to be solved, will be presented. It should be noted that there is no loss in information in the use of the RS variable reduction technique. However, there is a trade-off in that prior knowledge of a probability distribution function needs to be known. How this probability distribution function is obtained will also be provided in a later section.

3.3.4 Analysis of CWC-SPN by multi-plane Markov chain using Randomized states method
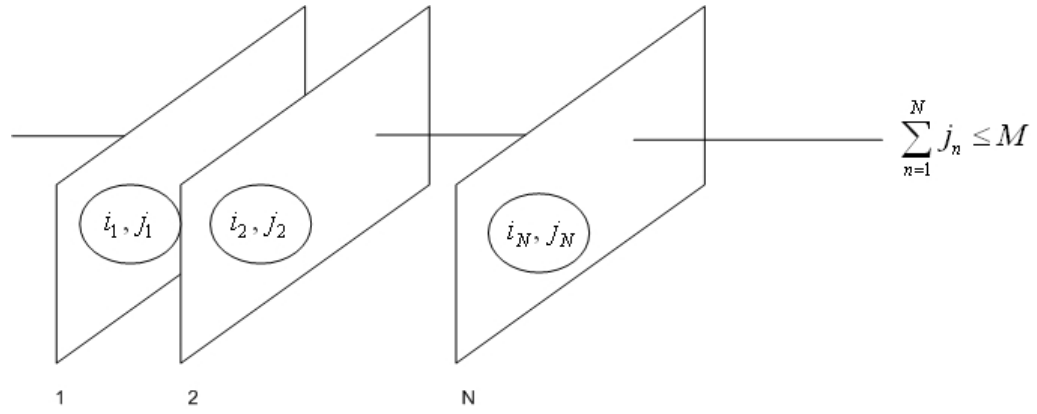
Figure 3-8:   Multi-plane state transition diagram for CWC-SPN

Figure 3-8 illustrates the concept of the Randomized states (RS) method. Each plane (i.e., flat surface) characterized by a two-dimensional (i_n, j_n) represents each output fiber in the CWC-SPN. Since there are N output fibers, there are correspondingly N of these planes. As before, i_n and j_n represent, respectively, the number of wavelengths and CWCs in use at the nth output fiber. Correspondingly, we define P_{i_n, j_n} to be the two-dimensional state probability for output fiber n. The following Theorem is now presented:

Theorem 3-3: As long as the behavior of the N planes in Figure 3-8, with respect to the constraint $\sum_{n=1}^{N} j_n \leq M$, is known in detail, solving for the multi-dimensional state probability $P_{i_1 j_1 \ldots i_n j_n \ldots i_N j_N}$, (as in **Theorem 3-2**), is equivalent to solving a series of two-dimensional Markov chain problems for P_{i_n, j_n} with no loss in information.

Proof

An important characteristic of OS scheduling is that once an optical data is scheduled on an output fiber, it is not possible for that scheduled optical data to be scheduled later onto another output fiber since this would affect the routing constraints of the optical data. This means that all CWC-SPN state transitions in an output fiber n occur independently of other output fibers. With respect to Figure 3-8, this means that a state transition, say in plane n (either due to a optical data arrival or departure in fiber n), is totally independent of state transitions in another plane n'. Thus, the CWC-SPN node can be viewed as a multi-plane system where each plane represents a two-dimensional Markov chain state system. Now the only connection among the N planes is the constraint on the number of used CWCs, i.e., $\sum_{n=1}^{N} j_n \leq M$.

The situation where this constraint applies is when there is a new optical data arrival and, it is necessary for this arrival to use a CWC. In other words, when there is transition from (i_n, j_n) to $(i_n + 1, j_n + 1)$, in any of the planes. This transition is valid provided $1 + \sum_{n=1}^{N} j_n \leq M$. Hence, as long as the behavior of the N planes with respect to this constraint, $\sum_{n=1}^{N} j_n \leq M$, is known in detail, solving the multi-dimensional state probability $P_{i_1 j_1 \ldots i_n j_n \ldots i_N j_N}$, as in **Theorem 3-2**, is equivalent to solving a series of two-dimensional Markov chain problems for P_{i_n, j_n}

End proof

The next Theorem provides details for solving P_{i_n, j_n}. For convenience, we first introduce the following notations:

W_n :   A random variable representing the number of CWCs currently in use at plane n (i.e., fiber n). It is clear that $0 \leq W_n \leq \min(K, M)$.

$\pi_n(t)$: Probability density function of W_n.

$$\pi_n(t) = \Pr(W_n = t) = \sum_{i_n} P_{i_n, j_n = t} \tag{3.15}$$

ϕ_n : The sum total of CWCs in use in the node but excluding those CWCs in use by plane n. Thus $\phi_n = \sum_{s \neq n} W_s$. As ϕ_n is the sum of several random variables W_s (where $s \neq n$), ϕ_n is a random variable itself that obeys some distribution.

$r_n(j_n)$: The probability that there is at least one CWC available, when currently there are j_n CWCs in use by fiber n. Hence,

$$r_n(j_n) = \Pr(\phi_n < M - j_n \,|\, W_n = j_n) \tag{3.16}$$

Now, with the assumption that $r_n(j_n)$ is known, the state equations for solving P_{i_n, j_n} is stated in the following theorem.

Theorem 3-4 : By virtue of the RS method, the state probability P_{i_n, j_n} (for all planes n) can be obtained from the following system of equations

$$\begin{cases} (A_{i_n, j_n} + B'_{i_n, j_n} + C_{i_n, j_n} + D_{i_n, j_n}) P_{i_n, j_n} = \\ A_{i_n-1, j_n} P_{i_n-1, j_n} + B'_{i_n-1, j_n-1} P_{i_n-1, j_n-1} + C_{i_n+1, j_n} P_{i_n+1, j_n} + D_{i_n+1, j_n+1} P_{i_n+1, j_n+1} \\ \sum_{i_n, j_n} P_{i_n, j_n} = 1 \quad \text{for each } n \in [1, N] \end{cases} \tag{3.17}$$

where A_{i_s, j_s}, B'_{i_s, j_s}, C_{i_s, j_s} and D_{i_s, j_s} are transition speeds for various scenarios to be described later

Proof

Similar to the previous analysis in **Theorem 3-1** and **Theorem 3-2**, for a particular plane *n*, there are four transition cases to consider for state $(i_n j_n)$. They are as follows:

Case 1: $(i_n j_n)$ to $((i_n+1), j_n)$, when $i_n + 1 \le K$. The transition speed is $A_{i_n, j_n} = (K - i_n)\lambda_n / K$.

Case 2: $(i_n j_n)$ to $((i_n+1),(j_n+1))$, when $i_n + 1 \le K$ and $j_n \le \min(M, K)$. It is noticed that the transition condition is no longer $1 + \sum_{k=1}^{N} j_k \le M$ (which is the case for **Theorem 3-2**). The transition speed is now $B'_{i_n, j_n} = r_n(j_n) i_n \lambda_n / K$.

Case 3: $(i_n j_n)$ to $((i_n-1), j_n)$, when $i_n - 1 \ge 0$ and $i_n > j_n$. The transition speed is $C_{i_n, j_n} = (i_n - j_n)\mu$.

Case 4: $(i_n j_n)$ to $((i_n-1),(j_n-1))$, when $i_n - 1 \ge 0$ and $j_n - 1 \ge 0$. The transition speed is $D_{i_n, j_n} = j_n \mu$.

It is noted that the difference between **Theorem 3-2** and **Theorem 3-4** is the case 2 transition. This is expected since as mentioned in the proof of **Theorem 3-3**, the only occasion where the *N* planes depend on each other is the transition from (i_n, j_n) to $(i_n + 1, j_n + 1)$.

End proof

The result in above analysis is also applicable to general data size distribution. Please refer to the **Appendix**.

Corollary 3-6 : The number of state probability equations $V_{RS}^{(N)}$ in (3.17) is given by:

$$V_{RS}^{(N)} = NV \tag{3.18}$$

Proof:

This is because the states of N planes are independent with each other by RS methods. Each plane has V number of variables so that overall number of states is NV.

End proof

Corollary 3-7 : The system of equations (3.17) is solvable theoretically, if $r_n(j_n)$ is available.

Proof:

For each plane, there are V state equations in (3.17), and for the Markov transition diagram, there is always one redundant state equation in (3.17), which (any one) can be deleted. However, there is one unity equation for every plane. Since there are $V_{RS}^{(N)}$ variables and also $V_{RS}^{(N)}$ equations, it is theoretically solvable.

End proof

Corollary 3-8: By solving for state probability P_{i_n,j_n} , many useful parameters can be obtained, as follows

$$P_{Drop,n} = \sum_{i_n \neq K,\ j_n} (1 - r_n(j_n)) i_n P_{i_n,j_n} / K + \sum_{j_n=0}^{\min(M,K)} P_{K,j_n} \tag{3.19}$$

In (3.19), the first term on the right side is the drop probability due to lack of CWC. We have to consider those new optical data arrivals whose wavelength corresponds to one of the i_n wavelengths currently in use. This explains the i_n / K factor in (3.19). The factor $(1 - r_n(j_n))$ indicates the probability that no available CWC when a new optical data arrives at fiber n. The second term represents the drop probability due to lack of available output wavelength. The overall drop probability of the node is thus

$$P_{Drop} = \sum_{n=1}^{N} (\lambda_n P_{Drop,n}) / \sum_{n=1}^{N} \lambda_n \qquad (3.20)$$

3.3.5   Estimation of probability $r_n(j_n)$

At this stage, the remaining hindrance to the RS method is the absence of knowledge on the explicit distribution function of $r_n(j_n)$. The $r_n(j_n)$ distribution function depends clearly on traffic patterns on each output fiber of the CWC-SPN node. Thus if random variables W_n are weakly correlated, then

$$\Pr(\phi_n = t) = \Pr\{\sum_{s \neq n} W_s = t\} \approx conv(\pi_1(t), ..., \pi_{n-1}(t), \pi_{n+1}(t), ..., \pi_N(t)) \quad (3.21)$$

is a good approximation. Accordingly, $r_n(j_n)$ is approximated to

$$
\begin{aligned}
r_n(j_n) &= \Pr(\phi_n < M - j_n \mid W_n = j_n) \approx \Pr(\phi_n < M - j_n) \\
&\approx \sum_{t=0}^{M-j_n-1} conv(\pi_1(t), ..., \pi_{n-1}(t), \pi_{n+1}(t), ..., \pi_N(t))
\end{aligned}
\qquad (3.22)
$$

The tail distribution function $f^{(N)}(w)$ of used CWCs is

$$f^{(N)}(w) = \Pr\{\sum_{n=1}^{N} W_n \geq w\} \approx \sum_{t=w}^{\infty} conv(\pi_1(t),...,\pi_n(t)...,\pi_N(t)) \qquad (3.23)$$

The approximation in (3.21) and (3.22) becomes an exact relationship if random variables W_n are independent. The scenario when random variables W_n are truly independent is when $M=NK$, i.e., there is no need to share CWCs since for every wavelength in the node, there is always an available CWC for its use. There is nonetheless a strong justification for the use of (3.21) and (3.22) as follows:

Justification for Weak Correlation of W_n : The objective of CWC-SPN is to evaluate that smaller number of CWCs that can achieve similar performance as FWC system. Therefore, the case where we have a small number of CWCs (which clearly increases the correlation factor in the planes of Figure 3-8) is not considered. It is also not the purpose of CWC-SPN to make optical data drops due to lack of CWC dominate over optical data drops due to lack of wavelengths. Clearly, if this happens, then the performance of a CWC-SPN node cannot equal that of a FWC system. Hence in that sense, there must be sufficient number of CWCs (but still fewer than a full wavelength system), so that the use of the weak correlation approximation for $r_n(j_n)$ in (3.22) is accurate enough to determine a close enough solution for states P_{i_n,j_n} .

Corollary 3-9: The system of equations in (3.17), with the help of above Justification, is an Nth order non-linear system of equation. Therefore, there is no explicit solution except by means of some numerical methods.

Proof:

Clearly $r_n(j_n)$ in (3.22) is a $(N\text{-}1)^{\text{th}}$ order polynomial in the variables P_{i_n,j_n}, because of convolution. Hence, when using (3.22) to obtain $r_n(j_n)$, the whole system of equations in (3.17) is order N. It is well known that a Nth-order non-linear system of equations with $V_{RS}^{(N)}$ variables does not have explicit solutions, and some numerical methods has to be used (normally the methods are iterative)

End proof

3.3.6 Iterative solution for solving the RS problem

It is noted that the system of equations in (3.17) is N^{th} -order polynomial only because of $r_n(j_n)$. If there is perhaps a numerical estimate of $r_n(j_n)$, then that numerical estimate can be used in (3.17) instead. In that case, (3.17) is now a system of **linear** equations with a manageable number of variables, i.e., *NV*, which can be conveniently solved. Notice that (3.17) solves for the state probabilities in a particular plane *n*. The overall solution is thus the simultaneous computation of *N* sets of independent simultaneous equations. The resulting complexity is indeed a significant reduction compared to the complexity resulting from ***Theorem 3-2***. A method, called **self-constrained iteration** (SCI) with **sliding window update** (SWU), is now contributed to calculate $r_n(j_n)$ and solve for P_{i_n,j_n} at the same time. For convenience, we use $r_n(j_n) = g_n(P_{i_1,j_1}...P_{i_{n-1},j_{n-1}}, P_{i_{n+1},j_{n+1}}.....P_{i_N,j_N})$, where $g_n(\cdot)$ is a general function to describe the functionality of (3.15) and (3.22), and we denote *q* as the iteration number. Accordingly, $r_n^{(q)}(j_n)$ is the value of $r_n(j_n)$ at the qth iteration. The description of SCI is as follows:

Step 1 ($q= 0$): Obtain initial $P_{i_n j_n}^{(0)}$, $n \in [1, N]$ - *We begin with initial*

guess $r_n^{(0)}(j_n) = 1$. *This guess is substituted into* (3.17) *to solve the resulting two-*

dimensional Markov chain state equations for the state probabilities $P_{i_n j_n}^{(0)}$, $n \in [1, N]$

Steps 2: *Start of SWU:* $q = q+1$, *with* ($P_{i_n j_n}^{(q-1)}$, $n \in [1, N]$) *available, a new* $r_n^{(q)}(j_n)$

is computed based on **SWU**

> *for n = 1 to N*
> $$r_n^{(q)}(j_n) = g_n(P_{i_1 j_1}^{(q)}, ... P_{i_{n-1} j_{n-1}}^{(q)}, P_{i_{n+1} j_{n+1}}^{(q-1)} ..... P_{i_N j_N}^{(q-1)})$$
> *endfor*

Step 3: *Comparing results* - *check for terminating condition*

$\sum_{n=1}^{N} \sum_{i_n j_n} (P_{i_n j_n}^{(q)} - P_{i_n j_n}^{(q-1)})^2 \le \varepsilon$ *where* ε *is a small user-defined accuracy value. If*

terminating condition is not satisfied, repeat iteration in the Step 2.

It is noted that in the SCI iteration, there is no step-size to adjust. Once the

iteration starts, the algorithm self-constrains to terminate when the terminating

condition is reached.

Observation on Iteration count of SCI. The iteration count of SCI increases with

decreasing *M*. As mentioned previously, the larger *M*, the closer the CWC-SPN node

is to the full wavelength system where $r_n(j_n)$ is indeed unity. Since we begin with

$r_n^{(0)}(j_n) = 1$, the convergence is very fast since the initial guess is very close to the

true result. When *M* is small, then $r_n(j_n)$ is distant from unity, hence more iterations

are required. For a $\varepsilon = 10^{-10}$, about 10 iterations are required for small *M* scenarios,

while for large *M*, about 2-3 iterations are all that is required. It should be noticed

that the initial guess, $r_n^{(0)}(j_n)$, can be any value besides zero and SCI can converge as well.

3.3.7   Numerical results of CWC-SPN

This section presents numerical results to verify the usefulness of the RS method and the SCI and SWU technique for obtaining CWC-SPN theoretical results. One of the main theoretical results is the drop probability measures for which one can make design choices on the value of M so that performance of a CWC-SPN node, given some loading situation, is on level par with a full wavelength system. Another main theoretical result is the saving of WC in CWC-SPN against FWC, when desired performance is achieved.

We assume a general asymmetric traffic model whereby loading on each output fiber is different. Hence, the probability υ_n ($n \in [1, N]$) of an optical data routed to an output fiber is different from other output probabilities. Traffic intensity on a particular output fiber is thus $\lambda_n = \upsilon_n \lambda$. If traffic is symmetric, then obviously, $\upsilon_n = 1/N$. Assuming υ_n is uniformly distributed in the range $[(1-Z)/N, (1+Z)/N]$ where $Z \in [0,1)$ represents the range of variation, the probability υ_n can be expressed as follows:

$$\upsilon_n = \frac{1}{N}[(1-Z) + \frac{2Z(n-1)}{N-1}] \tag{3.24}$$
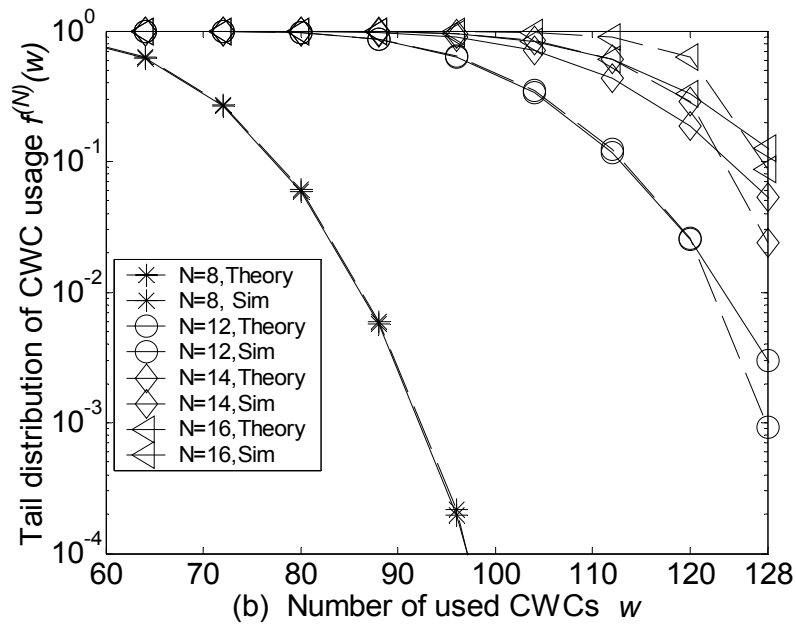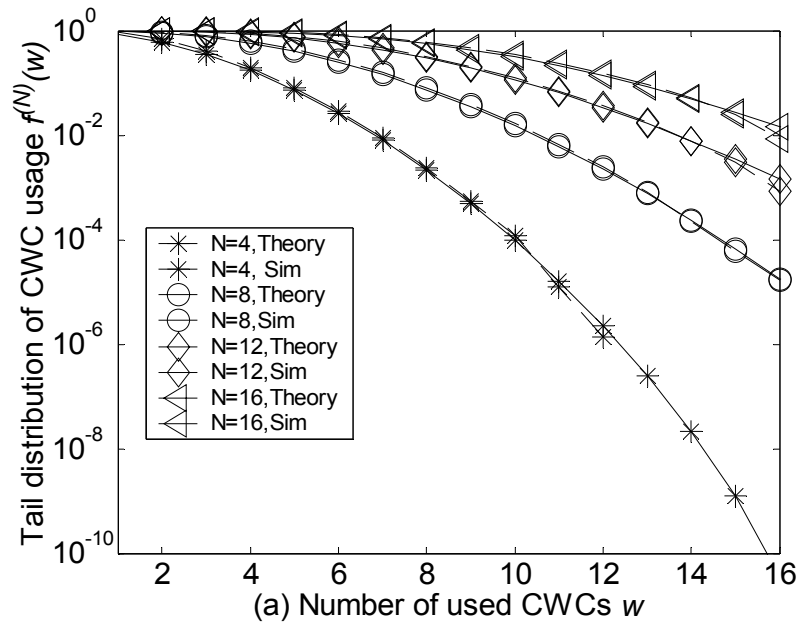
Figure 3-9: Tail distribution function of CWC-SPN with different number of output fibers, under asymmetrical traffic. (a) $K = 4$, $\rho = 0.4$, $Z = 0.4$, $M = 16$, $N = 4$, 8, 12, 16. (b) $K = 16$, $M = 128$, $\rho = 0.8$, $Z = 0.2$, $N = 8$, 12, 14, 16.

Figure 3-9(a) and (b) illustrates several $f^{(N)}(w)$ (theoretical and simulated) curves plotted against the number of used CWCs in the whole node. Asymmetric

traffic scenarios Z=0.4 (Figure 3-9 (a)) and Z=0.2 (Figure 3-9 (b)) are considered. (The numerical results are independent of optical data size distribution as stated in the **Appendix**, and therefore, it can be easily verified that the numerical results are exactly the same irrespective of optical data size distributions like Exponential, Gaussian or Fixed). The results in Figure 3-9 clearly show that the CWC-SPN analytical model is in close agreement with the simulated results. The function $f^{(N)}(w)$ decreases faster than exponential rate with larger w. Thereby, after a certain point, the usage probability of these CWCs is negligible. This means that the number of CWCs for the CWC-SPN scenario can be some value below the full CWC scenario. Several more interesting features can also be found in Figure 3-9. The offered load ρ and the load distribution parameter Z are related. If ρ increases, then Z has to be decreased to ensure that that loading on the highest index output fiber is less than one. For example, the loading on the highest index fiber for Figure 3-9 (a) and Figure 3-9 (b) is $\rho = 0.4 \times 1.4 = 0.56$ and $\rho = 0.8 \times 1.2 = 0.96$ respectively. The other feature in Figure 3-9 is that the loading ρ is kept as a constant parameter. Hence when the number of fibers N is increased, in order to keep ρ constant, more input traffic λ has to be generated. Thus we note that when input traffic λ increases, and the number of CWCs M is constant, it is obvious that the probability of using more CWCs should increase as illustrated in Figure 3-9. The discrepancy between the simulated results and the theoretical results is more pronounced with larger N than with smaller N. This is also obvious since for the same number of wavelength converters M, more fibers are sharing it, thereby creating more correlation between the various fibers and increase the correlation of

W_n. Thus, in this case, ***Justification of weak correlation of*** W_n is hard to be satisfied.
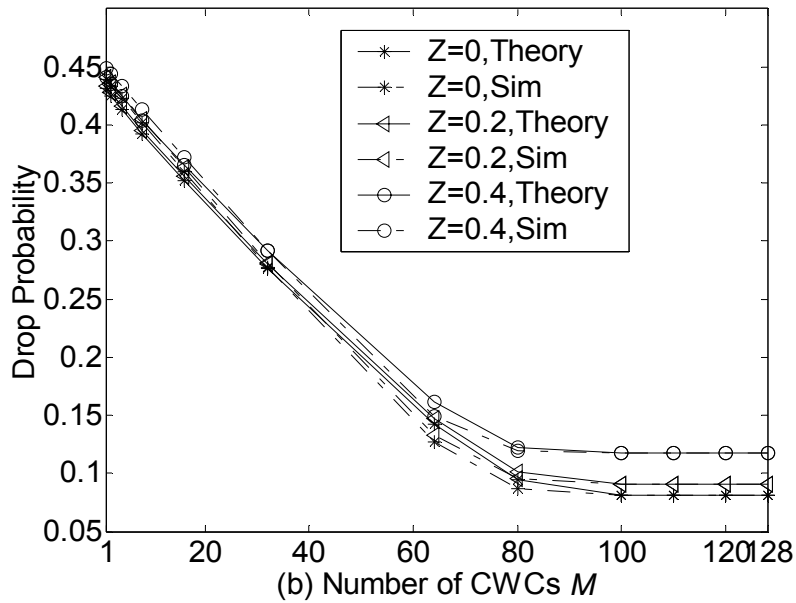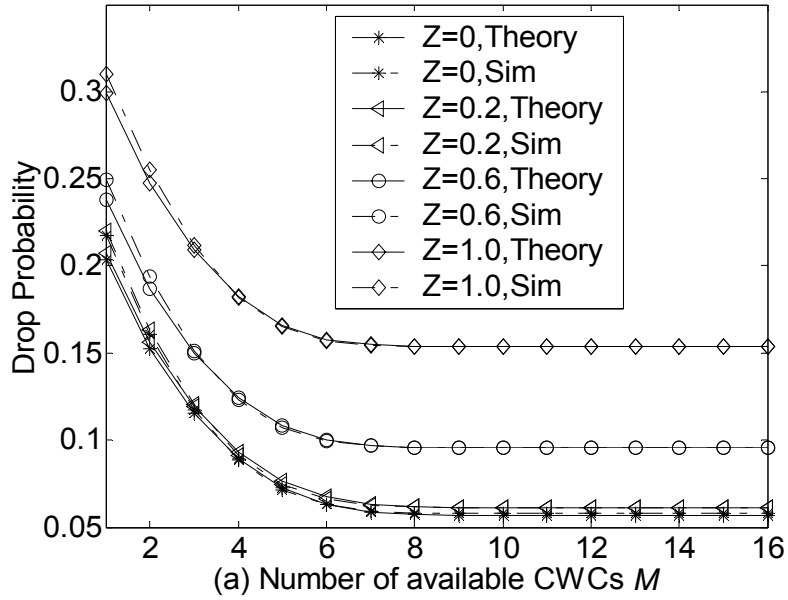
Figure 3-10 : Drop probability of CWC-SPN with different number of output fibers, under asymmetrical traffic. (a) $N = 4$, $K = 4$, $\rho=0.4$, $s = 0$, 0.2, 0.6, 1.0. (b) $N = 8$, $K = 16$, $\rho= 0.8$, $Z = 0$, 0.2, 0.4.

Figure 3-10 illustrates the overall drop probability performance in the node plotted against increasing number of wavelength converters M under different load distribution factor Z. The full wavelength converter point is the point on the extreme right (i.e., 16 and 128 CWCs for Figure 3-10 (a) and Figure 3-10 (b) respectively). The important design feature of Figure 3-10 is that x-axis point corresponding to that minimum number of CWCs needed so that the corresponding drop probability performance at that point has negligible difference compared to the drop probability performance at FWC condition. For example, for the case of light load conditions in Figure 3-10 (a), the theoretical curve has accurately predicted (i.e., gives the same result as the simulated curve) that the minimum number of CWCs needed is between 7 to 8 CWCs (depending on load distribution factor Z) to equal drop probability performance at FWC point of 16. In the case of high loading conditions, the theoretical plots of Figure 3-10 (b) has also accurately predicted that the minimum number of CWCs needed is about 100 CWCs to equal drop probability performance at the full CWC point of 128. In summary, it is not important whether the theoretical curve exactly coincides with the simulated curve as far as practical design considerations are concerned. What is clearly more important is whether the theoretical curves are able to accurately predict the minimum number of CWCs ensuring level-par performance with the FWC scenario. Clearly, Figure 3-10 demonstrates that the RS method (plus the SCI and SWU technique) is indeed useful and accurate enough to perform this prediction.

It is also noted that in Figure 3-10, the higher the degree of traffic asymmetry (i.e., higher Z), the higher is the drop probability. However, the minimum number of CWCs ensuring level-par performance with the FWC scenario is still similar to the case where traffic is symmetric (i.e., the case where $Z=0$). Henceforth, for

convenience and to reduce verbosity, the rest figures present results only for the case

of symmetric traffic, i.e., Z=0.
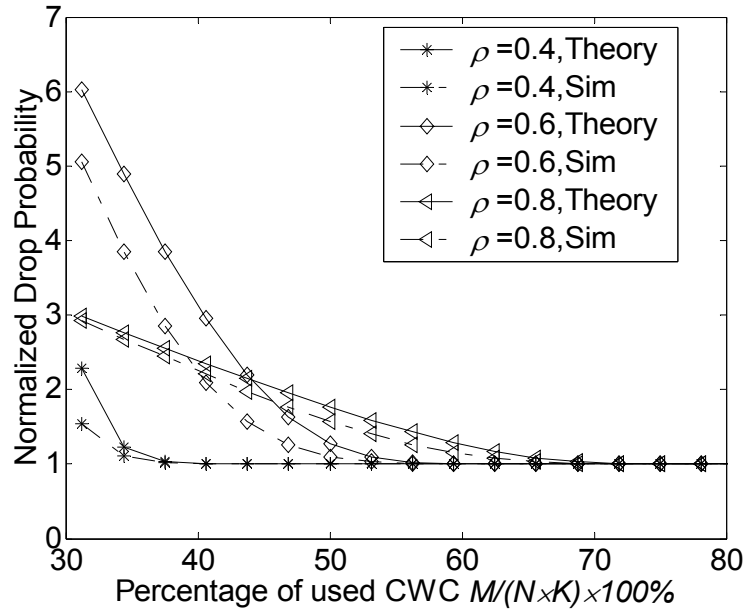
Figure 3-11: Normalized drop probability versus percentage of used CWCs in symmetric load of CWC-SPN. N = 8, K = 16. ρ=0.4, 0.6, 0.8.
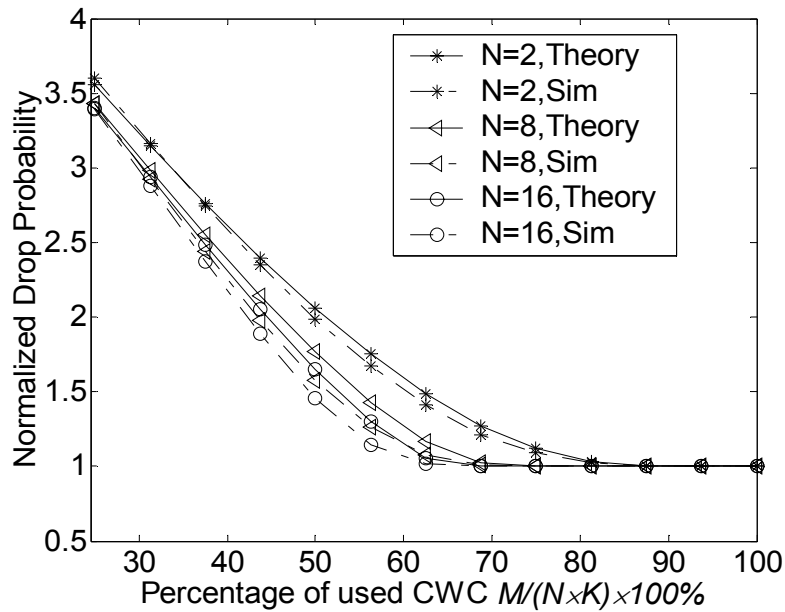
Figure 3-12: Normalized drop probability versus percentage of used CWCs in symmetric traffic of CWC-SPN. K = 16. ρ=0.8. N = 2,8,16

Figure 3-11 and Figure 3-12 illustrate clearer views for designers of CWC-SPN systems particularly when relative utilization $M/(N*K)*100\%$ (as compared to FWC utilization) of CWCs is important. To obtain the percentage savings in CWCs, one merely subtracts the relative utilization percentage from 100%. Also noted in Figure 3-11 and Figure 3-12 is that the *y*-axis is the normalized drop probability $P_{CWC-SPFdrop,M} / P_{FWCdrop}$. Hence the closer the normalized drop is to unity, the closer the performance to the full CWC performance. Hence the points of interests in Figure 3-11 and Figure 3-12 are when the normalized drop probability for the various scenarios diverges away from unity. In Figure 3-11, we vary the load ρ while keeping the number of fibers constant at $N = 8$. It is noted that as loading increases, percentage usage of CWCs must increase to keep drop performance on level-par with drop performance of the FWC system. In Figure 3-12, the loading ρ is kept constant while the number of output fibers is increased. This means the number of output fibers has increased for the same ρ and consequently, the percentage of used CWC can accordingly decrease. This means the larger the number of output fibers, the greater the savings in CWCs. Also noted in both Figure 3-11 and Figure 3-12 the theoretical curves are able to accurately predict (i.e., gives the same result as the simulated curve) the CWC percentage usage point where below that point, the performance of the CWC-SPN system diverges from the performance of the FWC system. Therefore, in the following figures, only theoretical results will be presented.

Similar to CWC-SPF, the CWC-SPN system, while being able to save wavelength converter cost, should ensure that its drop performance is also not compromised. It is expected that the blocking performance of the CWC-SPN system

will approach that of a FWC system monotonically with increasing M. However, the performance of CWC-SPN only approaches the performance of FWC asymptotically. Therefore, a target performance threshold of the drop probability is set to be achieved by the CWC-SPN as well. Therefore, if $P_{CWC-SPNdrop} / P_{FWCdrop} \leq \xi$, where $\xi > 1$ is a user-defined performance threshold, we consider the performance of CWC-SPN similar to that of FWC. The performance threshold adopted in this thesis is $\xi = 1.2$ throughout. It should be noted that $P_{FWCdrop}$ can be obtained from the ErlangB formula.

We can see that $P_{CWC-SPNdrop,M}$ will monotonically decease with increasing of M. Therefore, there must be a $\overline{M}_{CWC-SPN}$ to be the minimum number of CWCs required for the CWC-SPN node such that the performance threshold requirement is satisfied, i.e

$$\overline{M}_{CWC-SPN} = \min\{M \mid P_{CWC-SPNdrop,M} / P_{FWCdrop} \leq \xi\} \tag{3.25}$$

Accordingly, the minimum WC cost and minimum switch cost of CWC-SPN per fiber can be expressed as

$$\min WcCost_{CWC-SPN} = K \times \overline{M}_{CWC-SPN} / N \tag{3.26}$$

$$\min SwCost_{CWC-SPN} = (NK + \overline{M}_{CWC-SPN}) \times (NK + \overline{M}_{CWC-SPN}) \tag{3.27}$$

The saving of WC of CWC-SPN against FWC $\theta_1^{CWC-SPN}$ can be expressed as

$$\theta_1^{CWC-SPN} = (1 - \frac{\min WcCost_{CWC-SPN}}{WcCost_{FWC}}) \times 100\% \tag{3.28}$$

Figure 3-13 illustrates curves of $\theta_1^{CWC-SPN}$ via (3.28) against increasing number of output fibers for different loading conditions. Figure 3-13 curves

illustrate that the improvement in savings, by adding more output fibers, is more pronounced for the case of low loads than for high loads. The curves also illustrate that after a certain point, it is no longer worthwhile to keep on adding output fibers as the improvement in savings is no longer commensurate with the extra fibers that are added. This means that a CWC-SPN node need not be designed to always manage one large CWC resource pool for all output fibers (so as to maximize CWC savings). Instead, several independent CWC pools shared by a subset of output fibers can be designed. By sub-dividing the global shared pool, switch complexity in the CWC-SPN node can be reduced significantly with minor degradation on CWC savings
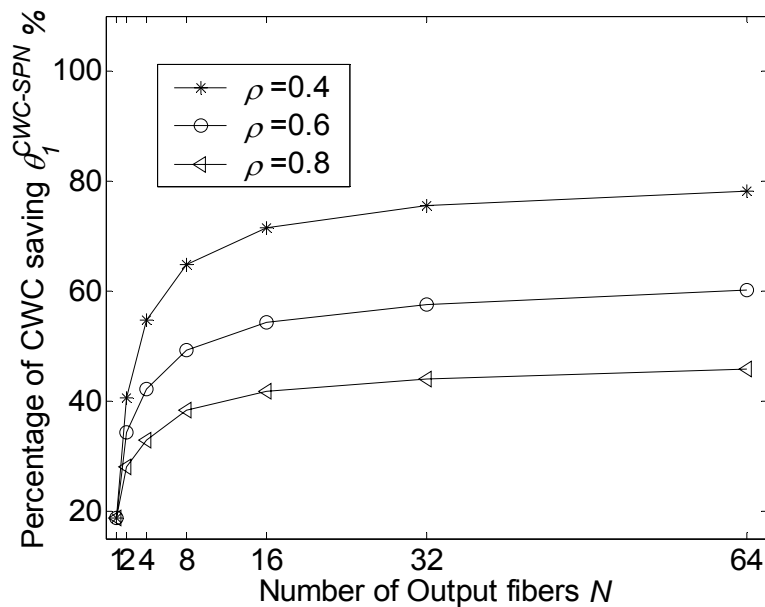
Figure 3-13: Saving of CWCs verses the number of output fibers, in symmetric traffic of SPN. $K = 16$. $\rho = 0.4\ 0.6\ 0.8$
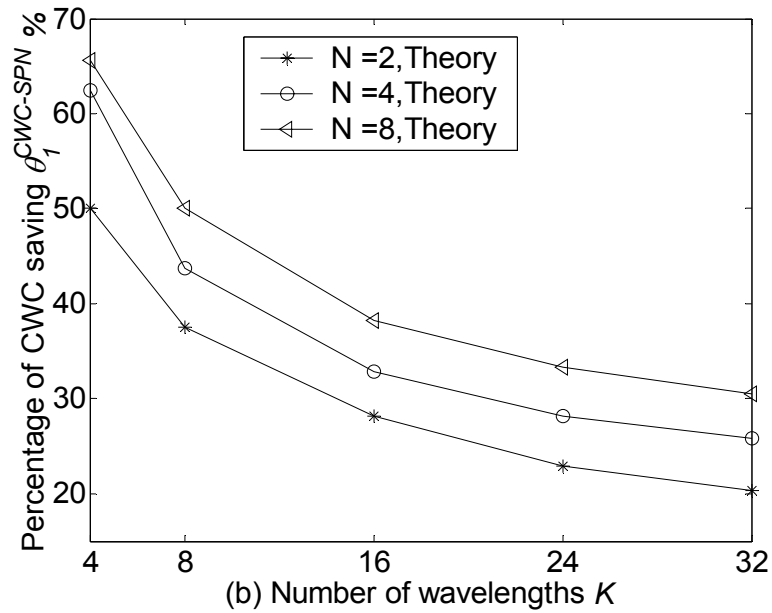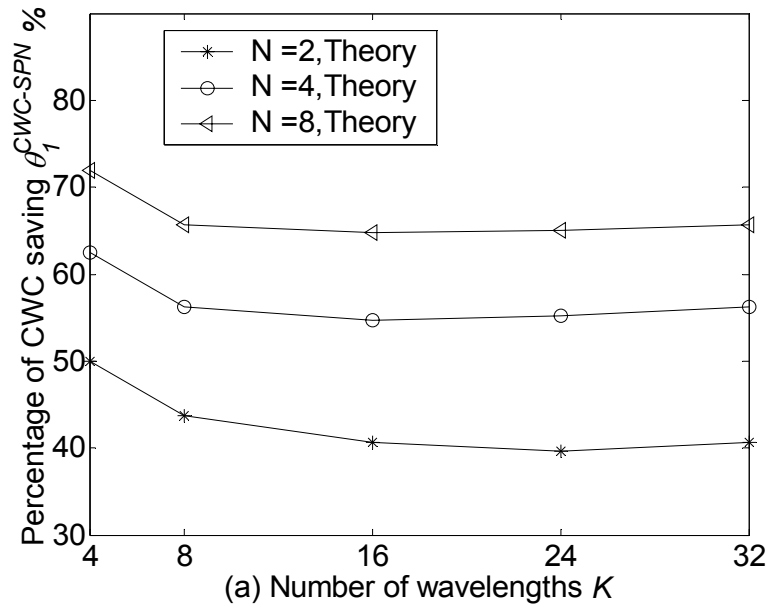
Figure 3-14:   Saving of CWCs verses the number of wavelengths K, in symmetric traffic, N=2, 4, 8; (a) ρ= 0.4 (b) ρ= 0.8

Figure 3-14 shows the saving of WC verses different number of wavelengths

for N under low load ($\rho = 0.4$ in Figure 3-14(a)) and high load ($\rho = 0.8$ in Figure

3-14(b). Both figures show that the saving of WCs decreases with increasing K. This is because with more wavelengths within one fiber, more optical data need CWCs to convert the data from input wavelength to an available output wavelength in order to achieve performance of FWC. Therefore, more CWCs are needed, leading to low saving of CWCs when K is larger. In addition, the trend of decreasing of saving for low load in Figure 3-14(a) is slower than the trend in Figure 3-14(b). This is because at low load, the requirement for CWCs is low as well. Thus, when K increases, the percentage of needed CWCs doesn't increase too much. This leads to the decreasing gradient of savings for low load is not as large as for high load.

3.4 Summary

In this chapter, both CWC-SPF and CWC-SPN architectures and their corresponding theoretical analysis are contributed.

In the analysis of CWC-SPF, an exact two-dimensional Markov chain analytical model was contributed. Numerical results showed that the CWC-SPF architecture can achieve similar performance as FWC, only with a WC saving percentage of 10-20%. The poor saving percentage is due to the poor sharing efficiency of the SPF architecture.

In the analysis of CWC-SPN, an exact multi-dimensional Markov chain analytical model was contributed. However, further analysis demonstrated that the multi-dimensional Markov chain may lead to intractable calculations. Therefore, in order to reduce the complexity of multi-dimensional Markov chain analysis, a novel set of methods namely, Randomized States, Self-Constrained Iteration with Sliding Window Update, are presented to approximate the performance of CWC-SPN.

These methods dramatically reduce the multi-dimensional problem to a numerically tractable problem where a series of seemingly unrelated two-dimensional Markov chain problems are solved. A number of useful numerical studies are presented, firstly, to confirm the accuracy of the novel theoretical approximation analysis results with actual simulated results and secondly, to show a practical use for the CWC-SPN architecture. It is demonstrated that the approximation theoretical results are indeed accurate enough. The numerical results also demonstrated that WC savings as high as 80% can be achieved for low load conditions like $\rho = 0.4$ and sometimes as high as 50% for high load conditions like $\rho = 0.8$, and such saving will increase with increasing number of fibers in one OS node. In addition, the results also show that with larger number of wavelength within one fiber, i.e., K, lesser saving can be achieved.

Generally, the CWC-SPN needs more switch fabric than CWC-SPF, but the saving of WC of CWC-SPN is better than that of CWC-SPF. This is because CWC-SPN shares all available CWCs in one common pool, leading to a higher sharing efficiency of CWCS and lesser CWCs.

So far, three existing NFWC architectures, i.e., PWC-only, CWC-SPF and CWC-SPN, have been analyzed and compared. Results show that PWC-only is not suitable to achieve similar performance as FWC, while CWC-SPF and CWC-SPN can achieve such performance while achieving a moderate amount of WC savings.

PWC is a cheap device but with undesirable performance. In contrast, CWC has better performance but is expensive. Therefore, our concern is to design a new architecture which can combine the benefits of both low cost PWC and high performance CWC.

Therefore, a new architecture, termed as two-layer wavelength conversion, which can save more WCs and even save switch fabric costs, will be presented in the next chapter.

4   Architecture and Modeling of Two-layer Wavelength Conversion

4.1   Introduction

In Chapter 2 and 3, the architectures and performance of PWC-only, CWC-SPF and CWC-SPN were presented. It is clear that using CWC is a waste, if a new incoming optical data can find an empty output wavelength within a small range of the input wavelength. If PWC is used under such scenario, the whole system will become more cost-efficient since PWC is cheaper than CWC. This means if we can combine PWC and CWC together in one architecture and assign the task of near wavelength conversion (Near-WC) to the PWC and the task of far wavelength conversion (Far-WC) to the CWC, the cost of such architecture is expected to be reduced further, while maintaining the same performance.

The above paragraph lends motivation to the consideration of a new optical switching architecture termed *two-layer wavelength conversion* (TLWC), where a combination of PWCs in the first layer and CWCs in the second layer is employed. The first layer PWCs perform the function of Near-WC thus cutting down the need for more expensive CWCs performing such functions, while the second layer CWCs can perform Far-WC. Specifically, the PWC layer is used to convert the input optical data to a near output wavelength first. If the Near-WC is unsuccessful, a CWC is then used to perform Far-WC. It is noted that one optical data can only be converted by either PWC or CWC instead of both. In TLWC, each input wavelength has one associated PWC, and CWCs are shared via some sharing mode (SPF or SPN)

at output side. In this chapter, we will study both TLWC-SPF and TLWC-SPN architectures.

For TLWC-SPF, every output fiber has its own pool of CWCs only for use by wavelengths belonging to that output fiber. For TLWC-SPN, all CWCs are pooled together for all fibers in one OS node.

The costs of TLWC-SPF/SPN are determined by the cost of its switch fabric and wavelength converters (PWC and CWC). The contributions in this chapter are to demonstrate that with TLWC-SPF/SPN, the implementation cost of wavelength converter in an optical switching node can be reduced, while achieving the same drop performance as a CWC-SPF/SPN optical architecture and/or a FWC optical architecture. In addition, the cost of the switch fabric of TLWC-SPF/SPN is likely to be lower than that of CWC-SPF/SPN, due to fewer CWCs are used.

Architectures and performance analyses of both TLWC-SPF and TLWC-SPN will be presented in section 4.2 and 4.3 respectively. Section 4.4 summarizes the performance of all TLWC-SPF/SPN and CWC-SPF/SPN architectures. Section 4.5 concludes this chapter. In addition, section 4.6 shows some network-wide simulation for NFWC architectures.

4.2   Architecture and analysis of TLWC-SPF

4.2.1   Architecture of TLWC-SPF

The TLWC-SPF architecture takes advantage of the cost savings and physical properties of the PWC (in the first layer) while adding a limited number of CWCs (in the second layer) to ensure drop performance approaches the drop

performance of FWC. In the architecture of TLWC-SPF since PWC is cheaply available and it has only one input wavelength as stated in Chapter 2, every input wavelength has an associated PWC so that contention of PWC does not happen. On the other hand, CWC an expensive device, is placed in a pool and shared by output wavelengths within one output fiber if needed. In addition, it should be noticed that PWC, which can only convert from one specific input wavelength to a sub-range of output wavelengths, cannot be shared like CWC.

Assume there are K wavelengths within one fiber. We number the wavelengths within one fiber from 0 to K-1. For the structure of PWC, we use the definition in section 2.1: assume that an optical data arriving on input wavelength k can only be converted to a wavelength m by the PWC, where $m \in \Omega(k)$ $\triangleq \{k \bmod K \mid k - d_1 \leq m \leq k + d_2\}$, where $d_1, d_2 \geq 0$. This means an input optical data may be converted to an output wavelength range of $S = d_1 + d_2 + 1$, where $S \leq K$.

Figure 4-1 shows the architecture of a TLWC-SPF OS node. A conventional cross-bar switching fabric is assumed. In this architecture each output optical fiber shares M number of CWCs and every wavelength in each output fiber has one associated PWC. Therefore, there are K PWCs and M CWCs per output fiber. If Near-WC by the associated PWC is successful, the optical data will be switched to the output port without using CWC. Otherwise one CWC out of the M pool will be used to perform Far-WC on the optical data. It should be noticed that when S=1, this means there is no PWC at all, and the TLWC-SPF node is reduced to CWC-SPF node.

It should be noted that the TLWC-SPF switch fabric in Figure 4-1 is non-blocking. This means that it is not possible for the switch to drop optical data due to

lack of switch resources. If optical data is dropped by the switch fabric, then it must be due to the lack of output wavelengths or failure in the two-layer PWC/CWC wavelength conversion process.
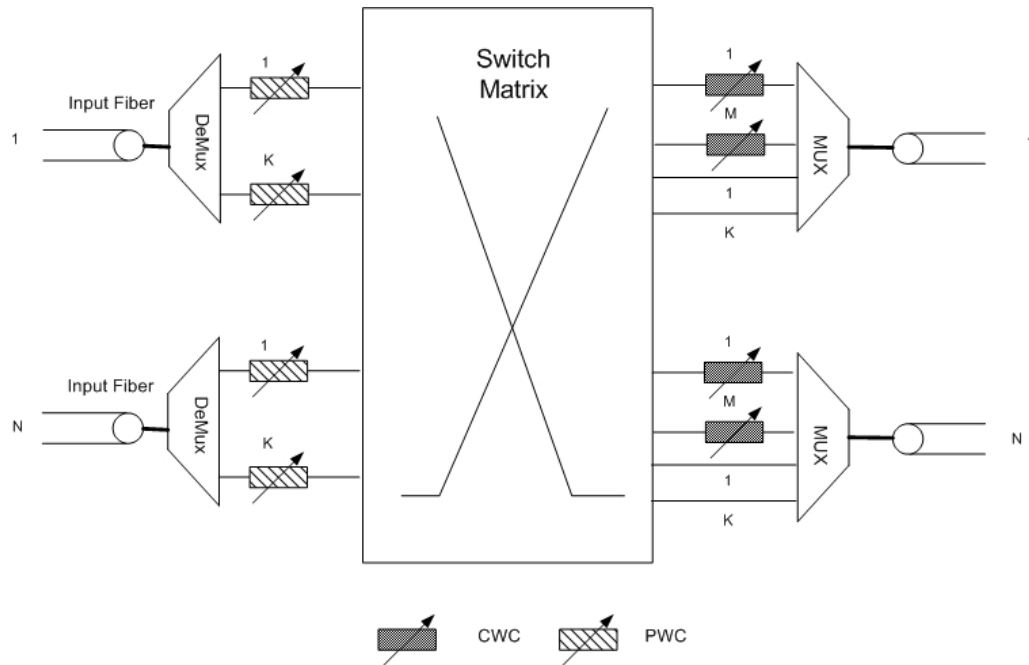
Figure 4-1:   Switch and conversion architecture of TLWC-SPF

In TLWC-SPF a wavelength converter assignment algorithm is needed to choose a suitable WC (either PWC or CWC). We denote $|\Omega(k,t)|$ to be the number of wavelengths in use by other optical data at time t within the range of PWC associated to wavelength k. When a new optical data arrives at time t on wavelength k, if $|\Omega(k,t)|=S$, it means that the input optical data cannot find a suitable output wavelengths via PWC, and thus a CWC from the common pool can be used. The assignment algorithm of TLWC-SPF is shown in Figure 4-2

> *Optical data arrives at wavelength k at time t.*
> *If $|\Omega(k,t)| \neq S$*
>   *Use PWC to find any available output wavelength*
> *Else*
>   *If one CWC is available and one wavelength is available*
>   *Use CWC to convert the optical data to an available*
>   *output wavelength*
>   *Else*
>
>   *Drop the optical data.*
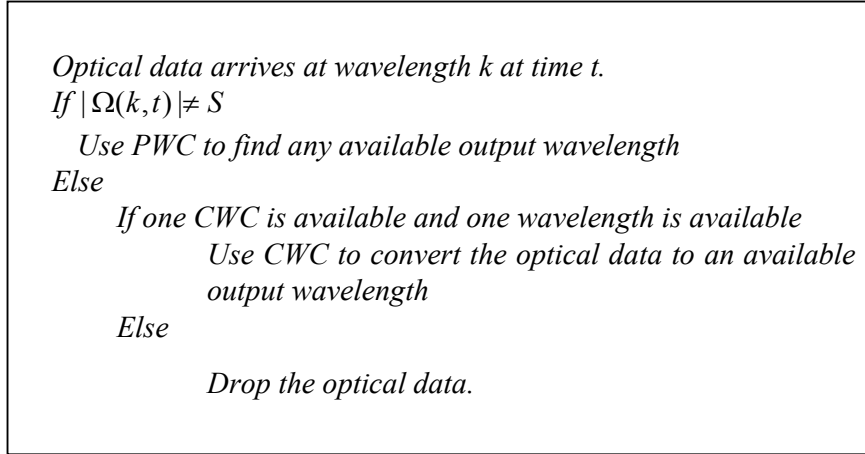
Figure 4-2:   TLWC-SPF wavelength converter assignment algorithm

4.2.2   Cost function of TLWC-SPF

In this section the implementation cost of the TLWC-SPF architecture is presented. The implementation cost includes two parts: switching fabric cost and wavelength converter cost.

It should be noted that if all the PWC elements are removed in Figure 4-1, the resulting node is indeed a CWC-SPF node. The complexity of the TLWC-SPF switching fabric can be expressed as in (4.1), which is the same as the CWC-SPF switching fabric as in (3.3), if M is the same in these two architectures.

$$SwCost_{TLWC-SPF} = NK \times (NK + NM) \tag{4.1}$$

In this thesis, in order to compare the WC implementation costs on the different wavelength conversion architectures, a simple linear cost structure is adopted such that the cost of a PWC or CWC is linearly proportional to its conversion range. This linear cost model is a conservative cost increase model (please refer to section 3.2.2 for detailed explanations)

The overall cost calculation is done by taking the product of the number of used wavelength converters and the conversion range of each wavelength converter. In the case of *M* CWCs, each with a range of *K*, the cost of implementation is *MK*; while for PWC, each with a range of *S*, the cost of implementation is *KS*. The general formula for the calculation of implementation cost per output fiber in a TLWC-SPF architecture is as follows:

$$WcCost_{TLWC-SPF} = \begin{cases} MK + KS & , \ S > 1 \\ MK & , \ S = 1 \end{cases} \qquad (4.2)$$

4.2.3 Theoretical analysis of TLWC-SPF

In this section, the analytical lower bound drop performance of TLWC-SPF is presented. Although the lower bound performance does not provide a conservative performance of the TLWC-SPF, it is nonetheless very useful as it closely approximates the TLWC-SPF performance very well (see numerical simulations later). In fact, as will be proven later, for the extreme cases of $S = 1$ (i.e., TLWC-SPF is reduced to a CWC-SPF model) and $S = K$ or $M = K$ (FWC model), the analytical lower bound drop performance is exactly equal to the actual drop performance.

We denote λ and μ to be the arrival rate of optical data and the service rate of each wavelength at the TLWC-SPF node respectively. Therefore, the traffic load on each output wavelength is $\rho = \lambda / (K\mu)$.

Now, notice from Figure 4-1 that the TLWC-SPF structure consists of a PWC section followed by a CWC section. It is not possible for optical data to be

dropped in the PWC section for two reasons: firstly, there is one PWC for each wavelength, hence it is not possible to suffer from lack of PWCs; secondly, any data not being able to be converted by the associated PWC will not be dropped but is passed to the CWC section to be handled. Hence all drop events will only occur at the CWC section. This being the case, our analysis begins by analyzing the CWC section. Drops occur in the CWC section due to: (1) lack of output wavelength or (2) lack of CWCs.

Hence, the analysis first seeks to obtain state probabilities $P_{i,j}$ for the two-dimensional state (i, j) in the CWC section indicating that there are i wavelengths in use by optical data, and j CWCs in use by some of these i wavelengths at the same time. The link between the PWC section and the CWC section is related by a set of probabilities α_i (more on this later) whereby for an input optical data arrival, say at a certain PWC and where there are currently i wavelengths currently in use by the output fiber in the TLWC-SPF node, all the associated S consecutive output wavelengths of that PWC are already in use. Hence the probability $(1 - \alpha_i)$ is the link which determines whether a CWC from the CWC section needs to be used. With this link in mind, we first present the following analysis on the CWC section and then determine probabilities α_i from the PWC section later

It should be noted that $0 \leq j \leq i \leq K$ and $j \leq M \leq K$. We now determine the state probability $P_{i,j}$ of the state (i, j).

Theorem 4-1: the state probability $P_{i,j}$ (for all valid states $0 \leq j \leq i \leq K$ and $j \leq M$) in the CWC section can be obtained from the following simultaneous equations

$$\begin{cases} (A_{i,j} + B_{i,j} + C_{i,j} + D_{i,j})P_{i,j} = \\ A_{i-1,j}P_{i-1,j} + B_{i-1,j-1}P_{i-1,j-1} + C_{i+1,j}P_{i+1,j} + D_{i+1,j+1}P_{i+1,j+1} \\ \sum_{i,j} P_{i,j} = 1 \quad \text{(for all } 0 \le j \le i \le K \text{ and } j \le M \le K) \end{cases} \tag{4.3}$$

where $A_{i,j}$, $B_{i,j}$, $C_{i,j}$ and $D_{i,j}$ are transition speeds for various scenarios to be described later.

Proof:

From (4.3), we can find that this equation is similar to the analysis of CWC-SPF. Therefore, like before, in this Markov chain analysis, we will only present the transition which is outgoing from each state.

Case 1: (i, j) to $(i+1, j)$, for $i+1 \le K$. This scenario indicates that the wavelength of the incoming optical data can be converted to an available output wavelength of the output fiber via a first layer PWC. The incoming optical data does not require any CWC to find a suitable output wavelength. Thus, the transition speed is $A_{i,j} = (1 - \alpha_i)\lambda$, where α_i is the important probability measure representing the probability that for an input optical data arrival, say at a certain PWC, all the associated S consecutive output wavelengths of that PWC are already in use. The probability α_i is also evaluated at state i. Hence the probability $(1 - \alpha_i)$ is the probability that for an optical data arrival, say at a certain PWC, there is an available wavelength amongst the associated S consecutive output wavelengths associated with that PWC. Accordingly, the new arrival can be converted to that available wavelength and accepted.

Case 2: (i, j) to $(i+1, j+1)$, for $i+1 \le K$ and $j+1 \le M$. This case indicates that the wavelength of the incoming optical data can not be converted to an available

output wavelength via the associated PWC. Thus, the optical data has to use one available CWC from the pool to find a suitable output wavelength. Thus, the transition speed is $B_{i,j} = \alpha_i \lambda$.

Case 3: (i, j) to $(i-1, j)$, for $i-1 \geq 0$ and $i > j$. This case indicates that an optical data not using any CWC has just been sent out completely. As there are $i - j$ optical data not using CWCs, the transition speed is therefore $C_{i,j} = (i - j)\mu$.

Case 4: (i, j) to $(i-1, j-1)$, for $i-1 \geq 0$ and $j-1 \geq 0$. This case indicates that an optical data using one CWC has just been sent out completely. As there are j optical data using CWCs, the transition speed is therefore $D_{i,j} = j\mu$.

Considering the fact that the sum of all state probabilities is equal to unity, the simultaneous equations in (4.3) are valid.

End Proof.

From the description of the four transition cases, we can find that this analysis is quite similar to that of CWC-SPF, except for one more parameter α_i, which is similar to PWC-only analytical model. Therefore, many theoretical features owned by CWC-SPF and PWC-only are also owned by TLWC-SPF. For example, the state transition diagram for state (i, j) is same as CWC-SPF shown in the Figure 3-3.

The result in above analysis is also applicable to general data size distribution. Please refer to the **Appendix**.

Corollary 4-1 The number of states in the simultaneous equations of (4.3) is $V = (2K - M + 2)(M + 1)/2$.

Corollary 4-2 The simultaneous equations in (4.3) are solvable.

Corollary 4-3: From state probabilities $P_{i,j}$, many useful parameters can be obtained as follows.

We denote random variable W as the number of CWCs being used. Thus the tail distribution function of used CWCs, $f(w)$, can be written as (4.4) and drop probability as (4.5)

$$f(w) = \Pr\{W \geq w\} = \sum_{i,j \geq w} P_{i,j} \tag{4.4}$$

$$P_{Drop} = \sum_{i=M}^{K-1} \alpha_i P_{i,M} + \sum_{j=0}^{M} P_{K,j} \tag{4.5}$$

In (4.5), the first term on the right side is the drop probability due to lack of CWC. The second term is the drop probability due to lack of available output wavelength.

Corollary 4-4: The Markov Chain analysis presented in ***Theorem 4-1*** is exact, i.e., not an approximation, ***provided the exact probabilities*** α_i ***from the PWC section is also known***.

The exact probabilities α_i can only be obtained using *K*-dimensional Markov chain analysis which leads to intractable analysis due to the large number of Markov chain states (2^K). For this reason, we now provide a method to obtain an approximation for α_i.

Approximation for α_i: In state *i*, there are *i* wavelengths in use out of a total of *K* wavelengths. It is assumed that when a new optical data arrives the optical data is uniformly filled amongst all of its *K* - *i* available wavelengths. The use of this assumption allows us to evaluate α_i easily as follows:

$$\alpha_i = \frac{i}{K} \times \frac{i-1}{K-1} \times ... \times \frac{i-(S-1)}{K-(S-1)} = \prod_{q=0}^{S-1} \frac{i-q}{K-q} \ , \ 0 \le i \le K \tag{4.6}$$

This approximation is the same as the approximation in Chapter 2 in (2.4).

Theorem 4-2 : The use of α_i in (4.6) to obtain the drop probability P_{drop} via (4.3) and (4.5) will result in a lower bound to the actual drop probability of the OS node. In other words, the actual α_i is larger than the α_i given in (4.6), because of grouping tendency.

Proof:

Please refer to proof of ***Theorem 2-3***

End proof

Theorem 4-3 : As *S* approaches *K* or *M* approaches to *K*, the approximation of α_i in (4.6) becomes more accurate. If *M=K* or *S=K*, the grouping tendency is removed completely and α_i in (4.6) is the exact value.

Proof

The proof is quite obvious if we consider the limit $S = K$. In this limiting case, grouping tendency is totally eliminated in the real system since it is clear that any available wavelength will now have exactly the same probability of being used by a new arrival.

Similar effect can be obtained if number of CWC M approaches to K, because when more CWCs are available, the distribution of occupied wavelength tends to be more uniformly distributed, which means the grouping tendency is alleviated to some extent as stated above. If M reaches the largest value, i.e., $M=K$, the grouping tendency is removed completely and the results presented in (4.6) and ***Theorem 4-1*** are exact

End proof

Theorem 4-4 : If S=1, which means the TLWC-SPF node is reduced to a CWC-SPF node, the α_i in (4.6) is exact. Consequently, the analysis in ***Theorem 4-1*** is also exact.

Proof

If S=1, this means the PWC cannot convert input wavelength to any other wavelength except itself, hence the PWC section can be deleted from the TLWC-SPF structure in Figure 4-1. The resulting structure is reduced to a CWC-SPF node. Since CWCs have the capability to convert input wavelengths to a full range it is impossible for CWCs to cause grouping tendencies. Consequently, all the occupied wavelengths are uniformly distributed. The α_i probabilities calculated in (4.6)

reduces to $\alpha_i = \dfrac{i}{K}$, which gives the same theoretical and exact result as the analysis

presented in ***Theorem 3-1*** for the CWC-SPF node.

End proof

Although calculating α_i by (4.6) leads to a lower bound of drop probability, this lower bound should be tight. This is because our objective of TLWC-SPF is to achieve similar performance as FWC. Therefore, there must be enough CWCs (only PWC cannot achieve such performance), i.e., large *M*. According to ***Theorem 4-3***, large enough *M* will alleviate grouping tendency leading to α_i probabilities calculated in (4.6) be close enough to the actual value.

4.2.4   Numerical results of TLWC-SPF

In this section we compare the theoretical results obtained by simultaneously solving (4.3) via (4.6) with simulation results. Poisson traffic is used in the simulations.

The following issues are addressed in this section: (a) the accuracy of the theoretical analysis; (b) the benefit of TLWC-SPF, in terms of WC savings and switch savings, compared to CWC-SPF and FWC.

Figure 4-3 demonstrates the theoretical and simulated drop performance of TLWC-SPF. Notice that as the number of CWCs increases to *K* (i.e., 16), the drop performance of TLWC-SPF becomes closer and closer to FWC (which is the case *M*=16). Figure 4-3 also demonstrates that as *S* (i.e., the range of the PWC) increases, fewer CWCs are required to obtain performance similar to FWC. The result is

obvious since larger range of PWC results in less reliance on the use of CWCs. Figure 4-3 also demonstrates that the analytical results although providing lower bound performance (by virtue of ***Theorem 4-2***), are very close to the simulated performance. As *M* increases, the deviation between the analytical and simulated results becomes smaller and smaller. This is expected by virtue of ***Theorem 4-3***. In addition, Figure 4-3 shows that low load (Figure 4-3(a)) needs fewer number of CWCs to achieve similar performance as FWC, compared to high load (Figure 4-3(b)).

Hence the following conclusions can be made: the TLWC-SPF node can achieve similar performance as FWC and the analytical model provides a very tight lower bound to the drop performance of TLWC-SPF.
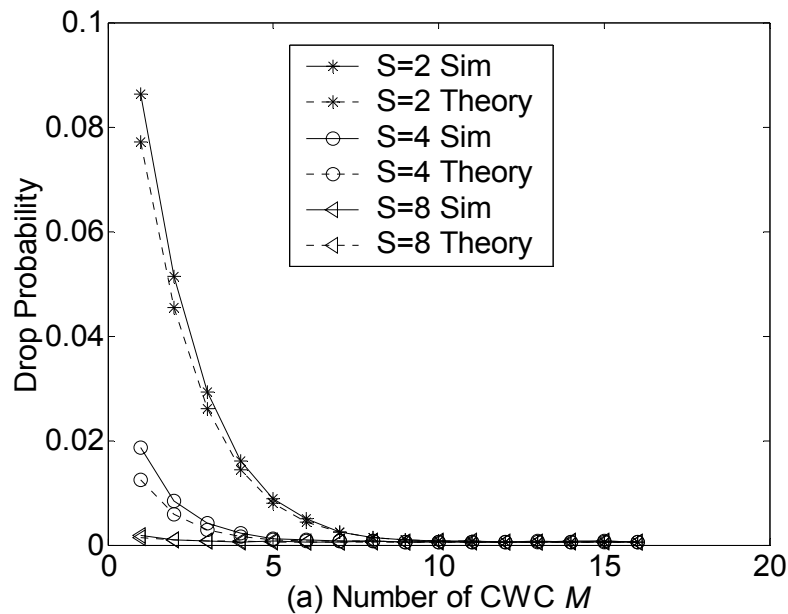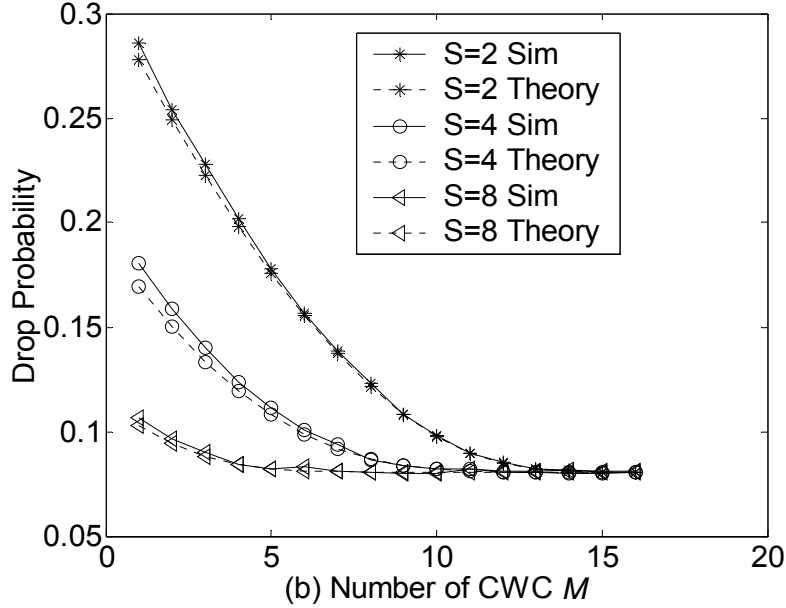
(a) Number of CWC *M*

Figure 4-3: Drop probability versus Number of CWCs in a TLWC-SPF architecture. K=16, M=1 to 16. (a) ρ =0.4. (b) ρ =0.8.

Like CWC-SPF and CWC-SPN architectures, from Figure 4-3, we can see that in TLWC-SPF system, for a given S, if the number of available CWCs increases, the drop probability of the system decreases and approaches that of a FWC system. This means that with a certain PWC range and certain number of CWCs, the blocking performance of the TLWC-SPF system will approach that of a FWC system. A target performance threshold of the drop probability as described in Chapter 3, is set to be achieved by the TLWC-SPF. Therefore, if $P_{TLWC-SPFdrop} / P_{FWCdrop} \leq \xi$, where $\xi > 1$ is a user-defined performance threshold. The performance threshold adopted throughout this thesis is $\xi = 1.2$.

For convenience, for a given S, we denote $\overline{M}_{TLWC-SPF,S}$ to be the minimum number of CWCs required for the TLWC-SPF node such that the performance threshold requirement is satisfied, i.e.,

$$\overline{M}_{TLWC-SPF,S} = \min\{M \mid P_{TLWC-SPFdrop,M} \,/\, P_{FWCdrop} \le \xi, \text{ for a given } S\} \quad (4.7)$$

Accordingly, the minimum WC cost per fiber of TLWC-SPF for a given S can be expressed as

$$\min WcCost_{TLWC-SPF,S} = \begin{cases} K \times \overline{M}_{TLWC-SPF,S} + KS & , \ S > 1 \\ K \times \overline{M}_{TLWC-SPF,S} & , \ S = 1 \end{cases} \quad (4.8)$$
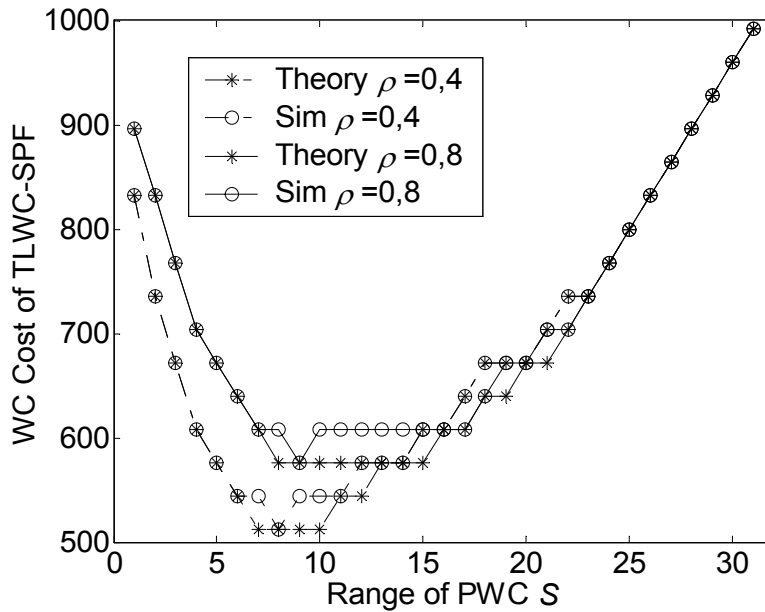
Figure 4-4:   The minimal WC cost of TLWC-SPF against the range of PWC for K=32. ρ=0.4, 0.8.

Figure 4-4 plots the minimum cost of TLWC-SPF against S for K=32 and different load to achieve threshold performance via (4.8) for both theoretical and simulation results. In Figure 4-4, when S=1, it should be noted that the TLWC-SPF node is reduced to a CWC-SPF node; when S=32, the TLWC-SPF node is reduced to a FWC node. In Figure 4-4, for given S, equation (4.7) is first used to find the

minimum number, i.e., $\overline{M}_{TLWC-SPF,S}$, of CWCs required so that the performance threshold is achieved. Thereafter, the cost formula in (4.8) is used to obtain the cost. The cost is U-shaped for the following reasons: when S is small the cost of WC is dominated by the need for more CWCs (since PWC range is too small to create a significant impact); when the PWC range increases there is no need for that many CWCs as before and hence the overall cost drops. But as the S range is further enlarged the PWC elements become more like a CWC element. This will cause the overall cost to rise again.

Therefore, from Figure 4-4, it can be seen clearly that there is an optimal S, S_{opt} , which achieves the lowest wavelength conversion cost while maintaining the desired drop performance. Note that for the S_{opt} , the wavelength conversion cost of TLWC-SPF is lower than that of CWC-SPF (i.e., the left starting point of the U-shape plot in Figure 4-4). It is also clear that there are many values of S_{opt} resulting in minimum TLWC-SPF WC cost. The main reason for this is that the cost function is an integer result and hence there are many S and M combinations meeting the minimum cost criteria. For low load, S_{opt} is a slightly smaller than that for high load since at low load, the requirements of WC are fewer.

We term $\overline{M}_{TLWC-SPF,S}$ at S_{opt} as $\widehat{M}_{TLWC-SPF}$. In the following presentation, only the S_{opt} and $\widehat{M}_{TLWC-SPF}$ are used to calculate the optimal cost of TLWC-SPF architecture. Therefore, when S_{opt} and $\widehat{M}_{TLWC-SPF}$ are, the optimal WC cost, $optWcCost_{TLWC-SPF}$, is expressed by (4.9), and the switch cost, $optSwCost_{TLWC-SPF}$, is expressed by (4.10)

$$optWcCost_{TLWC-SPF} = \min\{\min WcCost_{TLWC-SPF,S} \mid \text{ for all } S\}$$

$$= \begin{cases} K(S_{opt} + \widehat{M}_{TLWC-SPF}) & , \ S_{opt} > 1 \\ K\widehat{M}_{TLWC-SPF} & , \ S_{opt} = 1 \end{cases} \tag{4.9}$$

$$optSwCost_{TLWC-SPF} = NK \times (NK + N\widehat{M}_{TLWC-SPF}) \tag{4.10}$$

In the following, we will evaluate the cost saving of TLWC-SPF. We will compare the cost of both WC and switch of TLWC-SPF with FWC and CWC-SPF. Setting CWC-SPF as a comparison standard is because CWC-SPF also uses SPF mode to share CWC and the switch architecture of both TLWC-SPF and CWC-SPF are quite similar. The theoretical analysis will show that, if using TLWC-SPF, the costs of both WC and switch, can be saved compared to FWC and/or even CWC-SPF.

The saving of WC of TWC-SPF against FWC, $\theta_1^{TLWC-SPF}$, can be expressed as in (4.11), where $WcCost_{FWC}$ is obtained via (3.1). The saving of WC against CWC-SPF, $\theta_2^{TLWC-SPF}$, can be expressed in (4.12), where $\min WcCost_{CWC-SPF}$ is obtained via (3.8) .

$$\theta_1^{TLWC-SPF} = (1 - \frac{optWcCost_{TLWC-SPF}}{WcCost_{FWC}}) \times 100\% \tag{4.11}$$

$$\theta_2^{TLWC-SPF} = (1 - \frac{optWcCost_{TLWC-SPF}}{\min WcCost_{CWC-SPF}}) \times 100\% \tag{4.12}$$

From above theoretical analysis of WC cost we know that by using TLWC-SPF, both PWC and CWC cooperate to convert optical data. In order to achieve dedicated performance if PWC is used, the needed number of CWCs will decrease. Thus, we expect that the number of CWCs used in TLWC-SPF is fewer than in

CWC-SPF. Then, the switching cost of TLWC-SPF should be less than that of CWC-SPF, because the switching cost is only determined by the number of CWCs. The saving of switch of TWC-SPF against CWC-SPF, $\theta_3^{TLWC-SPF}$, can be expressed as in (4.13), where $\min SwCost_{CWC-SPF}$ is obtained via (3.9)

$$\theta_3^{TLWC-SPF} = (1 - \frac{optSwCost_{TLWC-SPF}}{\min SwCost_{CWC-SPF}}) \times 100\% \tag{4.13}$$

From above results, we know that the theoretical results can predict simulation results very well. Therefore, in the following only theoretical results will be presented. Figure 4-5 and Figure 4-6 illustrates the theoretical plot of $\theta_1^{TLWC-SPF}$ and $\theta_2^{TLWC-SPF}$ against increasing number of wavelengths in the optical switching node respectively. It is clear from Figure 4-5 that with increasing K the WC savings increases. For example, about 40% wavelength converter savings can be achieved for a 32-wavelengths TLWC-SPF node compared to a FWC node.

Against the CWC-SPF architecture, Figure 4-6 shows that about 35% wavelength converter savings can be achieved. It is also noted that wavelength converter saving in both Figure 4-5 and Figure 4-6 is not very sensitive to the load, and this feature is very useful for the design of TLWC-SPF. This means that parameters S and M which are optimized, say for a high load scenario, can just as well be used in a low load scenario with similar percentage savings performance.
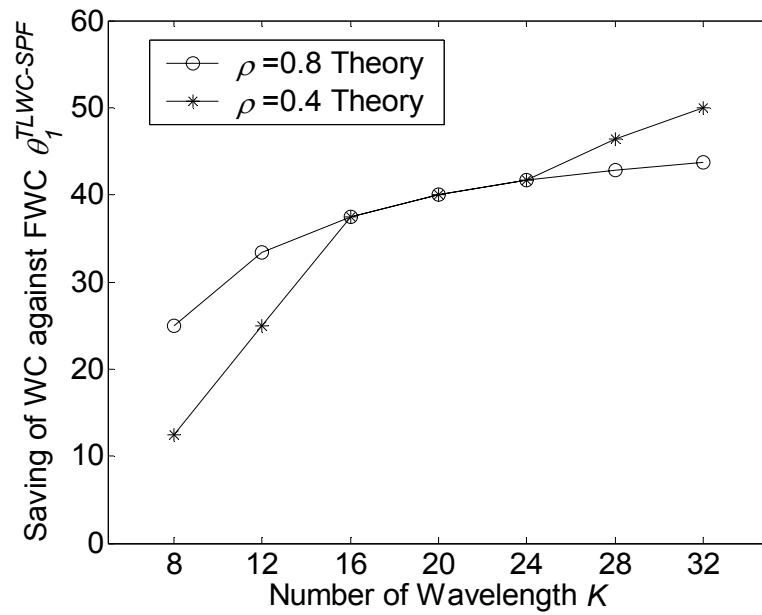
Figure 4-5:   Saving of WC of TLWC-SPF against FWC
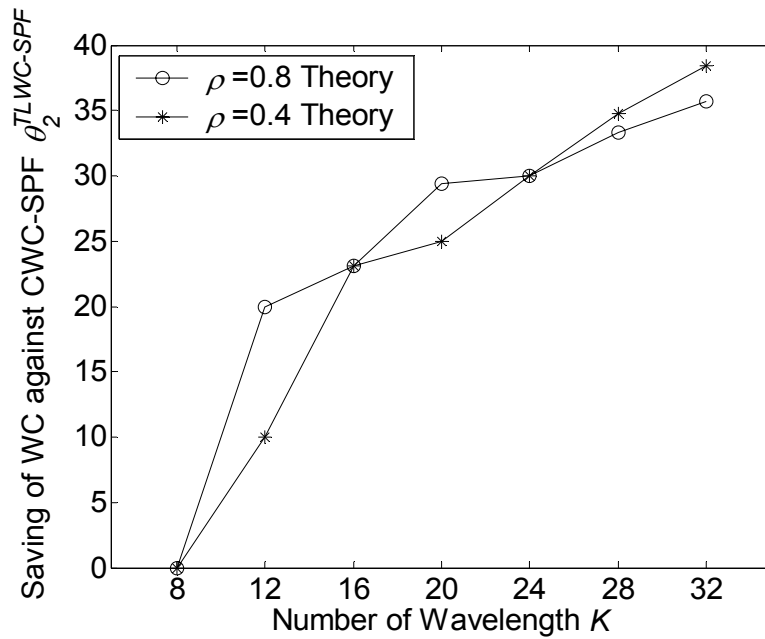
Figure 4-6:   Saving of WCs of TLWC-SPF against CWC-SPF architecture.
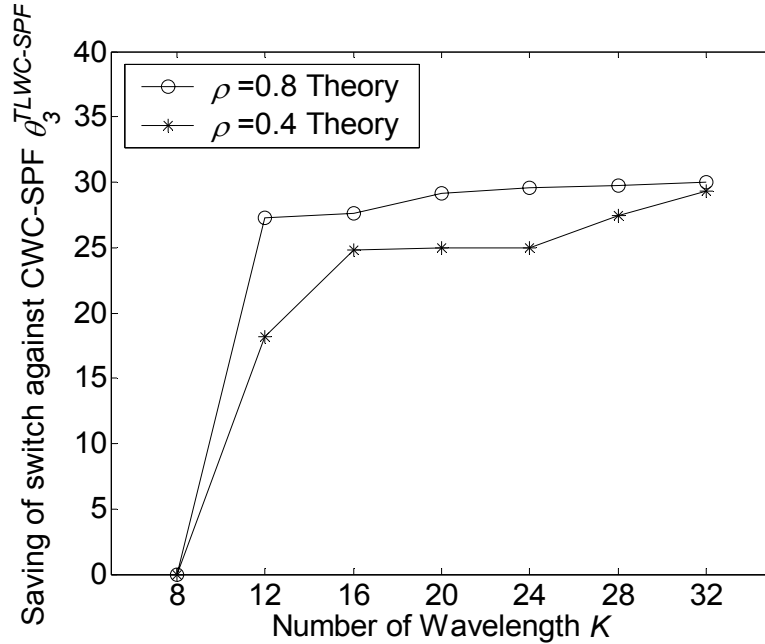
Figure 4-7:   Saving of switch of TLWC-SPF against CWC-SPF model.

Figure 4-7 shows the switch saving of TLWC-SPF against CWC-SPF can reach as high as 30%. High load scenario can save more switch than low load, since it needs fewer CWCs when S_{opt} applies. The switch saving is also not sensitive to traffic load, because of same reason stated above.

4.3   Architecture and analysis of TLWC-SPN

4.3.1   Architecture of TLWC-SPN

Similar to the architecture of TLWC-SPF, in TLWC-SPN every input wavelength has an associated PWC so that contention of PWC does not happen. On the other hand, CWC, an expensive device, is placed in a pool and shared by all

output fibers within one node. The definition of PWC used in TLWC-SPN is the same as TLWC-SPF and PWC-only, such as $d_1, d_2, S, \Omega(k),$ and $|\Omega(k,t)|$.

Figure 4-8 shows the architecture of a TLWC-SPN OS node. A conventional cross-bar switching fabric is assumed. In this architecture, the entire OS node share M number of CWCs, and every wavelength in each input fiber has one associated PWC. Therefore, there are K PWCs and M/N CWCs per output fiber. If Near-WC by the associated PWC is successful, the optical data will be switched to the output port. Otherwise, one CWC out of the M from the pool will be used to perform Far-WC; after the Far-WC, the optical data will be switched back to the output fiber. It should be noticed that when $S=1$, this means there is no PWC at all, and the TLWC-SPN node is reduced to CWC-SPN node.
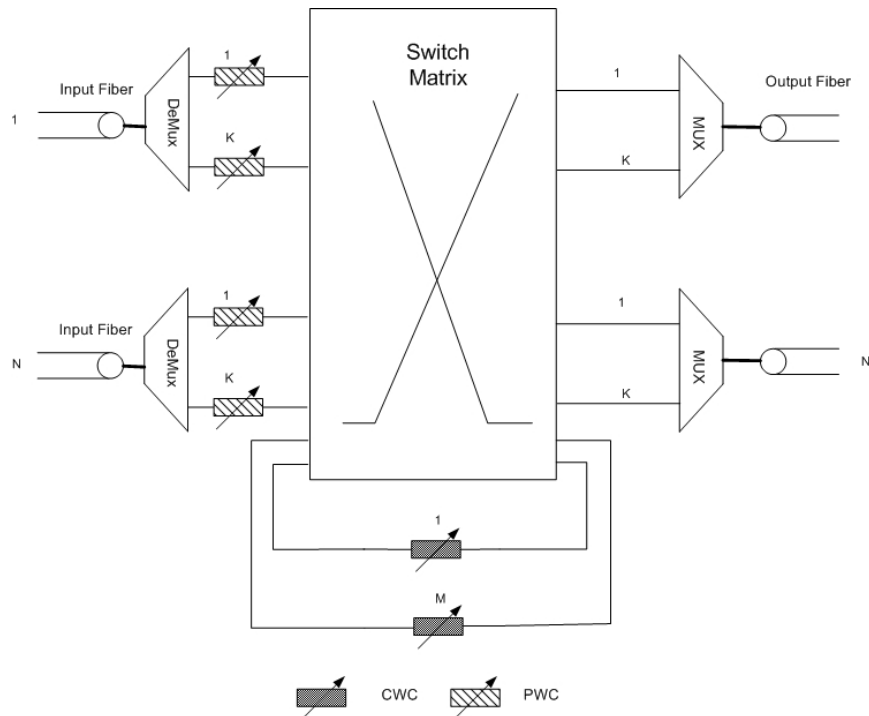
Figure 4-8:   Switch and conversion architecture of TLWC-SPN

Also, it should be noted that the TLWC-SPN switch fabric is non-blocking (cross-bar switch fabric). This means that it is not possible for the switch to drop optical data due to lack of switch resources. If optical data is dropped by the switch fabric then it must be due to the lack of output wavelengths or failure in the two-layer PWC/CWC wavelength conversion process. In TLWC-SPN the WC assignment algorithm is the same as TLWC-SPF shown in Figure 4-2.

4.3.2   Cost function of TLWC-SPN

Firstly, it should be noted that if all the PWC elements are removed in Figure 4-8, the resulting node is indeed a CWC-SPN node. The complexity of the TLWC-SPN switching fabric can be expressed as in (4.14), which is same as the CWC-SPN switching fabric as in (3.12), if M is the same in these two architecture.

$$SwCost_{TLWC-SPN} = (NK + M) \times (NK + M) \tag{4.14}$$

Similar to TLWC-SPF a simple linear cost function of PWC and CWC is used here. The general formula for the calculation of implementation cost of WC per output fiber in TLWC-SPN architecture is in (4.15). The reason why we use WC cost per fiber is that comparison between TLWC-SPN and TLWC-SPF can be made.

$$WcCost_{TLWC-SPN} = \begin{cases} MK/N + KS & , \ S > 1 \\ MK/N & , \ S = 1 \end{cases} \tag{4.15}$$

4.3.3 Theoretical analysis of TLWC-SPN using multi-dimensional Markov chain

It is noted that theoretical analysis of TLWC-SPN using multi-dimensional Markov chain is quite similar to that of CWC-SPN except a special parameter, α_i, which represent the function of PWC. Therefore, we expect here that the analysis of TLWC-SPN can also be similar to that of CWC-SPN. In the following the presentation of analysis of TLWC-SPN will be simplified, if the content is similar to that of CWC-SPN.

We denote λ_n as the optical data arrival rate of output fiber n ($1 \le n \le N$) so that the overall arrival rate at the node is $\lambda = \sum_n \lambda_n$, μ is the service rate of each wavelength. Therefore, the load on output fiber n is $\rho_n = \lambda_n /(K\mu)$, and the overall load on the node is $\rho = \lambda /(KN\mu)$. For generality we consider traffic as asymmetric which means that the traffic intensity λ_n on every output fiber may be different. We also assume that optical data arrive on each wavelength with equal probability, i.e., uniformly distributed amongst the wavelengths. In this thesis, we do not consider deflection routing.

We use (i_n, j_n) to indicate the state of the fiber n, where there are i_n wavelengths in use by optical data and j_n CWCs in use by some of these i_n wavelengths at the same time. It is clear that $0 \le j_n \le i_n \le K$ and $j_n \le \min(M,K)$. Thus, the state of a TLWC-SPN node is defined by $(i_1 j_1 ... i_n j_n ... i_N j_N)$. We now proceed to determine the state probability $P_{i_1 j_1 ... i_n j_n ... i_N j_N}$ of the state $(i_1 j_1 ... i_n j_n ... i_N j_N)$.

Theorem 4-5: the state probability $P_{i_1 j_1 \ldots i_n j_n \ldots i_N j_N}$ (for all valid states) can be obtained from the following simultaneous equations

$$\begin{cases} P_{i_1 j_1 \ldots i_n j_n \ldots i_N j_N} \times \sum_{n=1}^{N} (A_{i_n, j_n} + B_{i_n, j_n} + C_{i_n, j_n} + D_{i_n, j_n}) = \\ \sum_{n=1}^{N} \left\{ \begin{array}{l} A_{i_n-1, j_n} P_{i_1 j_1 \ldots (i_n-1) j_n \ldots i_N j_N} + B_{i_n-1, j_n-1} P_{i_1 j_1 \ldots (i_n-1), (j_n-1) \ldots i_N j_N} \\ + C_{i_n+1, j_n} P_{i_1 j_1 \ldots (i_n+1), (j_n-1) \ldots i_N j_N} + D_{i_n+1, j_n+1} P_{i_1 j_1 \ldots (i_n+1), (j_n+1) \ldots i_N j_N} \end{array} \right\} \\ \sum P_{i_1 j_1 \ldots i_n j_n \ldots i_N j_N} = 1 \quad \text{(for all } 0 \le j_n \le i_n \le K \text{ and } \sum_{n=1}^{N} j_n \le M) \end{cases} \quad (4.16)$$

where A_{i_n, j_n}, B_{i_n, j_n}, C_{i_n, j_n} and D_{i_n, j_n} are transition speeds for various scenarios to be described later

Proof:

In Markov chain analysis, like previous analyses in Chapter 3 and section 4.2, only outgoing transition is presented.

Case 1: From $(i_1 j_1 \ldots i_n j_n \ldots i_N j_N)$ to $(i_1 j_1 \ldots (i_n+1) j_n \ldots i_N j_N)$, when $i_n + 1 \le K$ for all $n \in [1, N]$. This scenario indicates the input optical data will be switched to the output fiber *n*, and the wavelength of the incoming optical data can be converted to an available output wavelength of the output fiber via a first layer PWC. The incoming optical data does not require any CWC to find a suitable output wavelength. Thus, the transition speed is $A_{i_n, j_n} = (1 - \alpha_{i_n}) \lambda_n$, where α_{i_n} is the same as the analysis in TLWC-SPF, representing the probability that for an input optical data arrival, say at a certain PWC, all the associated *S* consecutive output wavelengths of that PWC are already in use.

Case 2: From $(i_1 j_1 ... i_n j_n ... i_N j_N)$ to $(i_1 j_1 ... (i_n +1)(j_n +1) ... i_N j_N)$, when

$i_n +1 \leq K$ and $1 + \sum_{k=1}^{N} j_k \leq M$ for all $n \in [1, N]$. This case indicates that the input

optical data will be switched to the output fiber n, and that the wavelength of the

incoming optical data cannot be converted to an available output wavelength via a

PWC. Thus, the optical data has to use one available CWC to find a suitable output

wavelength. Thus, the transition speed is $B_{i_n, j_n} = \alpha_{i_n} \lambda_n$.

Case 3: From $(i_1 j_1 ... i_n j_n ... i_N j_N)$ to $(i_1 j_1 ... (i_n -1) j_n ... i_N j_N)$, when $i_n -1 \geq 0$

and $i_n > j_n$ for all $n \in [1, N]$. This case indicates that an optical data not using any

CWC has just been sent out completely from fiber n. As there are $i_n - j_n$ data not

using CWCs, the transition speed is therefore $C_{i_n, j_n} = (i_n - j_n)\mu$.

Case 4: From $(i_1 j_1 ... i_n j_n ... i_N j_N)$ to $(i_1 j_1 ... (i_n -1)(j_n -1) ... i_N j_N)$, when $i_n -1 \geq 0$

and $j_n -1 \geq 0$ for all $n \in [1, N]$. This case indicates that an optical data using one

CWC has just been sent out completely from fiber n. As there are j_n optical data

using CWCs, the transition speed is therefore $D_{i_n, j_n} = j_n \mu$.

Based on these four scenarios and the fact that the sum of all state

probabilities is equal to unity, simultaneous equations in (4.16) are obtained. It

should be noticed if the transition conditions specified in any of the above scenarios

are not satisfied, then the corresponding transition speeds A_{i_n, j_n}, B_{i_n, j_n}, C_{i_n, j_n} and

D_{i_n, j_n} are zero.

End proof

Corollary 4-5: From state probabilities $P_{i_1 j_1 \ldots i_n j_n \ldots i_N j_N}$, drop probability of the fiber n

can be written as

$$P_{Drop,n} = \sum_{i_1 j_1 \ldots i_N j_N} \left\{ \begin{array}{l} \sum_{i_n = j_n}^{K-1} \alpha_{i_n} \{ P_{i_1 j_1 \ldots i_n j_n \ldots i_N j_N} \mid \sum_{k=1}^{N} j_k = M \} + \\ \sum_{j_n = 0}^{\min(M,K)} \{ P_{i_1 j_1 \ldots i_n j_n \ldots i_N j_N} \mid i_n = K \} \end{array} \right\} \qquad (4.17)$$

Theorem 4-6 : The use of α_i in (4.6) to obtain the drop probability P_{drop} via (4.16)

and (4.17) will result in a lower bound of the actual drop probability of the OS node

using TLWC-SPN architecture. In other words, the actual α_i is larger than the

α_i given in (4.6), because of grouping tendency.

Proof

      Please refer to ***Theorem 4-2***

End proof

Theorem 4-7 : As S approaches K or M approaches to K, the approximation of α_i

in (4.6) becomes more accurate. If $M=K$ or $S=K$, the grouping tendency is removed

completely and α_i in (4.6) is the exact value.

Proof

      Please refer to ***Theorem 4-3***

End proof

Theorem 4-8 : If S=1, which means the TLWC-SPN node is reduced to a CWC-SPN node, the α_i in (4.6) is exact. Consequently, the analysis in ***Theorem 4-5*** is also exact.

Proof

Please refer to ***Theorem 4-4***.

End proof

Corollary 4-6: The simultaneous equations in (3.13) are theoretically solvable, but in practice, they are numerically intractable

Proof

Please refer to ***Corollary 3-4*** and ***Corollary 3-5***

End proof

4.3.4 Analysis of TLWC-SPN by multi-plane Markov chain using Randomized states method

Similar to the analysis of CWC-SPN, if using Randomized States (RS) method, the multi-dimensional Markov chain analysis for $(i_1 j_1 ... i_n j_n ... i_N j_N)$ can be reduced to multi-plane Markov chain analysis for (i_n, j_n). Before presenting the analysis several notations are introduced first.

W_n :   A random variable representing the number of CWCs currently in use at plane n (i.e., fiber n). It is clear that $0 \le W_n \le \min(K, M)$.

$\pi_n(t)$: Probability density function of W_n, i.e.,

$$\pi_n(t) = \Pr(W_n = t) = \sum_{i_n} P_{i_n, j_n = t} \tag{4.18}$$

ϕ_n: The sum total of CWCs in use but excluding those CWCs in use by plane n. Thus $\phi_n = \sum_{s \neq n} W_s$. As ϕ_n is the sum of several random variables W_s (where $s \neq n$), ϕ_n is a random variable itself that obeys some distribution.

$r_n(j_n)$: The probability that there is at least one CWC available, when currently there are j_n CWCs in use by fiber n. Hence,

$$r_n(j_n) = \Pr(\phi_n < M - j_n \mid W_n = j_n) \tag{4.19}$$

If random variables W_n are weakly correlated each other, then

$$\Pr(\phi_n = t) \approx conv(\pi_1(t), ..., \pi_{n-1}(t), \pi_{n+1}(t), ..., \pi_N(t)) \tag{4.20}$$

is a good approximation. Accordingly, $r_n(j_n)$ approximates to

$$\begin{aligned} r_n(j_n) &\approx \Pr(\phi_n < M - j_n) \\ &\approx \sum_{t=0}^{M-j_n-1} conv(\pi_1(t), ..., \pi_{n-1}(t), \pi_{n+1}(t), ..., \pi_N(t)) \end{aligned} \tag{4.21}$$

The approximation in (4.20) and (4.21) becomes an exact relationship if random variables W_n are independent. The scenario when random variables W_n are truly independent is when $M=NK$, i.e., there is no need to share CWCs since for every wavelength in the node there is always an available CWC for its use.

Theorem 4-9 : By virtue of the RS method, the state probability P_{i_n,j_n} (for all planes

n) can be obtained from the following system of equations

$$\begin{cases} (A_{i_n,j_n} + B'_{i_n,j_n} + C_{i_n,j_n} + D_{i_n,j_n})P_{i_n,j_n} = \\ A_{i_n-1,j_n}P_{i_n-1,j_n} + B'_{i_n-1,j_n-1}P_{i_n-1,j_n-1} + C_{i_n+1,j_n}P_{i_n+1,j_n} + D_{i_n+1,j_n+1}P_{i_n+1,j_n+1} \\ \sum_{i_n,j_n} P_{i_n,j_n} = 1 \quad \text{for each } n \in [1,N] \end{cases} \quad (4.22)$$

where A_{i_s,j_s}, B'_{i_s,j_s}, C_{i_s,j_s} and D_{i_s,j_s} are transition speeds for various scenarios to be

described later

Proof

Similar to the previous analysis in ***Theorem 3-4*** and ***Theorem 4-1***, for a

particular plane n, there are four transition cases to consider for state (i_n, j_n). They

are as follows:

Case 1: (i_n, j_n) to $((i_n+1), j_n)$, when $i_n + 1 \le K$. The transition speed

is $A_{i_n,j_n} = (1-\alpha_{i_n})\lambda_n$.

Case 2: (i_n, j_n) to $((i_n+1),(j_n+1))$, when $i_n + 1 \le K$ and $j_n \le \min(M,K)$. The

transition speed is now $B'_{i_n,j_n} = r_n(j_n)\alpha_{i_n}\lambda_n$.

Case 3: (i_n, j_n) to $((i_n-1), j_n)$, when $i_n - 1 \ge 0$ and $i_n > j_n$. The transition

speed is $C_{i_n,j_n} = (i_n - j_n)\mu$.

Case 4: (i_n, j_n) to $((i_n-1),(j_n-1))$, when $i_n - 1 \ge 0$ and $j_n - 1 \ge 0$. The

transition speed is $D_{i_n,j_n} = j_n\mu$.

It is noted that the difference between **_Theorem 4-5_** and this theorem is the case 2 transition speed from (i_n, j_n) to $(i_n + 1, j_n + 1)$.

End proof

The result in the above analysis is also applicable to general data size distribution. Please refer to the **Appendix**.

Corollary 4-7 *:* The number of state probability equations $V_{RS}^{(N)}$ in (4.22) is given by (4.23), and the system of equations (4.22) is solvable theoretically, if $r_n(j_n)$ is available.

$$V_{RS}^{(N)} = NV \tag{4.23}$$

Proof:

Please refer to **_Corollary 3-6_** and **_Corollary 3-7_**

End proof

Corollary 4-8: By solving state probability P_{i_n, j_n}, many useful parameters can be obtained as follows

$$P_{Drop,n} = \sum_{i_n \neq K, \ j_n} \sum (1 - r_n(j_n)) \alpha_{i_n} P_{i_n, j_n} + \sum_{j_n=0}^{\min(M,K)} P_{K, j_n} \tag{4.24}$$

In (4.24), the first term on the right side is the drop probability due to lack of CWC. We have to consider those new optical data arrivals which cannot find suitable wavelength via PWC when there are i_n wavelengths currently in use. This explains the α_{i_n} factor in (4.24). The factor $(1 - r_n(j_n))$ indicates the probability that there is no available CWC when a new optical data arrives at fiber *n*. The second

term represents the drop probability due to lack of available output wavelength. The overall drop probability of the node is thus as follows.

$$P_{TLWC-SPNdrop} = \sum_{n=1}^{N}(\lambda_n P_{Drop,n})/\sum_{n=1}^{N}\lambda_n \tag{4.25}$$

Similar to CWC-SPN, we can use (4.21) to estimate $r_n(j_n)$, leading to the system of equations in (4.22) be N^{th}-order polynomial. Therefore, **self-constrained iteration** (SCI) with **sliding window update** (SWU), is also applicable for the numerical calculation of TLWC-SPN. The SCI and SWU for TLWC-SPN are the same as CWC-SPN therefore, we will not present them here.

4.3.5   Numerical results of TLWC-SPN

This section presents numerical results to verify the usefulness of the RS method and the SCI SWU technique for obtaining TLWC-SPN theoretical results. The main theoretical results are the drop probability measures for which one can make design choices on the value of S and M so that performance of a TLWC-SPN architecture given some loading situations is on level par with a FWC architecture. At same time the cost of both WC and switch can be saved if TLWC-SPN architecture is used.

Similar to CWC-SPN we assume a general asymmetric traffic model whereby loading on each output fiber is different. Hence, the traffic intensity on a particular output fiber is thus $\lambda_n = \upsilon_n \lambda$, where the probability υ_n can be expressed as follows, where $Z \in [0,1)$ represents the range of variation.

$$\upsilon_n = \frac{1}{N}[(1-Z)+\frac{2Z(n-1)}{N-1}] \tag{4.26}$$

For the case of symmetric traffic, $Z=0$. When Z increases, the loading on output fibers with higher indexes is larger.

Figure 4-9 illustrates the overall drop probability performance plotted against increasing number of wavelength converters M under different load distribution factor Z. The FWC performance is the point on the extreme right (i.e., 16 and 128 CWCs for Figure 4-9 (a) and Figure 4-9 (b) respectively). The important design feature of Figure 4-9 is that the *x*-axis point corresponds to that minimum number of CWCs needed so that the corresponding drop probability performance at that point has negligible difference when compared to the drop probability performance at FWC condition. For example, for the case of light load conditions in Figure 4-9 (a), the theoretical curve has accurately predicted (i.e., gives the same result as the simulated curve) that the minimum number of CWCs needed is between 5 to 6 CWCs (depending on load distribution factor Z) to equal drop probability performance at FWC point of 16. For the case of high loading conditions the theoretical plots of Figure 4-9 (b) have also accurately predicted that the minimum number of CWCs needed is about 50 CWCs to equal drop probability performance at the FWC point of 128. In summary, it is not important whether the theoretical curve exactly coincides with the simulated curve as far as practical design considerations are concerned. What is clearly more important is whether the theoretical curves are able to accurately predict the minimum number of CWCs ensuring level-par performance with the FWC scenario. Hence the following conclusions can be made: the TLWC-SPN node can achieve similar performance as FWC and the RS method (plus the SCI and SWU technique) is indeed useful and accurate enough to perform this prediction.

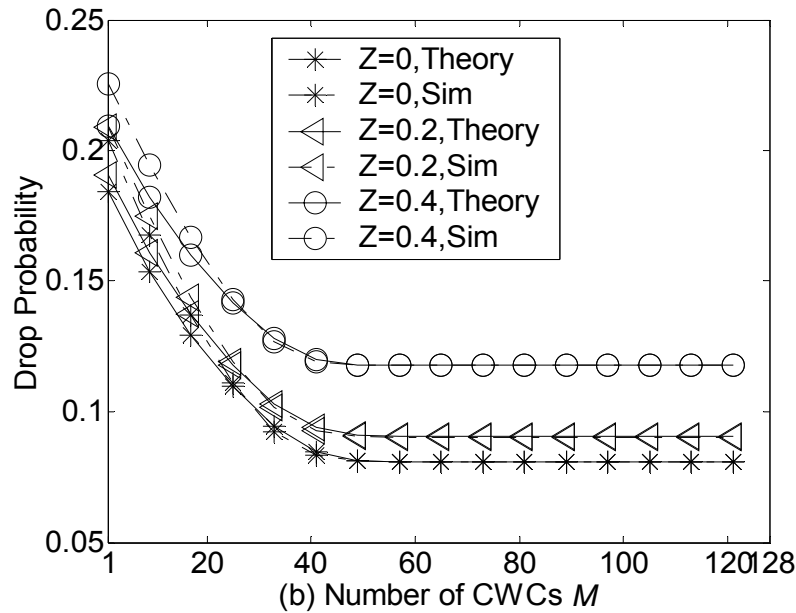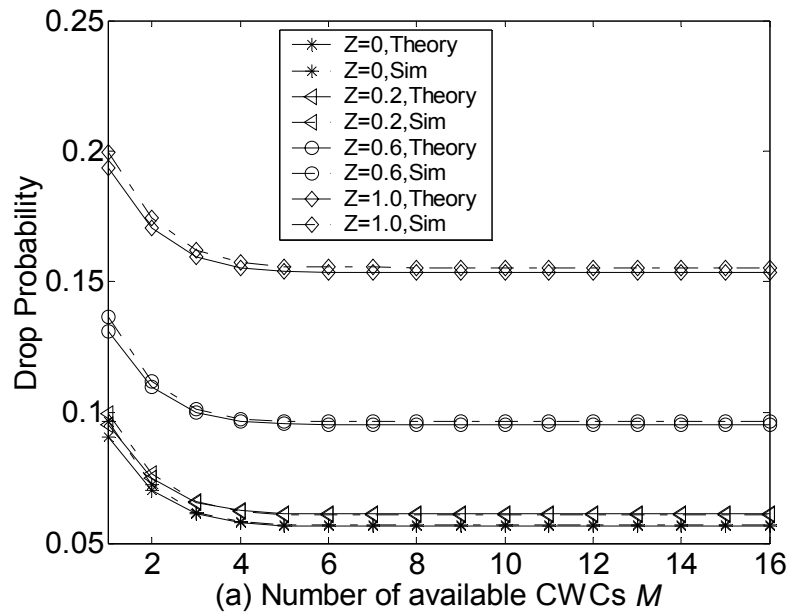Figure 4-9: Drop probability of TLWC-SPN with different number of output fibers, under asymmetrical traffic. (a) $N = 4$, $K = 4$, S=2, ρ=0.4, $Z = 0$, 0.2, 0.6, 1.0. (b) $N = 8$, $K = 16$, S=4, ρ= 0.8, $Z = 0$, 0.2, 0.4

It is also noted that in Figure 4-9, the higher the degree of traffic asymmetry

(i.e., higher Z), the higher is the drop probability. However, the minimum number of

CWCs ensuring level-par performance with the FWC scenario is still similar to the case where traffic is symmetric (i.e., the case where Z=0). Henceforth, for convenience and to reduce verbosity, Figure 4-10 and those above will present results only for the case of symmetric traffic, i.e., Z=0.

Figure 4-10 demonstrates the theoretical and simulated drop performance of TLWC-SPN under symmetrical load (i.e., Z=0) for different number of fibers within one OS node. Notice that as the number of CWCs per fiber (M/N) increases to K (i.e., 16), the drop performance of TLWC-SPN becomes closer and closer to FWC (which is the case M/N=16). Figure 4-10 also demonstrates that as S (i.e., the range of the PWC) increases, fewer CWCs are required to obtain performance similar to FWC. The result is obvious since increasing the range of the PWC results in less reliance on the use of a CWC. Figure 4-10 also demonstrates that the analytical results although providing approximated performance are very close to the simulated performance. As M increases the deviation between the analytical and simulated results becomes smaller. This is expected by virtue of **Theorem 4-7**

By comparing Figure 4-10 (a) and Figure 4-10 (b), we find that TLWC-SPN can approach to performance of FWC with fewer CWCs if N is larger. For S=2, if N=2, it needs 11 or 12 CWCs per fiber; if N=8, it needs only 8 or 9 CWCs per fiber. This is due to sharing efficiency of CWCs within the node. Therefore, it is expected that the saving of WC in TLWC-SPN will increase with N. Hence the following conclusions can be made: the TLWC-SPN node can achieve similar performance as FWC and the analytical model provides a good approximation to the drop performance of TLWC-SPN.
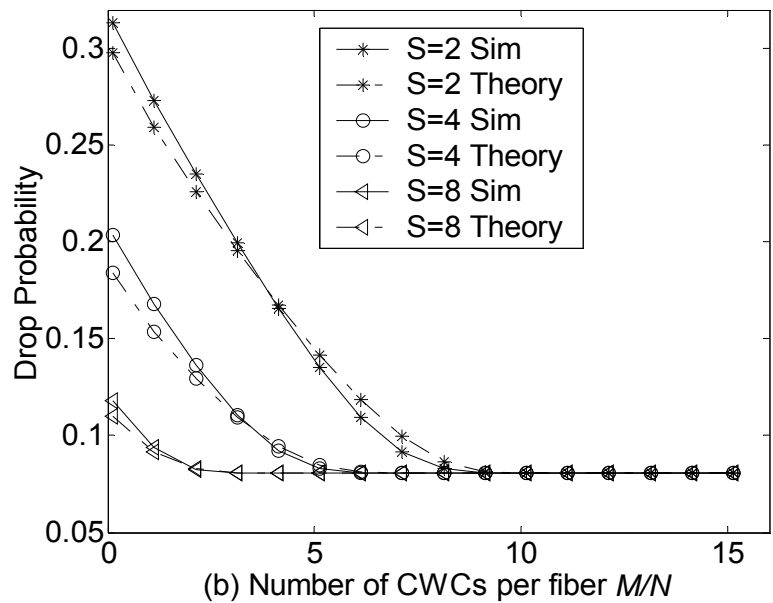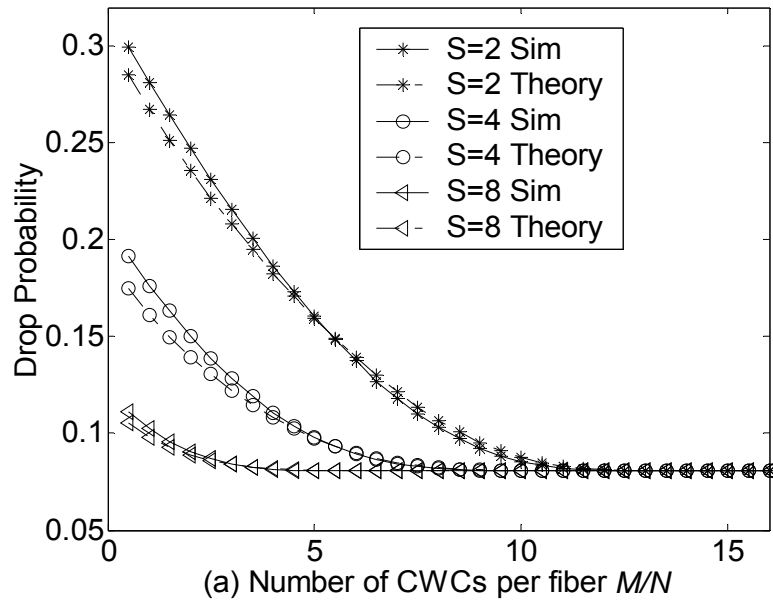
Figure 4-10: Drop Probability versus Number of CWCs in TLWC-SPN architecture. ρ=0.8, symmetric load, *K*=16, *M*=1 to 16 for different S=2, 4, 8. (a) N=2, (b) N=8.

From the above analyses we know that in TLWC-SPN system, for a given *S*,

if the number of available CWCs, i.e., *M*, increases, the drop probability of the

system decreases and approaches that of a FWC system. This means that with a certain PWC range and certain number of CWCs, the blocking performance of the TLWC-SPN system will approach that of a FWC system. A target performance threshold of the drop probability, like previous analyses for CWC-SPF/SPN and TLWC-SPF, is set to be achieved by the TLWC-SPN. Therefore, if $P_{TLWC-SPNdrop} / P_{FWCdrop} \leq \xi$, we consider that the TLWC-SPN can achieve similar performance as FWC.

For convenience, for a given S, we denote $\overline{M}_{TLWC-SPN,S}$ to be the minimum number of CWCs required for the TLWC-SPN architecture such that the performance threshold requirement is satisfied, i.e.,

$$\overline{M}_{TLWC-SPN,S} = \min\{M \mid P_{TLWC-SPNdrop,M} / P_{FWCdrop} \leq \xi, \text{ for a given } S\} \quad (4.27)$$

Accordingly, the minimum WC cost per fiber of TLWC-SPN for a given S can be expressed as

$$\min WcCost_{TLWC-SPN,S} = \begin{cases} K\overline{M}_{TLWC-SPN,S} / N + KS & , S > 1 \\ K\overline{M}_{TLWC-SPN,S} / N & , S = 1 \end{cases} \quad (4.28)$$
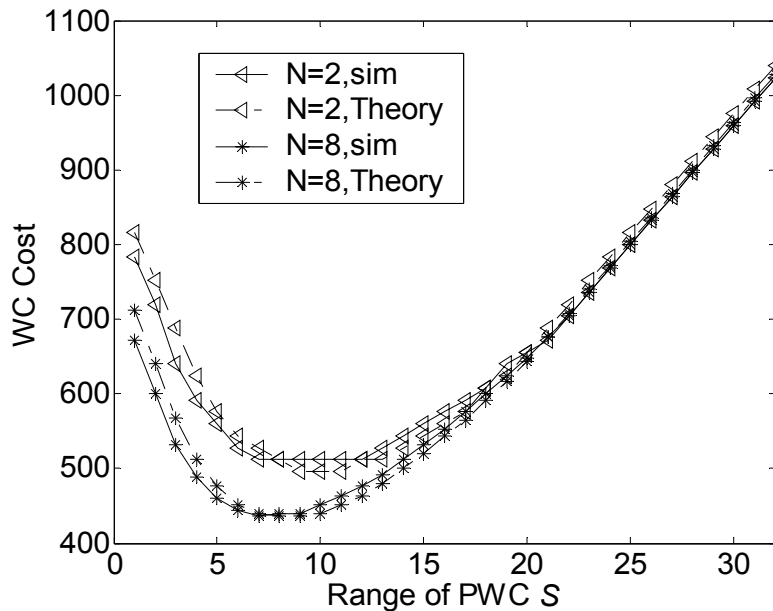
Figure 4-11: The cost of TLWC-SPN against the range of PWC for ρ =0.8 symmetrical load. K=32 N = 2, 8.

Figure 4-11 plots the minimum cost of TLWC-SPN against S for different number of wavelengths (K=16 and K=32) to achieve threshold performance via (4.28) for theoretical results. In this figure, when S=1, it should be noted that the TLWC-SPN node is reduced to a CWC-SPN node. In the figure, for given S, equation (4.27) is first used to find the minimum number, i.e., $\overline{M}_{TLWC-SPN,S}$, of CWCs required so that the performance threshold is achieved. Thereafter the cost formula in (4.28) is used to obtain the cost. The cost is U-shaped for the following reasons: when S is small the cost of WC is dominated by the need for more CWCs since PWC range is too small to create a significant impact; when the PWC range increases, there is no need for that many CWCs as before and hence the overall cost drops. But as the range of PWC is further enlarged, the PWC element becomes more like a CWC element. This will cause overall cost to rise again.

Therefore, from Figure 4-11, we can see clearly that there is an optimal S, S_{opt}, which achieves the lowest wavelength conversion cost for TLWC-SPN while maintaining the desired drop performance. Note that for the S_{opt}, the wavelength conversion cost is lower than the CWC-SPN wavelength conversion cost (i.e., the left starting point of the U-shape plot). It is also clear that there are many values of S resulting in minimum TLWC-SPN cost because the cost function is an integer result. Hence there are many S and M combinations meeting the minimum cost criteria.

We term $\overline{M}_{TLWC-SPN,S}$ at S_{opt} as $\widehat{M}_{TLWC-SPN}$. Therefore, when S_{opt} and $\widehat{M}_{TLWC-SPN}$ are used as a optimal configuration for TLWC-SPN, the optimal WC cost, $optWcCost_{TLWC-SPN}$, is expressed in (4.29). The switch cost, $optSwCost_{TLWC-SPN}$, is expressed in (4.30)

$$
\begin{aligned}
optWcCost_{TLWC-SPN} &= \min\{\min WcCost_{TLWC-SPN,S} \mid \text{ for all } S\} \\
&= \begin{cases} K(S_{opt} + \widehat{M}_{TLWC-SPN} / N) &, S_{opt} > 1 \\ K\widehat{M}_{TLWC-SPN} / N &, S_{opt} = 1 \end{cases}
\end{aligned}
\tag{4.29}
$$

$$
optSwCost_{TLWC-SPN} = (NK + \widehat{M}_{TLWC-SPN}) \times (NK + \widehat{M}_{TLWC-SPN})
\tag{4.30}
$$

Similar to the analysis of TLWC-SPF we will compare the cost of both WC and switch of TLWC-SPN with FWC and CWC-SPN. Setting CWC-SPN as a comparison standard is because CWC-SPN also uses SPN mode to share CWC, and the switch architecture of both TLWC-SPN and CWC-SPN are quite similar. The theoretical analysis will show that if using TLWC-SPN, the costs of both WC and switch can be saved compared to FWC and/or even CWC-SPN. As shown in the above figures the theoretical results coincide with simulation results very well, and only theoretical results will be presented in the following.

The saving of WC of TWC-SPN against FWC, $\theta_1^{TLWC-SPN}$, is expressed in (4.31), where $WcCost_{FWC}$ is obtained via (3.1). The saving of WC against CWC-SPN, $\theta_2^{TLWC-SPN}$, is expressed in (4.32), where $\min WcCost_{CWC-SPN}$ is obtained via (3.26). The saving of switch of TWC-SPN against CWC-SPN, $\theta_3^{TLWC-SPN}$, is expressed in (4.13), where $\min SwCost_{CWC-SPN}$ is obtained via (3.27)

$$\theta_1^{TLWC-SPN} = (1 - \frac{optWcCost_{TLWC-SPN}}{WcCost_{FWC}}) \times 100\% \tag{4.31}$$

$$\theta_2^{TLWC-SPN} = (1 - \frac{optWcCost_{TLWC-SPN}}{\min WcCost_{CWC-SPN}}) \times 100\% \tag{4.32}$$

$$\theta_3^{TLWC-SPN} = (1 - \frac{optSwCost_{TLWC-SPN}}{\min SwCost_{CWC-SPN}}) \times 100\% \tag{4.33}$$

The final set of results focuses on WC and switch savings made possible by TLWC-SPN compared to CWC-SPN and FWC.
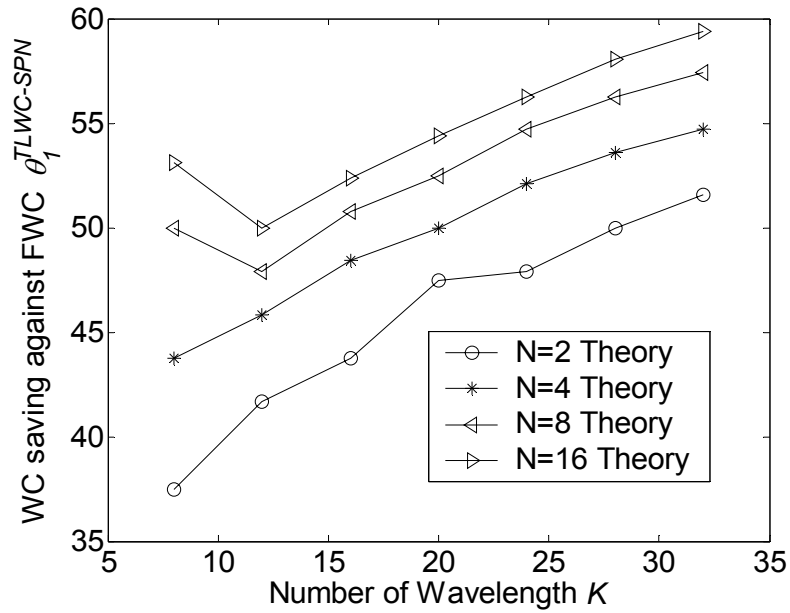
Figure 4-12:   Saving of wavelength conversion of TLWC-SPN against FWC under different number of fibers, symmetric traffic at $\rho = 0.8$.
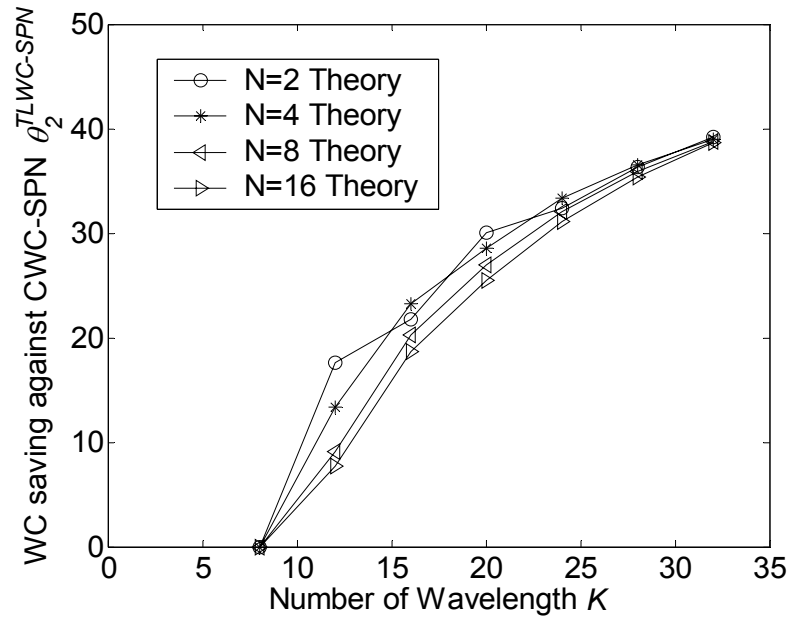
Figure 4-13:   Saving of wavelength conversion of TLWC-SPN against CWC-SPN, under different number of fibers, symmetric traffic at $\rho = 0.8$.

Figure 4-12 and Figure 4-13 illustrate the theoretical plot of $\theta_1^{TLWC-SPN}$ and $\theta_2^{TLWC-SPN}$ respectively under different number of output fibers at high loading scenario $\rho = 0.8$. It is clear from these two figures that with increasing K, the WC savings increases. The exception to this is in Figure 4-12 (comparison with FWC) for the scenario N large and K small. There is a reason for this: when N is large and K is small, the optimal combination of TLWC-SPN is that more CWCs are required to cover the lack of PWC range (due to small K). Therefore, the cost of TLWC is dominated by CWCs. This explains why savings curves of TLWC-SPN decreases under this scenario, as shown Figure 3-14, where we can see that the using of only CWC will cause the saving to decrease against the increasing of K. When K is increases the optimal combination of TLWC-SPF need fewer number of CWC but with a higher PWC range. Therefore, the cost of TLWC-SPN is dominated by PWC. Thus, the saving of WC increases again. On the other hand, for small N, the CWC saving feature is always dominated by PWC. That's why the saving of WC always increases against K for small N.

From Figure 4-12 it is clear that about 60% wavelength converter savings can be achieved for a 32-wavelength TLWC-SPN node compared to a FWC node for N=16. Wavelength converter saving against CWC-SPN, i.e $\theta_2^{TLWC-SPN}$ is shown in Figure 4-13. About 40% wavelength converter savings can be achieved additionally in TLWC-SPN.
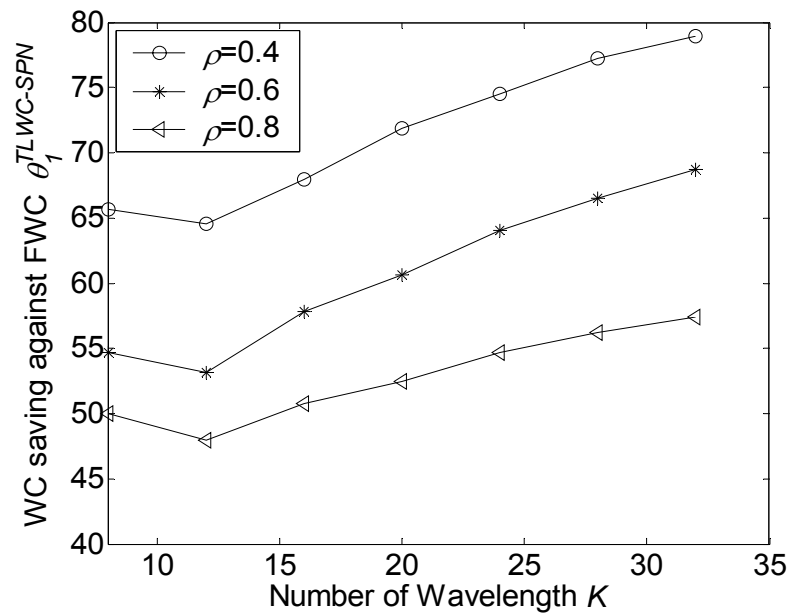
Figure 4-14: Saving of wavelength conversion of TLWC-SPN when N=8 for different load, compared to FWC
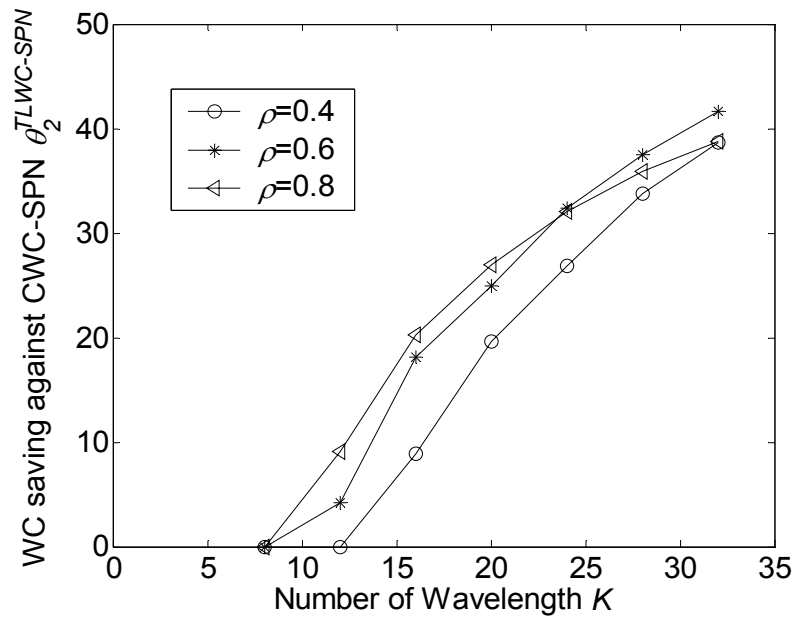
Figure 4-15: Saving of wavelength conversion of TLWC-SPN when N=8 for different load, compared to CWC-SPN.

Figure 4-14 and Figure 4-15 illustrate the theoretical plot of $\theta_1^{TLWC-SPN}$ and $\theta_2^{TLWC-SPN}$ respectively, under different load. Figure 4-14 shows that after suffering a slight dip in WC cost savings, the WC cost saving increases with increasing K. The reason for the slight dip is similar to the reason provided for Figure 4-12. Figure 4-15 also shows similar levels of relative cost saving compared to Figure 4-13 are seen to be achievable.
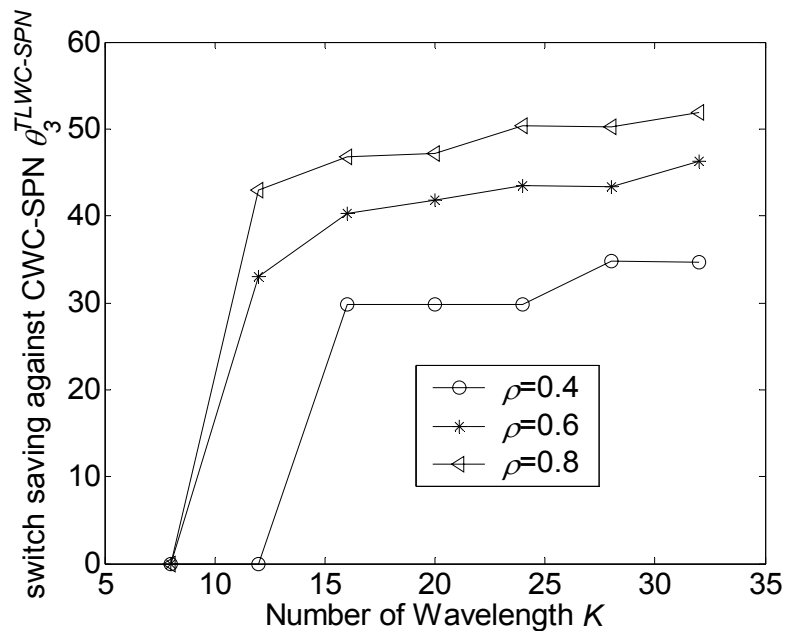
Figure 4-16:   Switch saving of TLWC-SPN when N=8 for different load compared to CWC-SPN model

Finally, Figure 4-16 illustrates switch fabric saving of TLWC-SPN compared to CWC-SPN, i.e., $\theta_3^{TLWC-SPN}$ in (4.33). Figure 4-16 shows that by using TLWC-SPN nearly half of switch can be saved even at high load scenario. Figure 4-16 also shows that saving of switch at high load is even better than at low load. This is because at high load S_{opt} is larger, so that $\widehat{M}_{TLWC-SPN}$ is significantly fewer than

$\overline{M}_{CWC-SPN}$; at low loads S_{opt} is smaller, so that $\overline{M}_{CWC-SPN}$ is comparable to $\overline{M}_{CWC-SPN}$.

4.4   Comparison of TLWC-SPF/SPN and CWC-SPF/SPN

Till now, all five NFWC architectures have been contributed and studied. The results show that PWC-only architecture is not suitable to achieve similar performance as FWC. Therefore in this section, we will compare the cost of both switch and WC for the remaining of the four architectures: CWC-SPF, CWC-SPN, TLWC-SPF, and TLWC-SPN.

For this comparison we use normalized cost function which is compared to the cost of FWC. For WC cost we use cost per fiber, while for switch cost we use the overall switch cost. The followings are the switch and WC cost of FWC.

$$WcCost_{FWC} = K \times K$$

$$SwCost_{FWC} = NK \times NK$$

Then, we will compare the costs of all the four architectures based on the costs normalized to FWC as follows.

$$NormWcCost_{CWC-SPF} = \frac{\min WcCost_{CWC-SPF}}{WcCost_{FWC}} \qquad (4.34)$$

$$NormSwCost_{CWC-SPF} = \frac{\min SwCost_{CWC-SPF}}{SwCost_{FWC}} \qquad (4.35)$$

$$NormWcCost_{CWC-SPN} = \frac{\min WcCost_{CWC-SPN}}{WcCost_{FWC}} \qquad (4.36)$$

$$NormSwCost_{CWC-SPN} = \frac{\min SwCost_{CWC-SPN}}{SwCost_{FWC}} \qquad (4.37)$$

$$NormWcCost_{TLWC-SPF} = \frac{optWcCost_{TLWC-SPF}}{WcCost_{FWC}} \qquad (4.38)$$

$$NormSwCost_{TLWC-SPF} = \frac{optSwCost_{TLWC-SPF}}{SwCost_{FWC}} \qquad (4.39)$$

$$NormWcCost_{TLWC-SPN} = \frac{optWcCost_{TLWC-SPN}}{WcCost_{FWC}} \qquad (4.40)$$

$$NormSwCost_{TLWC-SPN} = \frac{optSwCost_{TLWC-SPN}}{SwCost_{FWC}} \qquad (4.41)$$

From the above equations it can be seen that all normalized switch costs are larger than unity, while all normalized WC costs are less than unity. Figure 4-17 and Figure 4-18 show the theoretical normalized costs of WC and switch respectively, for N=8, $\rho = 0.8$. Figure 4-17 shows that TLWC-SPN always uses least WC cost, and CWC-SPN uses second-least WC cost when K is smaller. In contrast, TLWC-SPF will use second-least WC cost when K is larger. CWC-SPF always uses most WCs. In addition, the WC cost of TLWC-SPF/SPN tends to decrease with increasing K, while CWC-SPF/SPN tends to increase. Such observations are consistent with the trend shown in Figure 3-6 for CWC-SPF, Figure 3-14 for CWC-SPN, Figure 4-5 for TLWC-SPF and Figure 4-12 for TLWC-SPN.
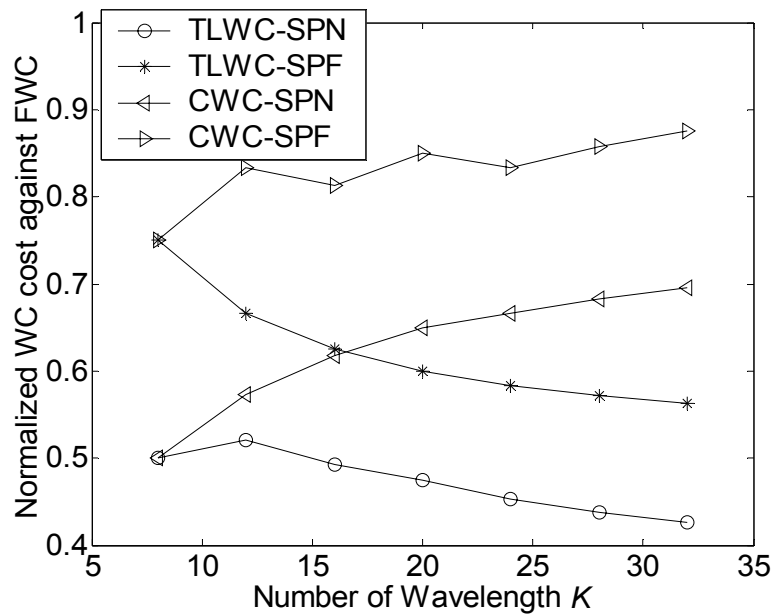
Figure 4-17: Normalized WC costs for all four NFWC architectures at *N*=8, $\rho = 0.8$
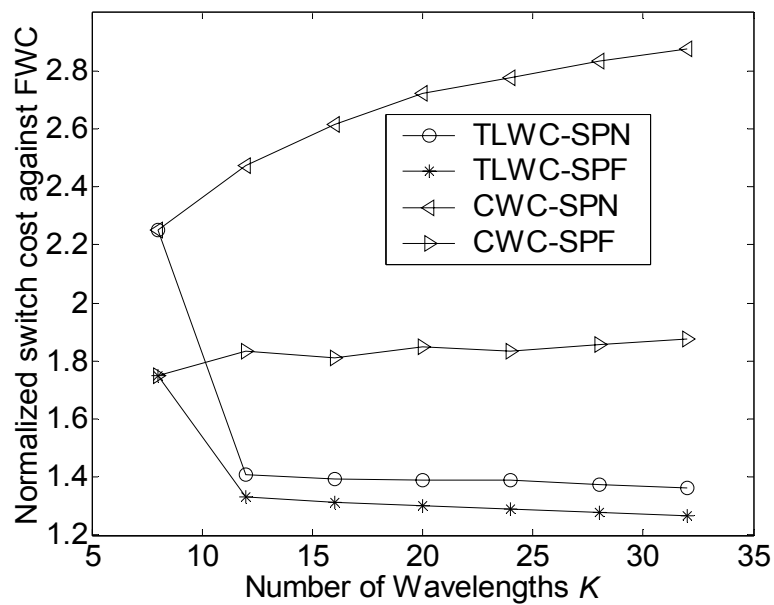
Figure 4-18: Normalized switch costs for all four NFWC architectures at *N*=8, $\rho = 0.8$

Figure 4-18 shows that TLWC-SPF always uses the least switch cost, and TLWC-SPN follows TLWC-SPF closely. CWC-SPN uses the most switch cost, and CWC-SPF uses second-most switch cost. The switch cost relationship between CWC-SPN and CWC-SPF coincides with our statement in Chapter 1, because SPN uses more switch to get the better sharing efficiency of wavelength converters. The switch cost relationship between TLWC-SPN and TLWC-SPF substantiates this statement as well.

From both Figure 4-17 and Figure 4-18 we can conclude that because of better architecture, TLWC-SPF/SPN always outperforms CWC-SPF/SPN, in terms of switch and WC costs. In terms of WC saving, TLWC-SPN is better than TLWC-SPF; while in terms of switch saving, TLWC-SPF is better than TLWC-SPN. Therefore, the choosing between TLWC-SPF and TLWC-SPN will depend on the real costs relationship between WC and switch. If cost of WC is dominated, TLWC-SPN is preferable; if cost of switch is dominated, TLWC-SPF is better.

4.5 Summary of TLWC

In this chapter, a novel two-layer wavelength conversion optical switching node operating in both share-per-fiber and share-per-node architectures, TLWC-SPF and TLWC-SPN, is contributed. In TLWC, PWC is used as the first layer to perform Near-WC and CWC is used as the second layer to perform Far-WC; thus the combination is more efficient than the CWC-SPF/SPN architectures.

For TLWC-SPF a two-dimensional Markov-chain analysis was presented to provide a tight lower bound theoretical drop performance of the TLWC-SPF architecture. Numerical studies demonstrated the closeness of the theoretical results

with actual simulated results, and also demonstrated how the theoretical results can be used to design TLWC-SPF nodes to achieve the best possible wavelength conversion savings compared to FWC architecture and CWC-SPF architecture. If compared to the FWC node, as high as 40% wavelength converter savings with TLWC-SPF can be achieved even at high load. If compared to CWC-SPF, TLWC-SPF architecture can achieve as high as 35% wavelength converter savings even in high load scenarios like $\rho = 0.8$. Finally, although the TLWC-SPF node has similar switch fabric architecture with the CWC-SPF node, the TLWC-SPF can save around 30% switch fabric because TLWC-SPF uses fewer CWCs.

A multi-dimensional Markov-chain describing the mechanics of a TLWC-SPN system is presented. Due to the complexity of multi-dimensional Markov chain analysis a set of methods namely, Randomized States, Self-Constrained Iteration with Sliding Window Update, were used. These methods dramatically reduce the multi-dimensional problem to a numerically tractable problem where a series of seemingly unrelated two-dimensional Markov chain problems are solved. Numerical studies demonstrated the closeness of the theoretical results with actual simulated results, and how the theoretical results can be used to design TLWC-SPN nodes to achieve the best possible wavelength conversion savings compared to FWC and CWC-SPN. Our numerical results demonstrated that WC savings as high as 80% can be achieved for low load conditions like $\rho = 0.4$ and sometimes as high as 55% for high load conditions like $\rho = 0.8$, compared to FWC. If compared to CWC-SPN, TLWC-SPN can save 40% more than CWC-SPN. Finally, although the TLWC-SPN architecture has similar switch fabric structure with the CWC-SPN node, the

TLWC-SPN node can save more switch cost since the TLWC-SPN uses fewer CWCs than CWC-SPN. The saving percentage is between 30-50%.

Comparison between TLWC-SPF and TLWC-SPN shows that the TLWC-SPN architecture always saves more WC than the TLWC-SPF architecture at the expense of a slightly more switch fabric costs.

4.6   Network performance evaluation for NFWC architectures

So far, performance evaluations for all NFWC architectures have been limited to a single node scenario. In this section, simulation results on NFWC architectures employed in a network environment are demonstrated.

The network environment of choice is the well-known NSF network of Figure 4-19 with asymmetrical traffic. Every node pair has a traffic flow, and the traffic intensity of the flow is proportional to the population density corresponding to the pair of the cities which the nodes represent. All nodes in the NSF network act as core nodes (i.e. forwards traffic originating from other nodes) as well as act as edge nodes (traffic originates or terminates from/into the node). Each flow finds a route to the destination by a shortest-path algorithm. For a particular load scenario, the relevant theoretical analysis model (as already presented in the previous sections/chapters) is used to calculate an optimal WC configuration to achieve similar performances as a FWC node. This WC configuration is then used to simulate the network performance. In this network-wide simulation, four NFWC architectures: CWC-SPF, CWC-SPN, TLWC-SPF and TLWC-SPN, are presented.
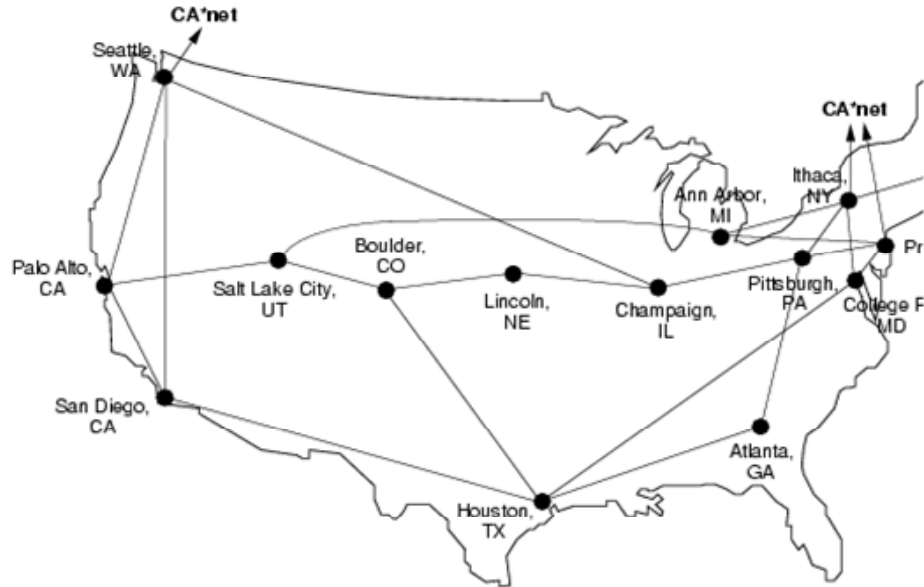
Figure 4-19:   NSF network topology

Figure 4-20 shows the NSF network's overall drop probability, defined as the ratio of overall dropped data in the network to the overall data fed into the network. The "load factor" used in this figure is not the same as the load factor used in previous chapters. This parameter is used to indicate the whole network's traffic intensity rather than the traffic load at each individual node. From this figure, it is noticed that with the optimal WC configurations employed in all the four NFWC architectures, there is not much differences in the drop performances. While the FWC architecture always achieves the lowest drop probability, the performance of the optimized NFWC architectures is not far from that of the FWC architecture. It should be noted that the optimal WC configuration for each node was designed independently of other nodes. As the traffic intensity for each node is known *a priori*, the usual threshold drop probability measure was used in each node to obtain its optimal WC configuration. This means that the WC optimization procedure for an individual node can just as well be applied in a network scenario.

Figure 4-21 shows the WC costs of the four NFWC architectures under the same simulation scenario as Figure 4-20. From the figure, we can find that the WC costs of the four NFWC architectures are different. The savings order beginning from the architecture with the highest saving is: TLWC-SPN, CWC-SPN, TLWC-SPF and CWC-SPF. The WC cost of TLWC-SPN is the lowest and this is consistent with our observation in Section 4.5. The reason why TLWC-SPF does not outperform CWC-SPN (as it is shown in Section 4.5) in the network-wide simulation scenario is as follows. The traffic load used in this simulation is not high, consequently, the sharing efficiency in CWC-SPN is very high, and this is coupled with the fact that the WC cost of CWC-SPN is lower than that TLWC-SPF. In addition, we can see that when the load increases, the cost of TLWC-SPF is shows a decreasing trend while the cost of CWC-SPN is always increasing. As the load factor increases, the savings in TLWC-SPF will eventually catch up with the savings in CWC-SPN.

In Figure 4-21, it is noted that when the load is extremely low, the WC costs of TLWC-SPN and CWC-SPN are very close. This is because when the load is low, S_{opt} in TLWC-SPN tends to be 1, which means the optimal configuration of TLWC-SPN tends to be CWC-SPN.

Figure 4-22 illustrates the switch cost of the NFWC architectures under the same simulation scenario as Figure 4-20. The results are consistent with earlier results presented in Figure 4-18 where it was demonstrated that TLWC-SPF can save the most switch costs compared to all other architectures.

Table 4-1 shows the WC configuration of NSF network when load factor is 3. The average number of CWC and the average range of PWC are shown in the table.

From the table, we can find that CWC-SPN architecture uses much less number of CWCs than CWC-SPF, since SPN architecture has better sharing efficiency. However, we cannot find similar scenario for TLWC, where the number of CWCs used in TLWC-SPN is much higher than TLWC-SPF. This is because in TLWC-SPF, larger range of PWC is used to compensate less number of CWCs. In overall by using the optimal configuration of PWC and CWC, the cost of TLWC-SPN is still better than TLWC-SPF, which is consistent with the results in previous sections.

From the network-wide simulations, it is clear that the single node theoretical analysis method can just as well be used in a network scenario. It is clear from the network-wide simulations that with the new cost saving NFWC architectures, similar performances as the FWC architecture can be achieved with WC costs just a fraction of the WC costs associated with the FWC architecture.
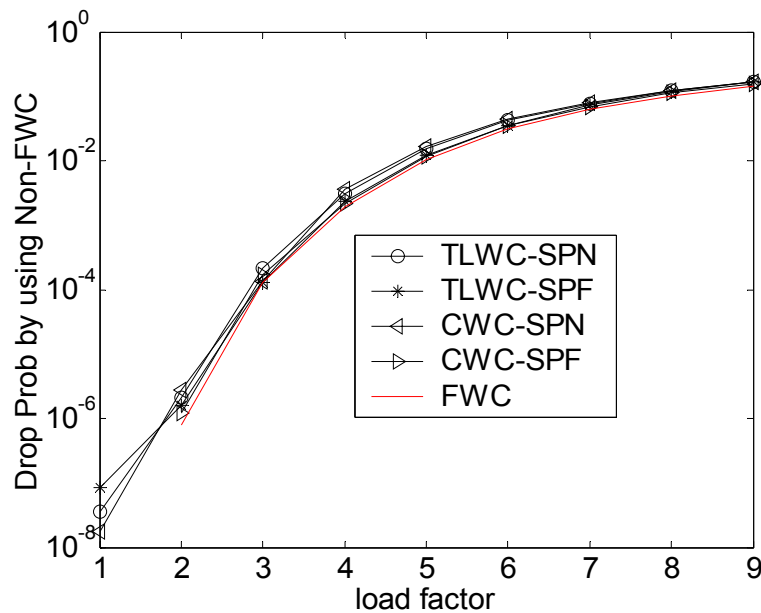
Figure 4-20: The overall drop probability of NSF network for different load and different NFWC architectures, *K=16*.
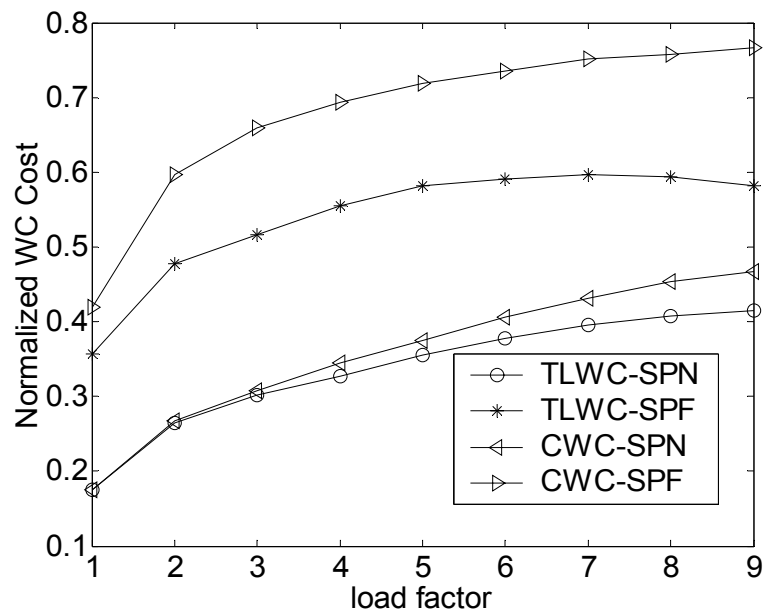
Figure 4-21:   Normalized WC cost in NSF network for different load
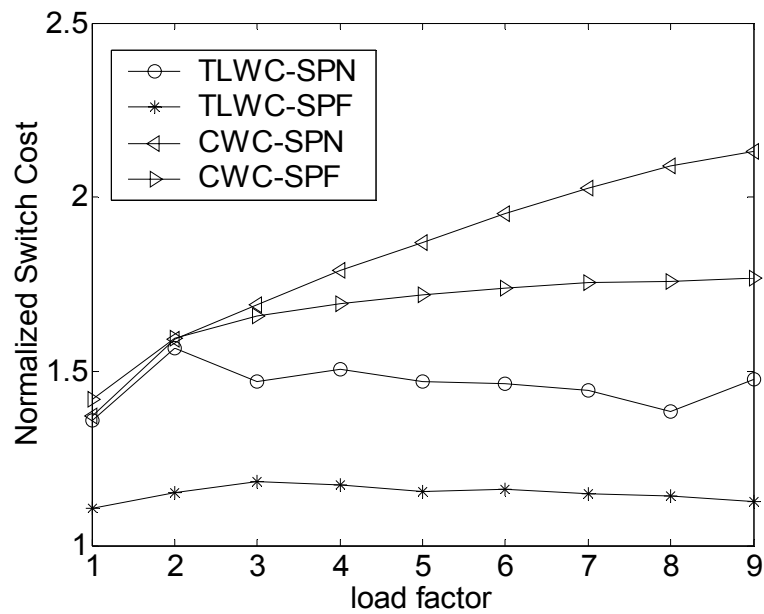
Figure 4-22:   Normalized switch cost in NSF network for different load

Table 4-1:   Comparison of WC configuration for different NFWC architectures under load factor =3 in NSF network

	FWC	CWC-SPF	CWC-SPN	TLWC-SPF	TLWC-SPN
Average number of CWC per link	16	10.5476	4.9286	2.9286	3.3333
Average range of PWC	N/A	N/A	N/A	5.3333	2.0476

5   Conclusions and Future Research

5.1   Conclusions

There are two major objectives in the work reported in this thesis. The first is to design a new NFWC architecture which can save more wavelength converters, compared to existing architectures like PWC-only, CWC-SPF and CWC-SPN. By combining PWC and CWC into a single architecture, we obtain a novel architecture called two-layer wavelength conversion (TLWC). In the TLWC architecture, PWCs available for each input wavelength form the first layer; while CWCs using some sharing policies form the second layer. According to different sharing policies, there are two kinds of TLWC: TLWC-SPF and TLWC-SPN. By assigning Near-wavelength conversion responsibilities to the PWC layer and Far-wavelength conversion responsibilities to the CWC layer, the cost of WC can be saved dramatically, compared to CWC-SPF/SPN architectures. When the cost of WC is reduced the switch fabric cost can also be further reduced. Therefore, TLWC-SPF/SPN savings always outperform CWC-SPF/SPN savings.

The other major objective of the work reported in this thesis is the development of a set of theoretical models under asynchronous traffic for different Non-Full wavelength conversion architectures. These include PWC-only, CWC-SPF, CWC-SPN, TLWC-SPF, and TLWC-SPN architectures. This has been achieved using Markov chain analysis. For the PWC-only architecture, both upper and lower bounds drop performance of the system were presented. Two-dimensional Markov chain analyses were contributed to achieve exact theoretical results and tight lower bound theoretical result for CWC-SPF and TLWC-SPF architecture respectively.

For both CWC-SPN and TLWC-SPN architectures, a new multi-plane Markov chain analytical model using Randomized States (RS) method, Self-Constrained Iteration and Sliding-Window Updating, were contributed to solve for the solution. Numerical results demonstrated that the contributed model was able to predict accurately how many wavelength converters can be saved using TLWC architecture compared to the FWC architecture.

In view of all the results presented in the earlier chapters, the following Table 5-1 compares all these five possible NFWC architectures, in terms of WC cost, switch fabric cost, and drop performance. From the table, we conclude that TLWC-SPN has the lowest WC cost, with an acceptable switch cost, and may be the best choice among all possible NFWC architectures.

Table 5-1:   Comparison of all NFWC architectures

Architectures	Switch Cost	WC Cost	Performance
PWC-only	Low	High	Poor
CWC-SPF	Middle	Middle-high	Good
CWC-SPN	High	Middle	Good
TLWC-SPF	Low-Middle	Low-middle	Good
TLWC-SPN	Low-Middle	Low	Good

The theoretical analytical models contributed in this thesis are also helpful for the OS designer to predict the performance of NFWC architectures and obtain optimized configuration for the switch fabric and the WC architecture.

5.2 Future research

5.2.1 Theoretical analysis of synchronous traffic for TLWC-SPF/SPN architectures

Another important traffic scenario often encountered in OS networks is the synchronous slotted traffic. Currently, analysis for the TLWC-SPF/SPN architecture under synchronous slotted traffic is not available. This work may be similar to the theoretical work on CWC-SPF/SPN under synchronous slotted traffic by Eramo in [77]-[80]. We expect that the WC saving percentage of TLWC-SPF/SPN under synchronous slotted traffic to be similar to the WC saving percentage under asynchronous traffic.

5.2.2 Theoretical analysis of NFWC when FDL is used.

Currently, all NFWC architectures assume a bufferless environment, which means no FDL is used. However, FDL is one essential device being used to resolve contentions due to lack of wavelength or lack of WC for OPS and OBS technologies. Therefore, it is important to analyze the performance of NFWC + FDL, as a kind of contention resolution method.

There are two possible methods to include the effect of the FDL. Firstly, let FDL be another dimension in the Markov chain to represent usage of the FDL for a particular wavelength. Secondly, assume FDL to be similar to a traditional buffer, which can delay data for any random time. Therefore, the FDL is a part of the queuing model while the current analytical model in this thesis represents the service model. The combination of the queuing model and service model is the new model to be analyzed. The first method may give better results than the second one,

because the assumption that the FDL is considered as a traditional buffer may introduce some discrepancies. However, the second method may be more easily analyzed, because the first method requires more Markov state dimensions which are expected to increase the complexity of the analysis.

5.2.3 The Impact of Switching Fabric on NFWC architectures

In this thesis, we use crossbar switch fabric throughout. This is because the crossbar is a simple and non-blocking switch fabric, which can simplify our analysis and can be used as a common comparison platform for all five NFWC in this thesis. However, the complexity of crossbar is the multiplication of the number of input and output port, such that the cost of the switches becomes very high when number of ports is large. Therefore, in order to reduce the cost of optical switching when NFWC architecture is used, some recent research works have shown in [90][91][92] that the switch and wavelength converter can be considered as whole and multi-stage non-blocking switching can be used, such that the cost of both WC and switch can be reduced significantly.

Therefore, in future, we will study and propose some multi-stage non-blocking switch fabrics with wavelength converter inside, especially for our new TLWC architectures. Some theoretical analysis can also be carried out to evaluate the performance of the corresponding architectures.

Appendix

The objective of this appendix is to show that the Markov chain state diagram analyses for PWC-only, CWC-SPF, CWC-SPN, TLWC-SPF and TLWC-SPN contributed in this thesis do not require any restrictive assumptions on the optical data size distribution. It should be noted that in the theoretical and numerical sections of this paper, the optical data size is stated to be of general distribution. In the following analysis, the term "server" is used instead of wavelength. The two terms are clearly interchangeable and the reason for using "server" is to be consistent with more familiar terms used in the field of queuing system. We use K as the number of servers (or number of wavelengths in the thesis) available in the system.

A.1 *M/G/K/K* **ErlangB loss formula**

We begin with the well known *M/M/K/K* Erlang B model. Let n represent the state where there are n servers in service currently (i.e., n wavelengths in use). Therefore, the Figure A-1 shows the state transition diagram of *M/M/K/K*. Thus the state probability P_n of state n, from any queuing theory textbook [76], can be expressed in (A.1) and (A.2), where λ is arrival rate and μ is service rate of one server.

$$
\begin{cases}
P_{n+1} = \dfrac{\lambda}{(n+1)\mu} P_n \;, \;\; 0 \le n \le K \\[2mm]
\sum_{n=0}^{K} P_n = 1
\end{cases}
\tag{A.1}
$$

$$
P_n = \frac{\dfrac{(\lambda/\mu)^n}{n!}}{\sum_{i=0}^{K} \dfrac{(\lambda/\mu)^i}{i!}}
\tag{A.2}
$$
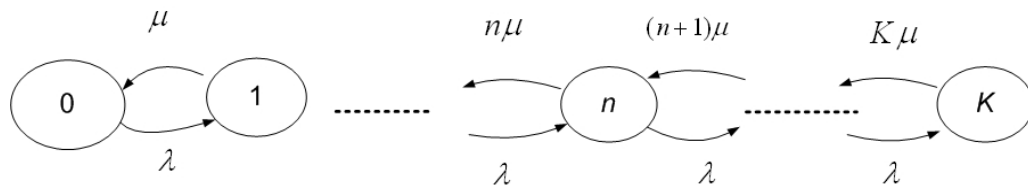
Figure A-1: *M/M/K/K* state transition diagram.

Since the service time distribution is linearly proportional to the data size distribution, we now consider service time distribution. Let X be the random variable representing the service time of a server, and let $g(t)$ and $G(t) = \int_0^t g(x)dx$, be the associated pdf (probability density function) and cdf (cumulative distribution function) of X. Define $\overline{G}(t) = 1 - G(t)$ to be the tdf (tail distribution function), $E[X] = \int \overline{G}(x)dx$ to be the average service time. The hazard rate function is thus given by $\upsilon(t) = g(t)/\overline{G}(t)$. The arrival process is Poisson and we assume the arrival rate is λ. The service rate is $\mu = 1/E[X]$. With these definitions, it is well known that:

Well known theorem A-1: The steady state probabilities of the *M/G/K/K* system is the same as the *M/M/K/K* system.

Proof

The proof is obtained from [89] but re-printed here as many parts of this proof will be used to prove that the analyses model contributed in the thesis are also independent of the service time distribution.

The state, at any time, of the *M/G/K/K* system can be defined to be the ordered ages of the data in service at that time. That is, the state will be $\bar{x} = (x_1, x_2, ... x_n)$, $x_1 \leq x_2 \leq .... \leq x_n$, if there are *n* servers in service (or *n* wavelength as used in this thesis), the most recent on having arrived x_1 time units ago, the next most recent arrived being x_2 time units ago, and so on. This ordering makes $\bar{x}$ be unique without duplications. Therefore, the process of successive states will be a Markov process in the sense that the conditional distribution of any future state given the present and all the past states, will depend only on the present state.

We will attempt to obtain the state probability density $p(\bar{x}) = p(x_1, x_2, ... x_n)$, where $1 \leq n \leq K$, and system empty probability $P(\phi)$. For any state $\bar{x}$, let $e_i(\bar{x}) = (x_1, ... x_{i-1}, x_{i+1} .... x_n)$. Now the state $\bar{x}$ will instantaneously go to $e_i(\bar{x})$ with probability density equal to $\upsilon(t)$. Similarly the state $e_i(\bar{x})$ will instantaneously go to $\bar{x}$ with probability density $\lambda g(x_i)$. Hence, according to the Markov chain state transition law

$$p(\bar{x})\upsilon(t) = p(e_i(\bar{x}))\lambda g(x_i) \tag{A.3}$$

$$p(\bar{x}) = p(e_i(\bar{x}))\lambda \overline{G}(x_i) \tag{A.4}$$

Letting $i=1$ and iterating the above yields

$$
\begin{aligned}
p(\bar{x}) &= \lambda \overline{G}(x_1)p(e_1(\bar{x})) \\
&= \lambda \overline{G}(x_1)\lambda \overline{G}(x_2)p(e_{2(}e_1(\bar{x}))) \\
&= ..... \\
&= P(\phi)\prod_{i=1}^{n} \lambda \overline{G}(x_i)
\end{aligned}
\tag{A.5}
$$

Integrating over all vectors $\bar{x}$ yields

$$
\begin{aligned}
P\{n \text{ in the system}\} &= P(\phi)\lambda^n \iint \dots \iint_{x_1 \le x_2 \le \dots \le x_n} \prod_{i=1}^{n} \overline{G}(x_i)dx_1 dx_2 \dots dx_n \\
&= P(\phi)\frac{\lambda^n}{n!} \iint \dots \iint_{x_1,x_2,\dots,x_n} \prod_{i=1}^{n} \overline{G}(x_i)dx_1 dx_2 \dots dx_n \\
&= P(\phi)\frac{(\lambda E[X])^n}{n!} \qquad n = 1,2,\dots.K
\end{aligned}
\tag{A.6}
$$

By using

$$P(\phi) + \sum_{n=1}^{K} P\{n \text{ in the system}\} = 1 \tag{A.7}$$

We can obtain

$$P\{n \text{ in the system}\} = \frac{\dfrac{(\lambda E[X])^n}{n!}}{\displaystyle\sum_{i=1}^{K}\dfrac{(\lambda E[X])^i}{i!}} = \frac{\dfrac{(\lambda/\mu)^n}{n!}}{\displaystyle\sum_{i=1}^{K}\dfrac{(\lambda/\mu)^i}{i!}} \tag{A.8}$$

We find that this formula is exactly same as the results from *M/M/K/K* analytical model in (A.2).

End proof

The above proof demonstrates that the steady state probabilities of the *M/M/K/K* model are the same as the steady state probabilities of the *M/G/K/K* model. This means that any analysis with exponential service distribution equally applies to general service distribution. However, it should be noted that the proof of equivalence for the *M/M/K/K* and the *M/G/K/K* model began as separate and unrelated sub-proofs and the final result just happens to be identical.

A.2 *The superset TLWC-SPN model*

It is noted that the TLWC-SPN Markov chain model is the most complicated and most demanding analytical model derived in the thesis. The other models like PWC-only, CWC-SPF, CWC-SPN and TLWC-SPF are all simpler models of the TLWC-SPN model. Rather than offering similar type of proofs for each of these models, we reduce verbosity by just considering the proof for the TLWC-SPN model. It should be obvious to the reader that the TLWC-SPN proof on its applicability to general size distribution is also just as relevant to the simpler PWC-only, CWC-SPF, CWC-SPN and TLWC-SPF models.

Now, the TLWC-SPN Markov chain analytical model presented in section 4.3 is not *M/G/K/K* but *p-M/G/K/K* where *p* stands for "probabilistic" (more on this later). The associated analytical contribution is based on a *p-M/M/K/K* model. While it has been shown that *M/M/K/K* and *M/G/K/K* are equivalent in their steady state probabilities, it is inappropriate to use this result to infer equivalence for *p-M/G/K/K* and *p-M/M/K/K* systems. Hence in the following sections, we define the *p-M/G/K/K* and *p-M/M/K/K* systems and a rigorous proof is provided to demonstrate the equivalence of the two systems.

A.3 Probability drop multi-server queue

Assume the arrival process is still Poisson and the service time is general distribution. The *p-M/G/K/K* model is described as follows: when there are *n* ($n < K$) data in service and a new data arrival, the data can be admitted into system with a probability β_n, which is not related to service time (data size) distribution. If the service time distribution is exponential, we term it as *p-M/M/K/K*. The TLWC-SPN architecture conforms to the p-M/G/K/K model as follows: when an optical data arrive and there are *n* ($n < K$) wavelengths in use, it is only with some β_n probability that the optical data may be served by an available wavelength. The β_n probability is the probability that there is an available wavelength converter which can be used to convert the optical data to one of the available wavelengths. A theorem will be provided later to demonstrate that the β_n probability in the TLWC-SPN model is indeed independent of the service time distribution. In the following, we will demonstrate that *p-M/M/K/K* has same steady probabilities with *p-M/G/K/K*, and we also will demonstrate that the Markov chain analysis in the thesis can be modeled as *p-M/G/K/K*.

The steady state probabilities of the *p-M/M/K/K* can be analyzed using the Markov chain state transition diagram as illustrated in the following figure. The associated steady state equations of the system can be expressed as in (A.9) and (A.10)
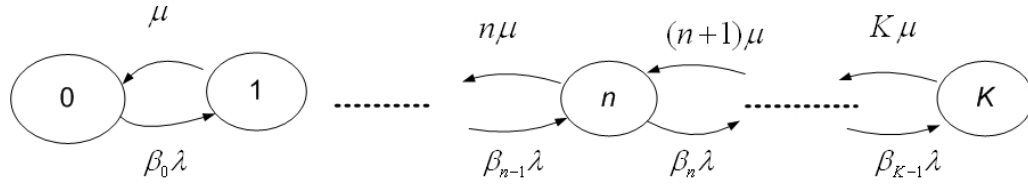
Figure A-2: Markov chain state diagram of *p-M/M/K/K* queue.

$$
\begin{cases}
P_{n+1} = \dfrac{\lambda \beta_n}{(n+1)\mu} P_n \quad , \quad 0 \le n \le K \\[2mm]
\displaystyle\sum_{n=0}^{K} P_n = 1
\end{cases}
\tag{A.9}
$$

$$
P_n = P_0 \frac{(\lambda/\mu)^n}{n!} \prod_{i=1}^{n} \beta_i \qquad n = 1, 2, \dots K \tag{A.10}
$$

Theorem A- 1: The steady state probabilities of the *p-M/G/K/K* system is the same as the *p-M/M/K/K* system

Proof

Using the same method for proving equivalence between the M/M/K/K and the *M/G/K/K* system, we replace λ in (A.3) and (A.4) with $\lambda\beta_n$, and obtain

$$
p(\bar{x})\upsilon(t) = p(e_i(\bar{x}))\lambda\beta_n g(x_i) \tag{A.11}
$$

$$
p(\bar{x}) = p(e_i(\bar{x}))\lambda\beta_n \overline{G}(x_i) \tag{A.12}
$$

Therefore, using the same progression as illustrated from (A.5) to (A.8), we obtain

$$
P\{n \text{ in the system}\} = P(\phi)\frac{(\lambda E[X])^n}{n!} \prod_{i=1}^{n} \beta_i \tag{A.13}
$$

Thus

$$P_n = P_0 \frac{(\lambda/\mu)^n}{n!} \prod_{i=1}^{n} \beta_i \qquad n = 1, 2, ... K \qquad (A.14)$$

where it is clear that (A.14) is identical with (A.10). Hence the *p-M/G/K/K* system has the same steady-state probabilities as the *p-M/M/K/K* system.

End proof

A.4 Applicability to General data size distribution

We now complete the proof for the applicability of the TLWC-SPN structure to general data size with the following Theorem:

Theorem A- 2: The β_n probability in the TLWC-SPN structure is independent of the service time distribution.

Proof:

We begin the proof with 2 important observations

Observation A-1: The occupancy distribution characteristics of a CWC (complete wavelength converter) in a TLWC-SPN node is a subset of the occupancy distribution characteristics of a "server" (i.e. wavelength). The observation is rather obvious since: (a) if an optical data arrives and it is admitted, it will definitely request one "server" (wavelength), but it may not request a CWC; (b) if a CWC is used or released by one optical data, a "server" must be used or released at same time. In other words, at all times, the number of servers in use is always larger or

equal to the number of wavelength converter in use. In addition, if there should be a CWC in use, it is without doubt that there is also a server in use that is directly responsible for the use of that CWC.

Similarly, the following observation, related to the use of a PWC to near-convert an optical data in a TLWC-SPN node, is also obvious:

Observation A-2: The occupancy distribution characteristics of a PWC (partial wavelength converter) in a TLWC-SPN node is also a subset of the occupancy distribution characteristics of a "server" (i.e. wavelength)

Now, we can write the β_n probability in terms of TLWC-SPN parameters as follows:

$$\beta_n = (1 - \alpha_n) + \alpha_n P\{\text{number of used CWC} < M | \text{n wavelengths in use}\} \qquad (A.15)$$

where α_n is the probability that a PWC is all used up (see Section 2.2). It is clear from (A.15) that by virtue of **Observation A-1** and **Observation A-2**, none of the parameters are related to the service time distribution. If any of the parameters in (A.15) are related, then they are only solely related to the "servers" (i.e. wavelengths) of the TLWC-SPN system.

End proof

Finally, the following theorem sums up all the work in this Appendix:

Theorem A- 3: The multi-dimensional Markov chain analysis and RS method for TLWC-SPN are also applicable to general service time (data size) distribution.

Proof

From ***Theorem A-2***, we know β_n in (A.15) has nothing to do with the service time (data size) distribution, therefore, it means the result of TLWC-SPN with general service time (data size) distribution is the same as Exponential data size distribution (by virtue of ***Theorem A- 1***).

Thus, any method, which obtain results for the Exponential service time (data size) model, e.g. multi-dimensional Markov chain model and RS/SCI methods, is just as applicable to the general service time (data size) distribution.

End proof

References

[1] A. Rodriguez-Moral, P. Bonenfant, S. Baroni, and R. Wu, "Optical Data Networking: Practical, Technologies, and Architectures for Next Generation Optical Transport Networks and Optical Internetworks", IEEE Journal of Lightwave Technology, vol. 18, 2000, pp. 1855-1870.

[2] N. Ghani, S. Dixit, and T. Wang, "On IP-over-WDM Integration", IEEE Communication Mag., vol. 38, 2000, pp. 72-84.

[3] R. Xu, Q. Gong, and P. Ye, "Novel IP With MPLS Over WDM-based Broadband Wavelength Switched IP Network," IEEE J. Lightwave Technology, vol. 19, no. 5, 2001, pp. 596-602.

[4] M. Renaud, et. al, "Network and system concepts for optical packet switching", Communications Magazine, IEEE , vol.35 , no. 4 , April 1997, pp. 96 -102

[5] C. Qiao and M. Yoo, "Optical Burst Switching (OS) - A New Paradigm for an Optical Internet", Journal of High Speed Networks, vol. 8, 1999, pp. 69-84.

[6] I. White, R. Penty, M. Webster, C. Y.J., A. Wonfor, and S. Shahkooh, "Wavelength Switching Components for Future Photonic Networks," IEEE Commun. Mag.,vol. 40, no. 9, 2002, pp. 74-81.

[7] B. Rajagopalan, J. Luciani, D. Awduche, B. Cain, and B. Jamoussi, "IP Over Optical Networks: A Framework," IETF RFC 3717.

[8] T. EL-Bawab and J. Shin, "Optical Packet Switching in Core Networks: Between Vision and Reality," IEEE Communication. Mag., vol. 40, no. 9, 2002, pp. 60-65.

[9] J. Diao and P. Chu, "Packet Rescheduling in WDM Star Networks With Real-time Service Differentiation," Journal of Lightwave Technology, vol. 19, no. 12, 2001, pp. 1818-1828.

[10] B. Meagher, G. Chang, G. Ellinas, Y. Lin, W. Xin, T. Chen, X. Yang, A. Chowdhury, J. Young, S. J. Yoo, C. Lee, M. Z. Iqbal, T. Robe, H. Dai, Y. J. Chen, and W. I. Way, "Design and Implementation of Ultra-low Latency Optical Label Switching for Packet-switched WDM Networks," IEEE Journal of Lightwave Technology, vol. 18, no. 12, 2000, pp. 1978-1987.

[11] B. Li, A. Ganz, and C. M. Krishna, "An In-band Signaling Protocol for Optical Packet Switching Networks," IEEE Journal. Select. Areas Communication, vol. 18, no. 10, 2000, pp. 1876-1884.

[12] M. Yoo and C. Qiao, "Just-Enough-Time (JET): A High Speed Protocol for Bursty Traffic in Optical Networks," Proc. IEEE/LEOS Conf. Tech. Global Info. Infrastructure, Aug. 1997, pp. 26-27.

[13] C. Qiao and M. Yoo, "Optical Burst Switching (OBS) A New Paradigm for an Optical Internet," Journal of High Speed Networks, vol. 8, no. 1, 1999, pp. 69-84.

[14] J. Turner, "Terabit Burst Switching", Journal of High Speed Networks, vol. 8, no. 1, 1999, pp. 3-16..

[15] Y. Xiong, M. Vandenhoute, and H. Cankaya. "Control architecture in optical burst-switched WDM networks". IEEE Journal on Selected Areas in Communications, vol 18, October 2000, pp. 1838-1851.

[16] C. Qiao and M. Yoo. Choices, "Features and issues in optical burst switching". Optical Network Magazine, vol. 1 no. 2, 2000, pp. 36-44.

[17]   J. White, M. Zukerman, and H. Vu. "A framework for optical burst switching network design". IEEE Communications Letters, vol. 6, June 2002, pp. 268-270.

[18]   C. Hsu, T. Liu, and N. Huang. "Performance analysis of deflection routing in optical burst-switched networks". In proceedings of INFOCOMM, vol. 1, 2002, pp. 66-73.

[19]   X. Wang, H. Morikawa, and T. Aoyama. "Burst optical deflection routing protocol for wavelength routing wdm networks". In Proceeding of Opticomm, 2000, pp. 257-266.

[20]   A. Zalesky, Hai Le Vu, Z. Rosberg, E.W.M. Wong, Zukerman M., "Modeling and performance evaluation of optical burst switched networks with deflection routing and wavelength reservation" INFOCOM 2004. Twenty-third Annual Joint Conference of the IEEE Computer and Communications Societies , vol. 3 , 7-11 March 2004 pp. 1864 – 1871

[21]   M. Yoo, C. Qiao, and S. Dixit, "QoS performance of Optical Burst Switching in IP-Over-WDM networks", IEEE Journal on Selected Areas in Communications, vol. 18, October 2000, pp. 2062-2071.

[22]   Huhnkuk Lim Chang-Soo Park, "An optical packet switch with hybrid buffer structure for contention resolution of asynchronous variable length packets", High Performance Switching and Routing, 2004. HPSR. 2004 Workshop on , 2004, pp. 162 - 166

[23]   S. Rangarajan, Zhaoyang Hu, L. Rau, D.J. Blumenthal, "All-optical contention resolution with wavelength conversion for asynchronous variable-length 40 Gb/s optical packets", Photonics Technology Letters, IEEE , vol. 16 , no. 2 , Feb. 2004, pp. 689 – 691.

[24]   V. M. Vokkarane and J. P. Jue, "Segmentation-Based Non-Preemptive Scheduling Algorithms for Optical Burst-Switched Networks" Proc. 1st International Workshop on OBS, Oct. 2003.

[25]   V. M. Vokkarane and J. P. Jue, "Prioritized Burst Segmentation and Composite Burst-Assembly Techniques for QoS Support in Optical Burst-Switched Networks," IEEE Journal on Selected Areas in Communications, vol. 21, no. 7, 2003, pp. 1198-1209.

[26]   A. Detti, V. Eramo, and M. Listanti, "Performance Evaluation of a New Technique for IP Support in a WDM Optical Network: Optical Composite Burst Switching (OCBS)," IEEE Journal of Lightwave Technology, vol. 20, no. 2, 2002, pp. 154-65.

[27]   B. Ramamurthy and B. Mukherjee, "Wavelength Conversion in WDM Networking," IEEE Journal on Selected Areas in Communications, vol. 16, no. 7, Sept. 1998, pp. 1061-1073.

[28]   E. Karasan and E. Ayanoglu, "Performance of WDM Transport Networks," IEEE Journal on Selected Areas in Communications, vol. 16, no. 17, Sept. 1998, pp. 1081-1096.

[29]   K.C. Lee and V. Li, "A Wavelength-Convertible Optical Network," IEEE/OSA Journal of Lightwave Technology., vol. 11, no. 5/6, May/June 1993, pp. 962-970.

[30]   T. Durhuus, B. Mikkelsen, C. Joergensen, S. L. Danielsen, K. E. Stubkjaer, "All-Optical Wavelength Conversion by Semiconductor Optical Amplifiers", Journal Lightwave Technology, vol. 14, no. 6, June 1996, pp. 942-954.

[31]   S.-C. Cao, J.C. Cartledge, "Time- and frequency-domain characterization of the modulated ASE noise in SOA-MZI wavelength converters", Photonics Technology Letters, IEEE , vol. 14 , no. 7 , July 2002 pp. 962 - 964

[32]   P. Ohlen, "Noise and crosstalk limitations in optical cross-connects with reshaping wavelength converters", Lightwave Technology, Journal of , vol. 17 , no. 8 , Aug. 1999, pp. 1294 - 1301

[33]   V. Eramo, M.Listanti, and M. Di Donato, "Performance Evaluation of a Bufferless Optical Packet Switch With Limited-Range Wavelength Converters", IEEE Photonic Technology Letters, vol. 16, no. 2, Feb 2004, pp. 644-646.

[34]   F.B. Shepherd, A. Vetta, "Lighting fibers in a dark network", Selected Areas in Communications, IEEE Journal on , vol. 22 , no. 9 , Nov. 2004 pp. 1583-1588.

[35]   C. Siva Ram Murthy, Mohan Gurusamy, "WDM Optical Networks : Concepts, Design, And Algorithms", Prentice-Hall, 2002.

[36]   S. Subramaniam, M. Azizoglu, A.K. Somani, "On optimal converter placement in wavelength-routed networks", Networking, IEEE/ACM Transactions on , vol. 7 , no. 5 , Oct. 1999, pp. 754 – 766.

[37]   Xiaowen Chu, Bo Li, I. Chlamtac , "Wavelength converter placement under different RWA algorithms in wavelength-routed all-optical networks", Communications, IEEE Transactions on , vol. 51 , vol. 4 , April 2003, pp. 607 – 617.

[38]   Bo Li, Xiaowen Chu, "Routing and wavelength assignment vs. wavelength converter placement in all-optical networks" Communications Magazine, IEEE , vol. 41 , no. 8 , Aug. 2003 pp. S22 - S28.

[39]   Peng-Jun Wan, Liwu Liu, O. Frieder, "Optimal placement of wavelength converters in trees and trees of rings", Computer Communications and Networks,

1999. Proceedings. Eight International Conference on , 11-13 Oct. 1999 pp. 392 - 397

[40]   V. Tamarapalli, S.H. Srinivasan, "Wavelength converter placement in WDM networks with non-uniform traffic", Local and Metropolitan Area Networks, 2004. LANMAN 2004. The 13th IEEE Workshop on , 25-28 April 2004 pp. 109 - 112

[41]   Suixiang Gao, Xiaohua Jia, Chuanhe Huang, Ding-Zhu Du, "An optimization model for placement of wavelength converters to minimize blocking probability in WDM networks", Journal of Lightwave Technology, vol. 21 , no. 3 , March 2003 pp. 684 - 694

[42]   X.-H Jia, D.-Z. Du, X.-D. Hu, H.-J. Huang, D.-Y. Li, "Placement of wavelength converters for minimal wavelength usage in WDM networks" INFOCOM 2002. Twenty-First Annual Joint Conference of the IEEE Computer and Communications Societies, vol. 3, 23-27 June 2002 pp. 1425 – 1431.

[43]   S.K. Bose, Y.N. Singh, A.B. Raju, B. Popat, "Sparse converter placement in WDM networks and their dynamic operation using path-metric based algorithms", Communications, 2002. ICC 2002. IEEE International Conference on, vol. 5 , 28 April-2 May 2002, pp. 2855 – 2859.

[44]   Lu Ruan, Dingzhu Du, Xiaodong Hu, Xiaohua Jia, Deying Li, Zheng Sun, "Converter placement supporting broadcast in WDM optical networks", Computers, IEEE Transactions on , vol. 50 , no. 7 , July 2001 pp. 750 - 758

[45]   Guangting Chen Guojun Li Guoliang Xue, "Optimal placement of wavelength converters in WDM optical networks with a general tree of rings topology", Computer Communications and Networks, 2000. Proceedings. Ninth International Conference on , 16-18 Oct. 2000 pp. 606 - 611

[46]   Gaoxi Xiao, Yiu-Wing Leung, "Algorithms for allocating wavelength converters in all-optical networks", Networking, IEEE/ACM Transactions on , vol. 7 , no. 4 , Aug. 1999 pp. 545 – 557.

[47]   Zhemin Ding, M. Hamdi, "On the management of wavelength converter allocation in WDM all-optical networks", Global Telecommunications Conference, 2003. GLOBECOM '03. IEEE, vol. 5, 1-5 Dec. 2003 pp. 2595 – 2600.

[48]   L.-W. Chen, E. Modiano, "Efficient Routing and Wavelength Assignment for Reconfigurable WDM Ring Networks With Wavelength Converters", Networking, IEEE/ACM Transactions on, vol. 13 , no. 1 , Feb. 2005 pp. 173 – 186.

[49]   C. Nuzman, J. Leuthold, R. Ryf, S. Chandrasekhar, C.R.Giles, D.T. Neilson, "Design and implementation of wavelength-flexible network nodes", Lightwave Technology, Journal of , vol. 21 , no. 3 , March 2003 pp. 648 - 663

[50]   Xiangdong Qin, Yuanyuan Yang, "Non-blocking WDM switching networks with full and limited wavelength conversion", Communications, IEEE Transactions on , vol. 50 , no. 12 , Dec. 2002 pp. 2032 - 2041

[51]   M.C. Yuang, Po-Lung Tien, J. Shih, A. Chen, "QoS scheduler/shaper for optical coarse packet switching IP-over-WDM networks", Selected Areas in Communications, IEEE Journal on , vol. 22 , no. 9 , Nov. 2004 pp. 1766 – 1780.

[52]   S.J.B. Yoo, et. al, "High-performance optical-label switching packet routers and smart edge routers for the next-generation Internet" Selected Areas in Communications, IEEE Journal on , vol. 21 , no. 7 , Sept. 2003 pp. 1041 - 1051

[53]   H. Overby, "An adaptive service differentiation algorithm for optical packet switched networks", Transparent Optical Networks, 2003. Proceedings of 2003 5th International Conference on , vol. 1 , 29 June-3 July 2003 pp. 158 – 161.

[54]   A. Kaheel, T. Khattab, A. Mohamed, H. Alnuweiri, "Quality-of-service mechanisms in IP-over-WDM networks", Communications Magazine, IEEE , vol. 40 , no. 12 , Dec. 2002 pp. 38 – 43.

[55]   Q. Zhang, V.M. Vokkarane, J.P. Jue, B. Chen, "Absolute QoS Differentiation in Optical Burst-Switched Networks", Selected Areas in Communications, IEEE Journal on , vol. 22 , no. 9 , Nov. 2004 pp. 1781 - 1795

[56]   V.M. Vokkarane, J.P. Jue., "Prioritized burst segmentation and composite burst-assembly techniques for QoS support in optical burst-switched networks", Selected Areas in Communications, IEEE Journal on , vol. 21 , no. 7 , Sept. 2003 pp.1198 – 1209.

[57]   Wanjiun Liao, Chi-Hong Loi, "Providing service differentiation for optical-burst-switched networks" Lightwave Technology, Journal of , vol. 22 , no. 7 , July 2004 pp. 1651 – 1660.

[58]   Jingxuan Liu, N. Ansari, T.J. Ott, "FRR for latency reduction and QoS provisioning in OBS networks", Selected Areas in Communications, IEEE Journal on , vol. 21 , no. 7 , Sept. 2003 pp. 1210 – 1219.

[59]   M. Yoo, C. Qiao, and S. Dixit. "QoS performance of Optical Burst Switching in IP-Over-WDM networks". IEEE Journal on Selected Areas in Communications, vol. 18, October 2000, pp. 2062-2071.

[60]   Soung Y. Liew, Gang Hu, H.J. Chao, "Scheduling algorithms for shared fiber-delay-line optical packet switches - the single-stage case", Global

Telecommunications Conference, 2004. GLOBECOM '04. IEEE , vol. 3 , 29 Nov -3 Dec 2004 pp. 1850 - 1856

[61]   Xin Li Hamdi M., "On scheduling optical packet switches with reconfiguration delay", Selected Areas in Communications, IEEE Journal on , vol. 21 , no. 7 , Sept. 2003 pp. 1156 – 1164.

[62]   J. Xu, C. Qiao, J. Li, G. Xu, "Efficient Burst Scheduling Algorithms in Optical Burst-Switched Networks Using Geometric Techniques" Selected Areas in Communications, IEEE Journal on , vol. 22 , no. 9 , Nov. 2004 pp. 1796 – 1811.

[63]   Jikai Li and Chunming Qiao, "Schedule burst proactively for optical burst switched networks", Computer Networks, vol. 44, no. 5, 5 April 2004, pp. 617-629

[64]   F. Callegati, W. Cerroni, G. Corazza, C. Develder, M. Pickavet, P. Demeester, "Scheduling Algorithms for a Slotted Packet Switch with either Fixed or Variable Length Packets", Photonic Network Communications , Sept, 2004, pp. 163-176

[65]   Hailong Li, Hanmeng Neo, Ian Li-Jin Thng, "Performance of the implementation of a pipeline buffering system in optical burst switching networks", Global Telecommunications Conference, 2003. GLOBECOM '03. IEEE, vol. 5 , 1-5 Dec. 2003 pp.2503 – 2507.

[66]   Jinhui Xu, Chunming Qiao, Jikai Li, Guang Xu, "Efficient channel scheduling algorithms in optical burst switched networks", INFOCOM 2003. Twenty-Second Annual Joint Conference of the IEEE Computer and Communications Societies. IEEE, vol. 3, 30 March - 3 April 2003 pp.2268 – 2278.

[67]   S.K. Tan, G. Mohan, K.C. Chua, "Burst rescheduling with wavelength and last-hop FDL reassignment in WDM optical burst switching networks ", Communications, 2003. ICC '03. IEEE International Conference on, vol. 2, 11-15 May 2003 pp. 1448 -1452.

[68]   A. Kaheel, H. Alnuweiri, F. Gebali, "A new analytical model for computing blocking probability in optical burst switching networks" Computers and Communications, 2004. Proceedings. ISCC 2004. Ninth International Symposium on , vol. 1 , June 28 - July 1, 2004 pp. 264 – 269.

[69]   A. Kaheel, H. Alnuweiri, F. Gebali, "Analytical evaluation of blocking probability in optical burst switching networks" Communications, 2004 IEEE International Conference on , vol. 3 , 20-24 June 2004 pp. 1548 – 1553.

[70]   N. Barakat, E.H. Sargent, "An accurate model for evaluating blocking probabilities in multi-class OBS systems", Communications Letters, IEEE , vol. 8 , no. 2 , Feb. 2004 pp. 119 – 121.

[71]   Z. Rosberg, Ha Le Vu, M. Zukerman, J. White, "Performance analyses of optical burst-switching networks", Selected Areas in Communications, IEEE Journal on , vol. 21 , no. 7 , Sept. 2003 pp. 1187 – 1197.

[72]   M. Neuts, H. Vu, and M. Zukerman, "Performance Analysis of Optical Composite Burst Switching". IEEE Communications Letters, vol. 6, August 2002. pp. 346-348.

[73]   S.L. Danielsen, C. Joergensen, B. Mikkelsen, K.E. Stubkjaer, "Analysis of a WDM packet switch with improved performance under bursty traffic conditions due to tuneable wavelength converters", Lightwave Technology, Journal of , vol. 16 , no. 5 , May 1998 pp. 729 – 735.

[74]   S.L. Danielsen, B. Mikkelsen, C. Joergensen, T. Durhuus, K.E. Stubkjaer, "WDM packet switch architectures and analysis of the influence of tunable wavelength converters on the performance", Lightwave Technology, Journal of , vol. 15 , no. 2 , Feb. 1997 pp. 219 – 227.

[75]   S.L. Danielsen, P.B. Hansen, K.E. Stubkjaer, "Wavelength conversion in optical packet switching", Lightwave Technology, Journal of , vol. 16 , no. 12 , Dec. 1998 pp. 2095 – 2108.

[76]   Donald Gross, Cal M. Harris, "Fundamentals of Queueing Theory",New York, Wiley, 1998.

[77]   V. Eramo, M. Listanti, "Packet Loss in a Bufferless Optical WDM Switch Employing Shared Tunable Wavelength Converters", IEEE Journal of Lightwave Technology, vol. 18, no. 12, Dec 2000, pp. 1818-1833.

[78]   V. Eramo, M. Listanti, P. Pacifici, "A comparison study on the number of wavelength converters needed in synchronous and asynchronous all-optical switching architectures", Lightwave Technology, Journal of , vol. 21 , no. 2 , Feb. 2003 pp. 340 – 355.

[79]   V. Eramo, M. Listanti, and M.D D, "Performance Evaluation of a Bufferless Optical Packet Switch With Limited-Range Wavelength Converters", IEEE Photonics Technology Letters, vol.16, no.2, Feb 2004, pp. 644-646.

[80]   V. Eramo, M. Listanti, "Input wavelength conversion in optical packet switches", Communications Letters, IEEE , vol. 7 , no. 6 , June 2003 pp. 281 – 283.

[81]   Zalesky, et, al, "Evaluation of limited wavelength conversion and deflection routing as methods to reduce blocking probability in optical burst switched networks" ICC, vol. 3 , 20-24 June 2004. pp. 1543 – 1547.

[82]   T. Durhuus, et, al, "All-Optical Wavelength Conversion by Semiconductor Optical Amplifiers", J. Lightwave Tech., vol. 14, no. 6, June 1996, pp. 942-954

[83]   Jin Cao, William S. Cleveland, Dong Lin, Don X. Sun, "Internet Traffic Tends Toward Poisson and Independent as the Load Increases", in the book Nonlinear Estimation and Classification, Springer 2003, pp. 83-109.

[84]   Thomas Karagiannis et al, "A Nonstationary Poisson View of Internet Traffic", INFOCOM 2004. Twenty-third Annual Joint Conference of the IEEE Computer and Communications Societies , 7-11 March 2004, vol. 3 , pp. 1558 - 1569.

[85]   R. Morris, Dong Lin, "Variance of aggregated Web traffic", INFOCOM 2000. IEEE Proceedings. vol. 1 , 26-30 March 2000, pp. 360 – 366.

[86]   Xiang Yu, Yang Chen and Chunming Qiao: "A study of traffic statistics of assembled burst traffic in optical burst switched network", Proceedings of Opticomm, vol. 4874, 2002. pp. 149-159.

[87]   Hailong Li, Ian Li-Jin Thng, "Edge Node Memory Usage in Optical Burst Switching Networks", submitted to Photonic Network Communications.

[88]   L.-W. Chen, E. Modiano, "Efficient Routing and Wavelength Assignment for Reconfigurable WDM Ring Networks With Wavelength Converters", Networking, IEEE/ACM Transactions on , vol. 13 , no. 1 , Feb. 2005 pp. 173 – 186.

[89]   Sheldon M. Ross, "Stochastic Processes", Wiley, 1983, pp. 168-171.

[90]   J. Ramamirtham and J. S. Turner, "Design of wavelength converting switches for optical burst switching", in Proceedings of the 21st Annual Joint Conference of the IEEE Computer and Communications Societies (INFOCOM). 2002, vol. 2, pp. 1162-1171, IEEE.

[91] Tony K. C. Chan, Eric W. M. Wong, Yiu-Wing Leung,"Shared-by-Wavelength-Switches: A Node Architecture Using Small Optical Switches and Shared Wavelength Converters", To be appeared in IEEE PHOTONIC TECHNOLOGY LETTERS.

[92] Hung Q. Ngo, D. Pan, and C. Qiao, "Nonblocking WDM switches base on arrayed waveguide grating and limited wavelength conversion", in Proceedings of the 23rd conference of the IEEE Communications Society (INFOCOM 2004), Mar 7-11, 2004, Hong Kong, China.

Biography

Author:	**Li Hailong**
Degree:	Doctor of Philosophy
Birth Date:	13 Dec, 1975
Place of Birth:	Ningxia, P.R.China

Educations

- Doctor of Philosophy in Electrical and Computer Engineering

  National University of Singapore, 2006

- Master of Engineering in Signal and Information Processing

  Beijing University of Posts and Telecommunications

  Beijing, P.R.China, April 2001

- Bachelor of Engineering

  Beijing University of Posts and Telecommunications

  Beijing, P.R.China, July 1998

Publication List

Published Journal Papers

1. **Hailong Li,** Ian Li-Jin Thng, "Cost Saving Two-Layer Wavelength Conversion in Optical Switching Network", IEEE/OSA Journal of Lightwave Technology, vol. 24, no. 2, Feb 2006. pp. 705-712.

2. **Hailong Li**, Malvin Tan Wei Liak, Ian Li-Jin Thng, "Fairness Issue and Monitor-based Algorithm In Optical Burst Switching Networks", Computer Networks, vol 50, issue 9, June 2006, pp. 1384-1405.

3. Caroline H. E. Chin, Yuqin Mong, Xiaosong TANG, Ian Li-Jin Thng and **Hailong Li**, "A FSLE-based transceiver for combined synchronization and equalization in partial response systems", WSEAS Trans. on Systems, issue 2, vol. 5, ISSN:1109-2777, pp. 368-373, Feb 2006.

4. **Hailong Li**, Ian Li-Jin Thng, "Performance Analysis of a Limited Number of Wavelength Converters in an Optical Switching Network", IEEE Photonics Technology Letters, vol. 17, no. 5, May 2005, pp. 1130-1132

5. **Hailong Li**, KimHui Ling, Li-Jin Ian Thng, Malvin Tan Wei Liak, "Dual Control Packets in Optical Burst Switching Networks", OSA Journal of Optical Networking, vol 3. no. 11, Nov 2004, pp. 787-801.

6. Xin Guan, Ian Li-Jin Thng, Yuming Jiang, and **Hailong Li**, "Providing Absolute QoS through Virtual Channel Reservation in Optical Burst Switching Networks", Computer Communications, vol 28, no. 9, June 2005, pp. 967-986.

7. Kian Jui Tan, Ian Li-Jin Thng, and **Hailong Li**, "Absolute Priority Just-Enough-Time Scheme For Absolute Quality of Service in Optical-Burst-Switching Networks", OSA Journal of Optical Networking, vol 3, no. 8, Aug, 2004, pp. 573-588.

Published conference papers

8. **Hailong Li,** Ian Li-Jin Thng, "A Novel Cost Saving Two-Layer Wavelength Conversion Structure in Optical Switching Node", accepted for presentation at the 2006 IEEE International Conference on Communications (ICC 2006)

9. **Hailong Li**, Malvin Tan Wei Liak, Ian Li-Jin Thng, Xiaorong Li, "Fiber Delay Line-Random Early Detection QoS Scheme for Optical Burst Switching

Networks" , Proceedings of 7th IEEE International Conference on High Speed Networks and Multimedia Communications HSNMC'04, June 30 - July 2, 2004. Toulouse, France, published by Springer, pp. 761-765.

10. **Hailong Li**, Tan Wei Liak Malvin, Ian Li-Jin Thng, "A Distributed Monitoring-based Fairness Algorithm In Optical Burst Switching Networks", IEEE International Conference on Communication, 20-24 June 2004, Paris, France, vol 3 , pp. 1564 - 1568.

11. **Hailong Li**, Hanmeng Neo, Ian Li-Jin Thng, "Performance of The Implementation of A PipeLine Buffering System In Optical Burst Switching Networks", Global Telecommunications Conference, 2003. GLOBECOM '03. IEEE, vol 5, 1-5 Dec 2003 pp. 2503 – 2507.

12. Caroline H. E. Chin, Yuqin Mong, Xiaosong TANG, Ian Li-Jin Thng and **Hailong Li**, "A new combined equalization/synchronization technique for partial response systems", Proceedings of the 4th WSEAS International Conference on Electronics, Control and Signal Processing (ICECS '05), Miami, Florida, USA, November 17-19, 2005, pp. 126-131.

Journal papers being reviewed

13. **Hailong Li**, Ian Li-Jin Thng, "Cost Effective Two-Layer Wavelength Conversion by Sharing per Node in Optical Switching Networks", submitted to IEEE Transaction on Networking.

14. **Hailong Li**, Ian Li-Jin Thng, "Performance Analysis of a Limited Number of Wavelength Converters by Share per Node in Optical Burst Switching Network", submitted to Computer Networks.

15. **Hailong Li,** Ian Li-Jin Thng, and Qun Zhao, "Upper and Lower Bounds of Performance Analysis for Partial Wavelength Converters in Optical Burst Switching Networks", submitted to Optical Switching Networks.

16. **Hailong Li**, Ian Li-Jin Thng, "Edge Node Memory Usage in Optical Burst Switching Networks", submitted to Photonic Network Communications.